THE SOLAR WIND INTERACTION WITH THE GEOMAGNETIC FIELD

JOHN H. WOLFE and DEVRIE S. INTRILIGATOR*

Space Sciences Division,
Ames Research Center, NASA, Moffett Field, Calif., U.S.A.

(Received in final form 12 July, 1969)

Abstract. A review is presented of the interaction of the solar wind with the magnetic field of the earth. The material is developed primarily from an observational point of view. The early observations are covered through late 1963, with primary emphasis on the sunward interaction region. The historical review of the early results is discussed in terms of the significant contributions of each satellite observation and in the light of our present concept of the solar wind-geomagnetic field interaction. Subsequent to 1963 the observations tend to overlap such that a strictly historical treatment is not tractable and the material is presented from a phenomenological approach. The daytime and night-time hemispheres are covered separately in terms of the significant and separable phenomena which dominate the structure and dynamics of these two regions. Satellite and deep space probe data are compared with relevant theory. Further observational efforts needed to improve our understanding of the details of the solar wind-geomagnetic field interaction are also discussed.

1. Introduction

It is well established today that the geomagnetic field does not extend indefinitely into interplanetary space, but rather is fairly well confined by the pressure exerted on the earth's field by the continuous outward flow from the sun of the solar plasma or solar wind. The terminating boundary of the geomagnetic field, the magnetopause, produces a cavity in the solar wind flow inside of which the solar plasma is excluded from direct penetration. This cavity is comet-like in shape, extending to a geocentric distance of approximately 10 earth radii, R_E, in the solar direction and flaring out to a mean distance of 12–14 R_E at the dawn-dusk meridian. Downstream from the sunlit hemisphere the magnetopause continues to flare out but to a lesser degree and eventually forms a presumably cylindrical-like tail, quite analogous to cometary tails, with a mean diameter of approximately 40–50 R_E. The geomagnetic tail seems to be well defined (i.e., dominated by geomagnetic field lines and the absence of solar plasma) out to at least the orbit of the moon (approximately 60 R_E) but probably begins to break up on the order of 100–200 R_E downstream from the earth. Effects of the tail have been observed, however, as far downstream as 1000 R_E.

Standing upstream from the magnetopause is a magnetohydrodynamic shock front. Since the wave modes, which are evidently dominant in this region of space, propagate with a group velocity much lower than the solar wind speed, information regarding the presence of the magnetic field of the earth cannot, in general, be transmitted upstream. As a result, the solar wind undergoes a shock transition quite analogous to

* NAS-NRC Postdoctoral Resident Research Associate. Present address: Physics Dept., California Institute of Technology, Pasadena, Calif.

Space Science Reviews **10** (1970) 511–596.

the gas dynamic bow shock that stands off from a blunt body encountering supersonic gas flow. The shock front is located ahead of the magnetopause some 3–4 R_E at the subsolar point and the standoff distance increases with increasing angle with respect to the stagnation point.

With the possible exception of evidently less dominant wave modes that can propagate upstream, the first principal encounter of the solar wind with the earth is at the bow shock. Here the solar wind undergoes a shock-like transition, which, in general, manifests itself as a decrease in the flow speed and a deflection in the flow direction associated with an increase in density and random energy. As the solar plasma proceeds inward, its flow direction is contoured to the shape of the magnetopause and the plasma flows around the geomagnetic cavity, carrying with it the imbedded interplanetary magnetic field. The position of the cavity at any point is then a consequence of the equalization of the normal component of total pressure on each side of the magnetopause. The region between the shock and magnetopause, called the magnetosheath, is dominated by hot, frequently nonthermal plasma, showing significant deviations from solar radial flow, the distorted interplanetary magnetic field, and a variety of complex wave-particle interactions.

An ecliptic plane view of the general features of this simplified picture is shown in Figure 1, together with the projected intial orbits and trajectories of a few selected

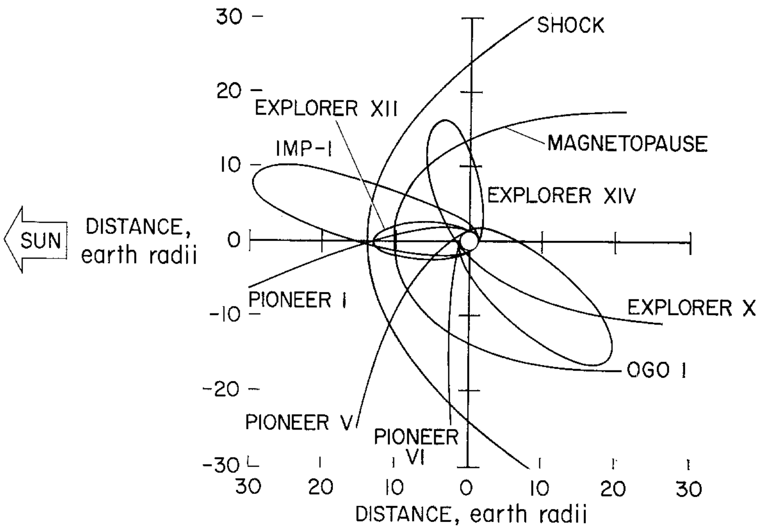

Fig. 1. Ecliptic plane view of the orbits and trajectories of a few selected satellites and deep space probes. The trajectories are shown with respect to the mean positions of the magnetopause and shock fronts.

satellites and deep space probes. This picture is oversimplified since the interaction of the solar wind with the geomagnetic field is a highly dynamic one. As we shall see later, the observational evidence indicates that the position, stability, and structure of the shock and magnetopause, the character of the magnetosheath with regard to plasma, low energy particles, magnetic and electric field conditions, and even the appearance of the outer radiation zone are highly dependent on the state of the interplanetary medium at any given time. In addition, the shape of the magnetopause is not symmetric with respect to the earth–sun line due to the nonradial flow characteristics of the solar wind. Neither is the magnetopause a surface of revolution, since one would expect in a noon-midnight meridian view, illustrated in Figure 2, two neutral points on

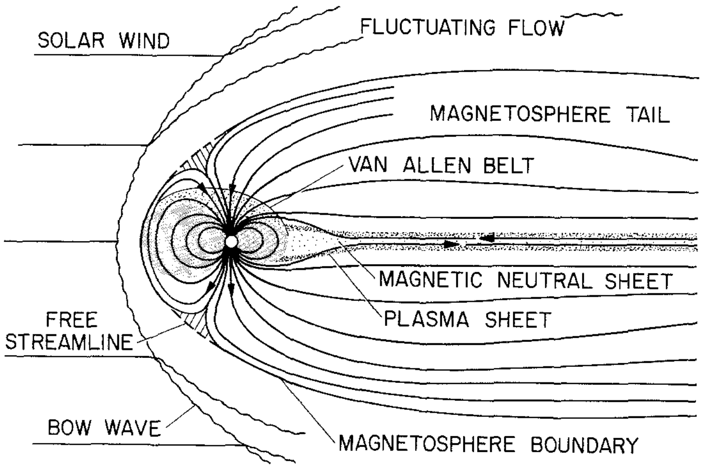

Fig. 2. Noon-midnight meridian plane view of the present concept of the magnetosphere and shock front interaction region.

cavity boundary, each associated with the two adjacent field lines that emanate near a geomagnetic pole and separate to form the outermost field lines in the sunlit and tail regions.

This general picture has evolved over the last 10 years. Many of the general features of our present concept of the geomagnetic field termination process were predicted by early theoretical work, while some of the more subtle features were not contemplated at all. The purpose of this review concerns all aspects of the solar wind-geomagnetic field interaction, but primarily from an observational point of view. Although the history of the early theoretical predications and some of the astronomical observations that led to these predictions is a fascinating subject in itself, it is outside the scope of the present review. Rather, the interested reader is referred to the many excellent reviews that include the early theoretical work (see, e.g., Dessler, 1967; Mackin and Neugebauer, 1966; Wilcox, 1968; Hess, 1968; Hess and Mead, 1968; and many others).

2. Early Observations

The first spacecraft to observe the distant geomagnetic field and to penetrate the near interplanetary medium was Pioneer 1. This vehicle was launched October 11, 1958, with an objective to survey the magnetic state of the medium between the earth and the moon. The spin stabilized spacecraft carried a single axis search coil magnetometer, which measured the component of the ambient magnetic field perpendicular to the spacecraft spin axis ($B_\perp$). The results from this experiment were first reported by Sonett (1959) and later in more detail by Sonett *et al.* (1960). Although the objective of placing the Pioneer I spacecraft into lunar orbit was not achieved, considerable data were obtained from the magnetometer experiment on the outbound trajectory between the geocentric distances from 3.7 to 7 and from 12.3 to 14.8 R_E. As can be seen from Figure 1, the Pioneer I trajectory was near the noon meridian, and the distance interval from 3.7 to 7 R_E was well within the outer part of the magnetosphere, whereas the distance interval between 12.3 and 14.8 R_E in all likelihood included the outer magnetosheath and the shock transition.

The magnetometer results from the first interval are shown in Figure 3, where $B_\perp$ is plotted as a function of geocentric distance and the solid line represents the expected value for an extrapolated dipole field of the earth (Sonett *et al.*, 1960). The agreement with the extrapolated value of $B_\perp$ was approximately within 10% and thus lent cre-

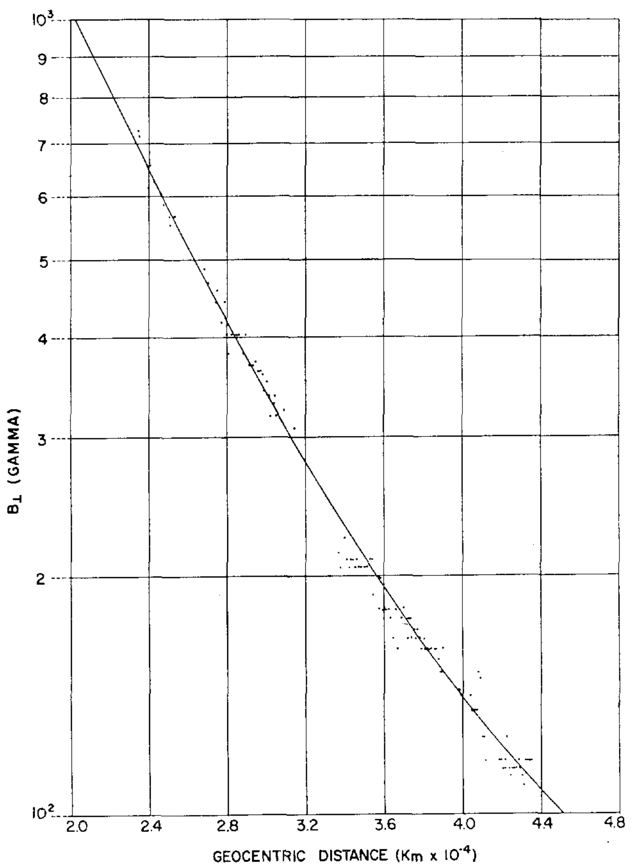

Fig. 3. Pioneer 1 magnetic field measurements from 2.0×10^4 to 4.8×10^4 km. The solid line represents the expected value for the extrapolated dipole field for the earth.

dence to the expected $1/r^3$ dependence of the earth's field. The variations of the measured field from the extrapolated dipole, particularly for the outer portion of this region, are characteristic of the fluctuations in the geomagnetic field in the outer magnetosphere as subsequently observed by numerous satellites and deep space probes launched since the flight of Pioneer 1.

The data obtained from 12.3 to 14.8 R_E are shown in Figure 4. Here again $B_\perp$ is

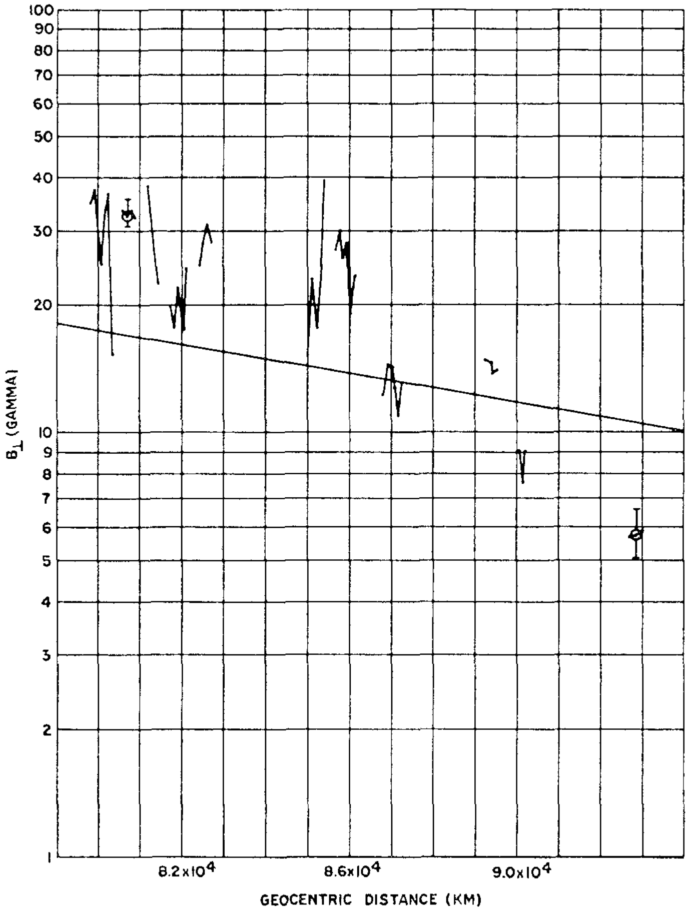

Fig. 4. Pioneer 1 magnetic field measurements from 7.9×10^4 to 9.4×10^4 km (12.3 to 14.8 R_E). The solid curve shows the extrapolated dipole field for the earth.

plotted as a function of geocentric distance with the solid curve showing the extrapolated dipole field (Sonett *et al.*, 1960). In view of our present picture of the interaction of the solar wind with the geomagnetic field, the field values recorded up to about 90000 km (14.1 R_E) were probably within the magnetosheath, with the shock transition occurring near this distance. The exact location of the shock for the Pioneer 1 traversal cannot be ascertained unambiguously, however, due to the intermittent data that resulted from ground tracking operations. The shock location, e.g., could have been as close as 86000 km (13.5 R_E) as evidenced by the large drop in field magnitude near this distance. In any event, the field magnitude of approximately 6 γ (1 $\gamma = 10^{-5}$ gauss) obtained at a distance near 93000 km (14.6 R_E) is, with little doubt, that of the interplanetary magnetic field. The large fluctuations in the magnetosheath field and the decrease in the mean ambient field from greater than 10 to less than 10 γ across the bow shock have been verified by numerous magnetic field measurements obtained since the Pioneer 1 observations.

The flights of the Russian lunar vehicles, Luna I, II, and III, launched on January 2, September 12, and October 4, 1959, respectively, provided the first opportunity of observing the plasma environment from within the magnetosphere near earth out to large distances beyond the shock. The results from these missions (Gringauz *et al.*, 1960a, b; Shklovskiy *et al.*, 1960) were somewhat difficult to interpret due to vehicle orientation, spacecraft and instrument photoeffects, and only integral energy resolution capability. Each spacecraft carried four charged particle traps, located with different orientations, each of which consisted of a hemispherical outer grid, a middle suppression grid, and a charged particle current collector. The outer grids of the various detectors had bias voltages applied that ranged between -10 and $+15$ V with respect to the vehicle skin. The suppression grids were generally held at -200 V, and the collectors were biased at $+90$ V. Two very significant results were obtained from these observations. The first concerned the detection of relatively soft electrons ($E > 200$ eV) at a geocentric distance from about 55000 to 75000 km. Within this range the electron fluxes recorded were on the order of 2×10^8 cm^{-2} sec^{-1}, whereas up to approximately 50000 km, the $E > 200$ eV electron fluxes were much lower, less than 2×10^7 cm^{-2} sec^{-1}. This region of geocentric distance was referred to as the 'third' or 'outermost' radiation zone. This seemed consistent with the second significant observation of continuously streaming positively charged particles with $E > 15$ eV (limited by the $+15$ V potential applied to the outer grid of one of the four charged particle traps) at greater distances from the earth (i.e., greater than 75000 km). The fluxes observed here were on the order of 2×10^8 cm^{-2} sec^{-1}. This continuous flux of positively charged particles was correctly identified as the streaming solar wind. It was argued that the third radiation zone resulted from the collision and partial penetration of this proton stream into the earth's magnetic field, with the subsequent redistribution of energy between the protons and electrons.

Although one could argue semantics, since the concepts of the magnetopause, magnetosheath, and shock were not established at that time, the third radiation zone is interpreted today as the observation of the superthermal electrons associated with the outer magnetosphere and magnetosheath. The outer magnetosphere electrons in this energy range are generally only quasi-trapped, and the magnetosheath electrons result from shock thermalization and wave-particle heating and thus form an integral part of the flowing plasma of the magnetosheath. Even though one would expect significant changes in the flow and spectral characteristics of these soft electrons between the magnetosphere and magnetosheath, the integral fluxes tend to be roughly equal and thus these early charged particle trap results failed to detect the magnetopause. These early measurements, however, did indicate the complex nature of the geomagnetic field termination process and were, without doubt, the first to show that an interplanetary solar wind did indeed exist and did interact with the earth's magnetic field.

The next spacecraft mission that provided information with regard to the interaction of the solar wind with the geomagnetic field was Pioneer 5. This spacecraft was launched March 11, 1960, into an escape trajectory near the dusk meridian (see Figure 1). Like Pioneer 1, Pioneer 5 was spin stabilized and carried a single axis search coil magnetometer that recorded the magnetic field perpendicular to the spacecraft spin axis. The preliminary results from this experiment were first reported by Coleman *et al.* (1960) and Smith *et al.* (1960) and, with respect to the interaction region, in great detail by Coleman (1964). The observed values of $B_\perp$ between 5.2 and 30.2 R_E are shown in Figure 5 (Coleman, 1964). The values plotted are 1 min averages (aver-

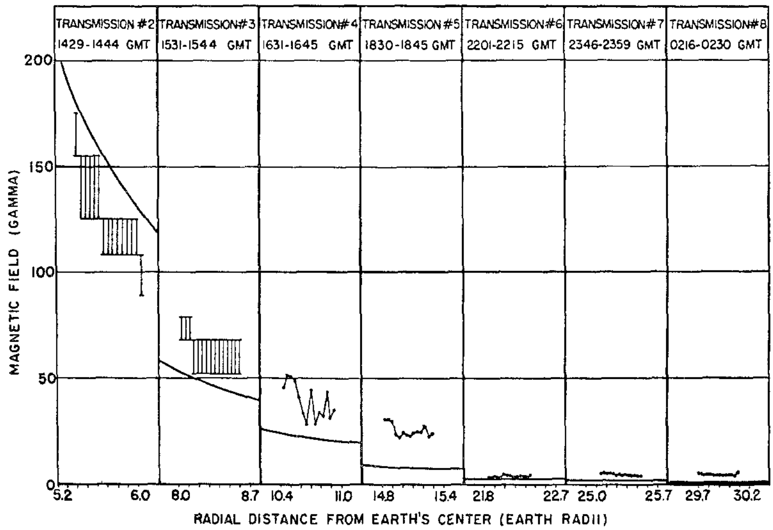

Fig. 5. Pioneer 5 magnetic field measurements between 5.2 and 30.2 R_E. The values plotted are 1 min averages with the use of flags representing the limits of a given digitization channel instead of points when the corresponding digitization channel was the only one recorded during a particular 1 min averaging period. The solid curves represent the extrapolated dipole field of the earth.

aged over 40 measurements), with the use of flags representing the limits of a given digitization channel instead of points when the corresponding digitization channel was the only one recorded during a particular 1 min averaging period. The solid curves shown in Figure 5 represent the extrapolated $B_\perp$ component of the geomagnetic dipole. Figure 6 shows the individual measurements of $B_\perp$ taken at 1.5 sec intervals for selected periods within transmissions 3–8. As in Figure 5, the solid curves are the extrapolated dipole field.

The results from Pioneer 5 were somewhat difficult to interpret, primarily because the spacecraft was launched during the recovery phase of a geomagnetic storm. If the interplanetary medium was still disturbed at this time, then it is likely that the interaction region had a much more complex character than would be expected for quieter times. Coleman (1964), e.g., has interpreted the large increase in the amplitude of the magnetic field fluctuations from transmission 3 to 4 as evidence that the Pioneer 5

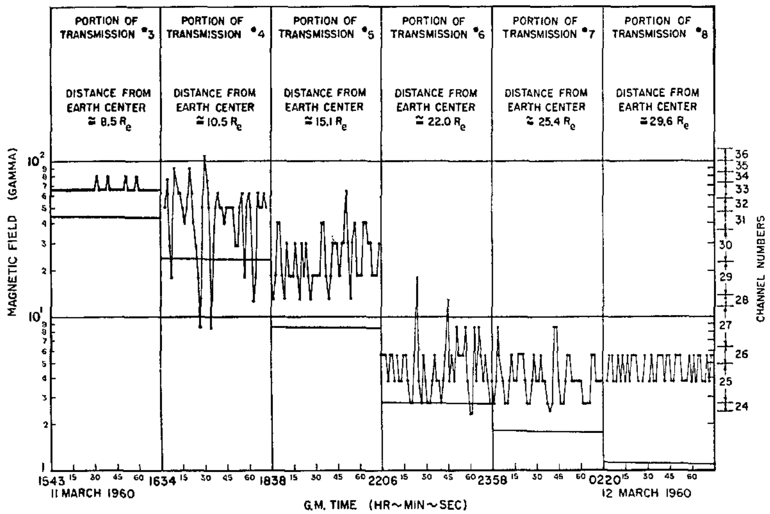

Fig. 6. Pioneer 5 individual measurements of the magnetic field taken at 1.5 sec intervals for selected periods within transmissions 3–8. The solid curves are the extrapolated dipole field.

spacecraft entered the magnetosheath somewhere between 8.5 and 10.5 R_E. It seems just as likely, however, that the spacecraft entered the magnetosheath between transmissions 4 and 5, where the mean field decreased from 41.0 to 26.8 γ and the rms deviation of the field decreased from 20.7 to 11.0 γ. This then would place the magnetopause somewhere between approximately 11.0 and 14.8 R_E and would imply that the fluctuations observed during transmission 4 were associated with the outer magnetosphere. A magnetopause location between these two later transmissions would be more consistent with subsequent measurements of the mean boundary position in this region of space as determined by later spacecraft flights.

The location of the shock is perhaps more easily identified in Figures 5 and 6 between 15.1 and 22.0 R_E, where the mean field decreased from 26.8 to 4.5 γ, while the rms deviation of the field decreased from 11.0 to 2.2 γ. As pointed out by Coleman (1964), however, the greatest difficulty encountered in attempting to reconcile the Pioneer 5 measurements with the shock wave model concerns the relatively large amplitude fluctuations observed out to at least 25.6 R_E, presumably some 4–10 R_E upstream from the shock front (see transmissions 6 and 7 in Figure 6). Although these measurements may have been the first observations of upstream wave phenomena, the possibility that the field fluctuations observed out to 25.6 R_E may have been interplanetary in character cannot be discounted. In any event, the Pioneer 5 observations confirmed and extended the earlier conclusions concerning the complex nature of the interaction between the solar wind and the geomagnetic field.

With the flight of Venera I (Sputnik III) came the first *in situ* observational evidence that the solar wind was related somehow with geomagnetic activity as observed by ground magnetic stations. Results from this Soviet Venus probe, launched February 12, 1961, revealed that the charged particle traps (similar to those flown on the earlier Luna vehicles) indicated an increase in the incident solar wind flux associated with an increase in geomagnetic activity resulting from a magnetic storm (Gringauz *et al.*, 1963). It was hypothesized at that time that there was good correspondence between the geomagnetic field fluctuations and changes in the solar wind flux near the beginning of the geomagnetic storm and that this correspondence disappeared somewhat later in the storm, presumably due to the development of local ionospheric current systems. The short time duration of the spacecraft transmission sessions (approximately $\frac{1}{2}$ hour) unfortunately precluded an unambiguous identification of the correlation between solar wind characteristics and geomagnetic phenomena.

Explorer 10, launched March 25, 1961, was the first attempt to investigate the distant geomagnetic field and plasma environment in the night hemisphere. The Explorer 10 satellite was a spin stabilized, battery powered spacecraft and carried an ac modulated Faraday cup-type plasma probe (Bonetti *et al.*, 1963) and a rubidium vapor and two tilted fluxgate (saturable core) magnetometers (Heppner *et al.*, 1963). Useful data were available only on the outbound leg of the spacecraft trajectory out to a geocentric distance of approximately 42 R_E in the evening quadrant. The Explorer 10 trajectory is shown in Figure 1. Note, however, that the Explorer 10 orbit plane was highly inclined, so that the outer portion of the outbound leg generally lay some 35° to 50° below the ecliptic.

A unique feature of this mission was the capability of the instrumentation to obtain vector measurements of the ambient magnetic field and approximate spectral information with regard to the incident ion fluxes. During the portion of the flight between approximately 8 and 22 R_E, the magnetometer experiment detected a large scale field generally directed away from the direction of the earth and sun. At a distance of about 22 R_E, the plasma experiment observed a positive ion flux that had a streaming velocity (assuming the positive ions were protons) of about 300 km/sec. In summary, the remaining observations out to about 42 R_E revealed intermittent periods characterized by one of two general features. The first concerned the appearance of substantial plasma fluxes on the order of 10^8 cm^{-2} sec^{-1} with an inferred streaming velocity near 300 km/sec. Although the plasma probe could not provide precise flow direction information, the streaming angle that was observed lay within an angular window of about 20° by 80°, which included the direction from the sun. Associated with this observed plasma flux, the magnetometer indicated the presence of irregular fields generally forming large angles with respect to the earth–spacecraft line. This was in contrast to periods where the plasma flux was either below or just above the detection threshold and the ambient magnetic field was observed to be generally radial from the earth. An example of these two regimes is given in Figure 7, which shows a comparison of magnetic field and plasma data taken between approximately 21 and 28 R_E (Bonetti *et al.*, 1963). The bottom curve gives the positive ion fluxes as a function of time in the various energy channels shown, and the top three curves give the magnetic field values in solar-ecliptic coordinates. Here ϕ is the ecliptic projection of the angle of the field vector

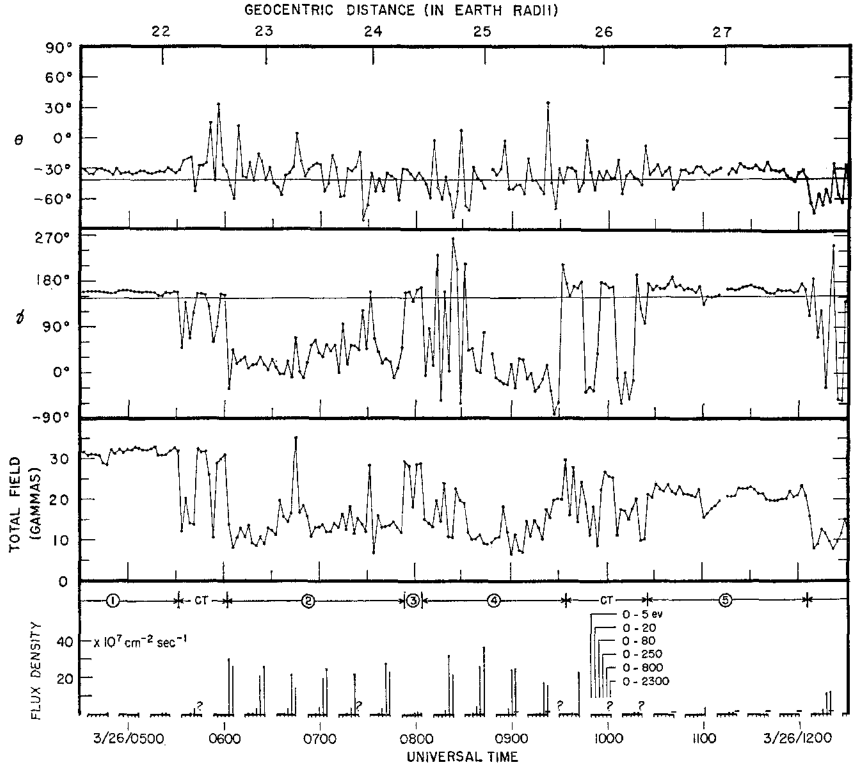

Fig. 7. A comparison of Explorer 10 magnetic field and plasma data taken between approximately 21 and 28 R_E. The bottom curve gives the positive ion fluxes as a function of time in the various energy channels shown, and the top three curves give the magnetic field values in solar ecliptic coordinates.

measured positively counterclockwise from the spacecraft–sun line, and θ is the angle out of the ecliptic with positive values for northward directed vectors. As can be seen in this figure, the lack of positive ion fluxes before 22 R_E and between approximately 26.2 and 27.8 R_E is well correlated with a relatively steady magnetic field directed approximately radially away from the earth. In addition, Figure 7 also shows that coincident with the observation of substantial plasma fluxes, the spacecraft encountered relatively unsteady magnetic field conditions.

It is clear from the Explorer 10 results that the geomagnetic cavity has great radial extent in the antisolar direction. Perhaps of even greater significance, these results illustrated the exclusion of the solar wind plasma from the geomagnetic cavity. We know today, of course, that these observations were in the magnetosheath and therefore not characteristic of the interplanetary medium. However, the oscillatory nature of the presence of the two plasma-field regimes clearly demonstrated that the magnetopause was not spatially static but, on the contrary, was capable of significant gross motion.

The Explorer 12 spacecraft was launched on August 16, 1961, and included in the experiment payload was a triaxial fluxgate magnetometer capable of simultaneous sampling of the three components of the ambient magnetic field. The results from this experiment (Cahill and Amazeen, 1963) were highly significant in that the satellite instrumentation and trajectory (see Figure 1) provided the first opportunity for systematic and recurrent sampling of the termination of the geomagnetic field. With an orbit apogee of only 13.1 R_E, it is unlikely that the spacecraft ever crossed the shock front even though the initial line of apsides was only 2.5° East of the noon meridian. This is somewhat uncertain, however, since the lowest digitization level of the mag-

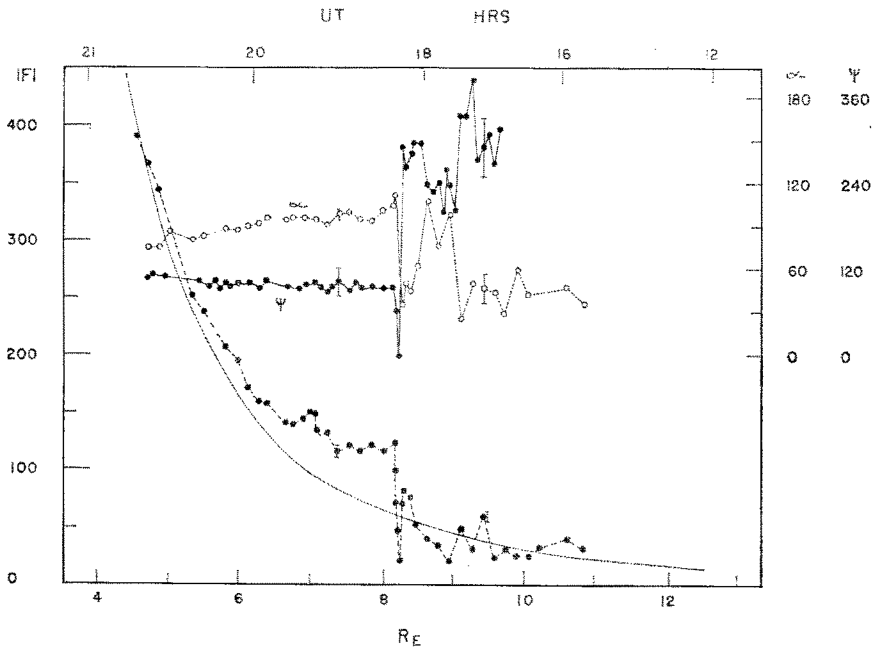

Fig. 8. Explorer 12 observations of the distant geomagnetic field during the September 13, 1961, inbound pass. The solid curve is the extrapolated dipole, and the magnetopause is located here just beyond 8 R_E.

netometer was 12γ and the field changes across the shock might have been difficult to distinguish.

Two examples of the distant geomagnetic field observations are shown in Figures 8 and 9. Here, $|F|$ is the total field magnitude in gamma and α and Ψ are the angular components of the ambient field vector in spacecraft coordinates. (See original article by Cahill and Amazeen, 1963, for the definition of this coordinate system.)

The magnetopause is clearly observed just beyond 8 R_E in Figure 8 for the September 13, 1961, inbound pass, and at approximately 10.5 R_E in Figure 9 for the September 30 – October 1, 1961, outbound pass. As illustrated in these figures, the magnetopause is most easily discernible by the changes in the field direction and in the level of the

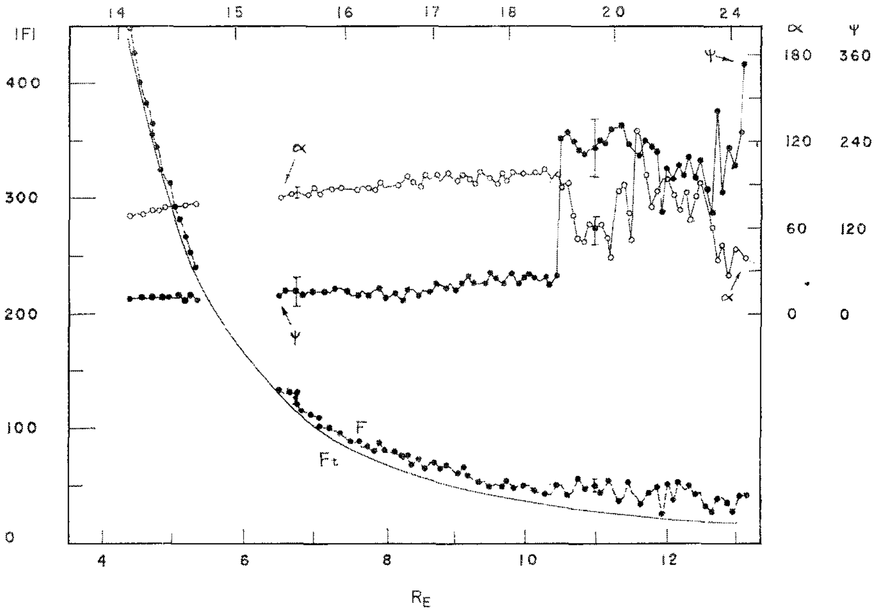

Fig. 9. Explorer 12 observations of the distant geomagnetic field during the September 30 – October 1, 1961, outbound pass. The solid curve is the extrapolated dipole field, and the magnetopause is located here at approximately 10.5 R_E.

fluctuations in field magnitude rather than a distinct change in magnitude itself. One of the most significant findings of Explorer 12 was that the detailed structure of the magnetic field across the magnetopause from one traversal to the next was never identical and that observations at different times could only be compared in a gross sense. This has been verified in subsequent measurements and is evidently associated with the state of the interplanetary medium at the time of the magnetopause traversal and perhaps somewhat dependent on the position of the traversal with respect to the stagnation point.

The magnetopause locations that were observed during the first 6 weeks of spacecraft life ranged over geocentric distances from 8.2 to 11.7 R_E. These observations were made within the angular extent with respect to the earth–sun line corresponding to local times between 0822 and 1302 hours (Cahill and Amazeen, 1963). The thickness of the magnetopause, as determined by the time required for the ambient field to undergo a complete change in direction, was never observed to be less than about 100 km, assuming no motion of the boundary back or forth past the spacecraft. The magnetosheath field near the boundary, although capable of large fluctuations in magnitude and direction, was found to be generally contained in a plane parallel to the earth's field just inside the magnetosphere.

The termination of the geomagnetic field as detected by the magnetometer was also observed to be coincident with the boundary for geomagnetically trapped electrons having energies $E > 40$ keV (Freeman *et al.*, 1963). In addition to the above, the presence of large intensities of relatively low energy electrons to significant distances beyond the magnetopause was also observed. These particles were detected in a CdS crystal detector, which could only respond to total energy deposition. Although the inferred high fluxes are somewhat difficult to reconcile in view of later measurements, it is clear that their identification with the superthermal electrons of the magnetosheath seems quite reasonable. It should also be noted that these lower energy electron fluxes in the magnetosheath provided the first indication of the true nature of the third radiation belt reported in the earlier U.S.S.R. measurements.

Although the Mariner II spacecraft, launched August 27, 1962, did not observe the solar wind-geomagnetic field interaction region, the onboard plasma measurements (Snyder and Neugebauer, 1964; Neugebauer and Snyder, 1966) demonstrated unambiguously that the solar wind was a persistent feature of the interplanetary medium. The velocities, temperatures, and densities that were observed ranged over the intervals 320–770 km/sec, 3×10^4–6×10^5 K, and 0.2–70 cm^{-3}, respectively, for the hydrogen component of the solar wind. In addition, a definite correlation was observed between the magnitude of the solar wind velocity and the dynamic state of the geomagnetic field as measured by the K_p index.

Explorer 14 was a spin stabilized spacecraft launched October 2, 1962, into an eccentric orbit having an apogee of 16.5 R_E geocentric and a period of approximately 36 hours. The orbit was inclined 33° to the equatorial plane, and the initial line of apsides made an angle of 72° with respect to the earth–sun line on the dawn side of the earth. In addition to instrumentation similar to that flown on Explorer 12, this spacecraft also carried a quadraspherical curved plate electrostatic analyzer. This plasma probe, although sensitive to solar uv, was able to detect the magnetosheath plasma and bow shock during the October 7, 1962, magnetic storm (Wolfe and Silva, 1965). This storm was also observed on Mariner II in interplanetary space (Neugebauer and Snyder, 1962; Sonett *et al.*, 1964) some 4 hours 39 min prior to its detection at earth. The significant results from Explorer 14 were the observation of the back and forth motion of the magnetopause across the spacecraft and, at least on one occasion, the back and forth motion of the shock front. The observations were consistent with solar wind flow in interplanetary space from the general direction of the sun with a deflection of the flow direction across the shock and around the geomagnetic cavity. In addition, it provided the first observation of plasma heating at the shock front as evidenced by the large increase in ion temperature within the magnetosheath as compared to the upstream value.

The next spacecraft to obtain significant information with regard to the solar wind-geomagnetic field interaction region was the IMP 1 satellite. IMP 1 (Explorer 18) was unique in both its orbit and the instrumentation that it carried. This spin stabilized spacecraft was launched on November 27, 1963, into a highly elliptical orbit with an initial apogee of approximately 31 R_E. The orbit plane was tipped 33° from the earth's equatorial plane, and the initial line of apsides was about 27° from the earth-sun line toward the dawn meridian and lay approximately 5° below the ecliptic (see Figure 1). This orbit enabled the IMP 1 spacecraft to sample nearly the entire interaction region in the morning quadrant during the first $2\frac{1}{2}$ months of useful lifetime. In addition, the magnetospheric tail region out to the limits of the orbit was also investigated over the subsequent several months. The instrument complement consisted of a rubidium vapor magnetometer, two monoaxial, tilted flux-gate magnetometers, an ac modulated Faraday cup plasma probe, a quadraspherical electrostatic analyser plasma probe, and a variety of thermal and higher energy particle detectors. The initial results from these experiments were first reported in the *IG Bulletin* (1964) and, with regard to the magnetic field, Faraday cup, and electrostatic analyzer, in greater detail by Ness *et al.* (1964), Bridge *et al.* (1965a), and Wolfe *et al.* (1966a), respectively.

Probably the single most important contribution by IMP 1 to our present understanding of the solar wind-geomagnetic field interaction region was the extensive mapping of the shock front, magnetosheath and magnetopause locations, and the repetitive observations of the general characteristics of the interaction region. It should be noted, however, that this mapping resulted from observations made by

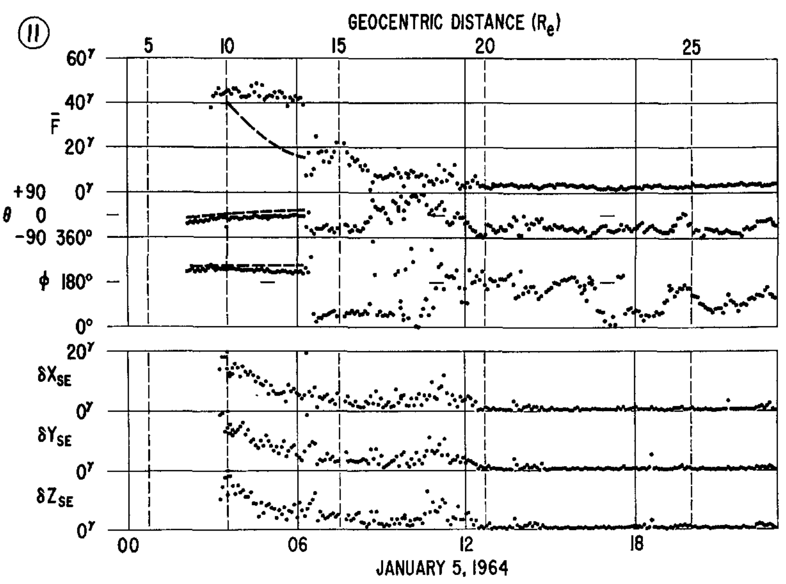

Fig. 10. An example of magnetic field measurements obtained on the 11th outbound pass of the IMP 1 satellite on January 5, 1964. The points shown are 5.46 min averages with the top three curves representing the field magnitude, $\bar{F}$, and the field orientation, θ and ϕ, in a solar ecliptic coordinate system. The dashed lines in the upper three curves represent the extrapolated dipole field. The bottom three curves give the rms deviations of the solar ecliptic, X, Y, and Z magnetic field components over the 5.46 min averaging intervals. For this case, the magnetopause was located at a geocentric distance of about 13.6 R_E.

several of the instruments aboard the spacecraft, and the results sometimes led to different inferences.

Figure 10 shows an example of magnetic field data obtained on the 11th outbound pass of the satellite on January 5, 1964 (Ness *et al.*, 1964). The points given are 5.46 min averages with the top three curves representing the field magnitude, $\bar{F}$, and the two angular components, θ and ϕ, in a solar ecliptic coordinate system identical to that defined for Figure 7. The dashed lines in the upper three curves represent the extrapolated dipole field. The three bottom curves give the rms deviations of the solar ecliptic X, Y, and Z magnetic field components over the 5.46 min averaging interval. Here the X axis points toward the sun, Y antiparallel to the earth's orbital motion, and Z toward the North ecliptic pole. Inspection of the data shows that the magnetopause was located on this pass at a geocentric distance of 13.6 R_E. It is interesting to note that the magnetospheric field magnitude just prior to the magnetopause traversal was approximately twice the extrapolated dipole value, which verified similar observations by Explorer 12 (Cahill and Amazeen, 1963). Large amplitude fluctuations in both magnitude and direction are then observed in Figure 10 as the spacecraft crossed the magnetosheath. At 19.7 R_E, the field became relatively stable both in magnitude and direction as seen in the values of $\bar{F}$, θ, and ϕ but observed more dramatically in the field variances given in the bottom three curves. This sudden decrease in the amplitude of the field fluctuations was interpreted as the shock traversal and seemed to be a fairly constant feature of the IMP 1 magnetic field results. The

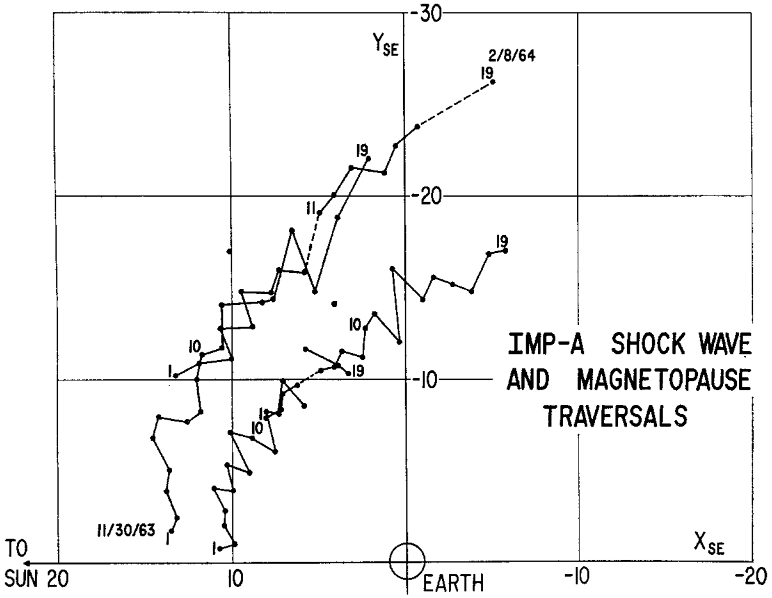

Fig. 11. A summary of the magnetopause and shock front locations determined by the IMP 1 magnetic field measurements. The data cover the first 19 orbits of the satellite, and the boundary points have been rotated from the spacecraft orbital plane into the ecliptic, assuming rotational symmetry about the earth–sun line.

criteria of the sudden drop in field magnitude and change in direction from the magnetosphere to the magnetosheath were used to define the magnetopause location, and the decrease in the amplitude of the variances from the magnetosheath to interplanetary space was used to define the location of the shock front. A summary of the magnetopause and shock front locations using the above criteria is shown in Figure 11 (Ness *et al.*, 1964). The data cover the first 19 orbits of the IMP 1 satellite, and the boundary points have been rotated from the satellite orbital plane into the ecliptic, assuming rotational symmetry with respect to the earth–sun line.

The IMP 1 quadraspherical analyzer, although capable of only crude angular and energy/unit charge information, was capable of defining three distinct regions of space on a given magnetosheath traversal (Wolfe *et al.*, 1966a). Within the geomagnetic cavity, no ion fluxes larger than the detection threshold of the instrument were observed. Within the magnetosheath, broad energy spectra were generally observed, along with great variability in flow direction and flux amplitude. This was in contrast to the relatively steady flow and the much lower temperature associated with the interplanetary medium.

The electrostatic analyzer had a fan shaped angular acceptance function approximately 90° by 15°. The instument was mounted on the spinning IMP 1 satellite so that the 90° acceptance angle was measured in the polar plane containing the vehicle

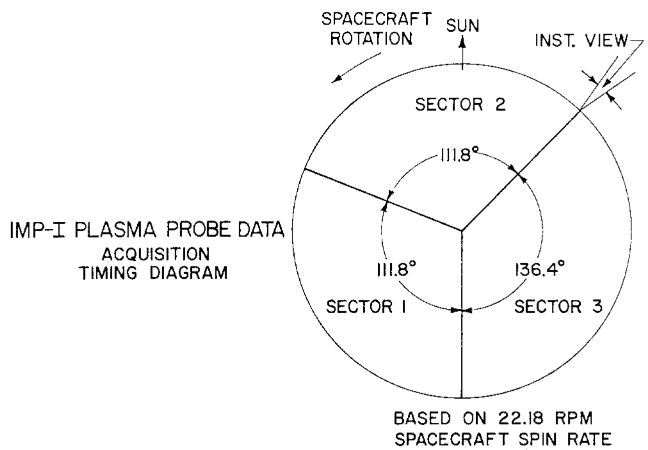

Fig. 12. Data acquisition and timing diagram for the IMP 1 electrostatic analyzer showing the angular sector widths and locations with respect to the spacecraft–sun line.

spin axis, and the instrument normal was perpendicular to the spin axis. The polar angle view was thus symmetrical above and below the spacecraft equatorial plane. With this mounting, the instrument acceptance geometry swept a band approximately 90° wide around the celestial sphere with each vehicle rotation. Angular indexing in the satellite equatorial plane was defined by dividing it into three sectors, using the optical aspect sensor as a reference. This division is shown in Figure 12. Note that the solar direction is always contained in the second sector. Figure 13 shows an example of the plasma observations for the 17th inbound pass of IMP 1 (Wolfe *et al.*, 1966a). The ion current over the range from 10^{-14} to 10^{-12} A (approximately 20 telemetry quantization levels) for the four lowest analyzer voltage steps is plotted as a

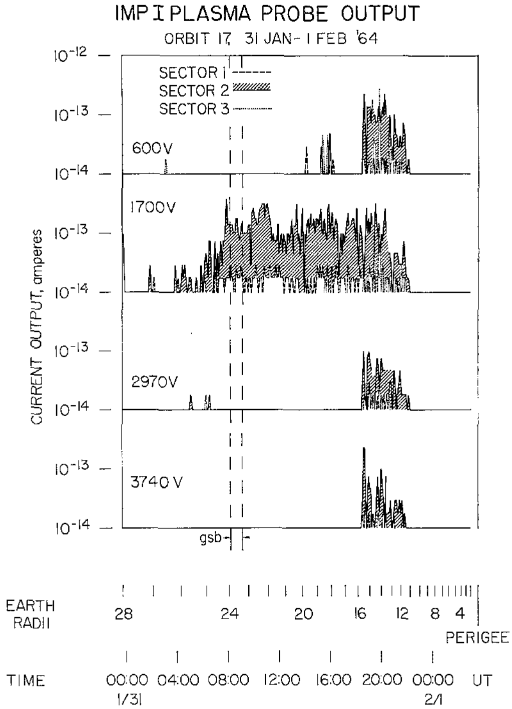

Fig. 13. Positive ion flux data from the IMP 1 electrostatic analyzer for the 17th inbound pass of the satellite showing the incident ion current in the three angular sectors for the four lowest energy channels as a function of UT and geocentric distance in earth radii. The shock front is located here at 15.7 R_E and the magnetopause at 11.3R_E. The gradual storm beginning, gsb, is indicated starting at about 0800.

function of the geocentric distance in earth radii and time in UT. The observed ion current was approximately proportional to the incident ion flux. For a normal incidence parallel beam in the 600 V channel, 10^{-14} A corresponds to approximately 3×10^5 protons cm^{-2} sec^{-1}. Only the four lowest energy levels were plotted since ion current was infrequently observed in the channels above 3740 V (846 km/sec for protons) for this instrument. The ion currents observed in the three sectors of rotation are plotted and identified by the legend. Figure 13 reveals the shock location at 15.7 R_E and the magnetopause at 11.3 R_E and illustrates the more disturbed character of the plasma ions within the magnetosheath. It is cautioned, however, that this particular magnetosheath traversal was subsequent to a gradual storm beginning (denoted by gsb in Figure 13) and showed a much higher degree of disturbance than was observed during more geomagnetically quiet traversals. The magnetosheath observations, however, consistently showed a lower plasma velocity, higher temperature, and a greater variability in flow direction as compared to the interplanetary solar wind characteristics.

The vast majority of the satellite passes showed a rather sharp cutoff in plasma flux associated with the magnetopause. Several passes, however, were anomalous in that they revealed a gradual rather than a sharp decrease in ion flux at the magnetopause. A few passes, particularly beyond a sun–earth probe angle of 90°, indicated a transient behavior for this boundary. This observation was thus consistent with the earlier Explorer 10 results. The shock location was more difficult to define because of its frequently diffuse and evanescent appearance.

In any event, the observational criteria of plasma thermalization at the shock transition and flow cessation at the magnetopause were used to determine the extent of the magnetosheath, and the results from the first 33 orbits are shown in Figure 14

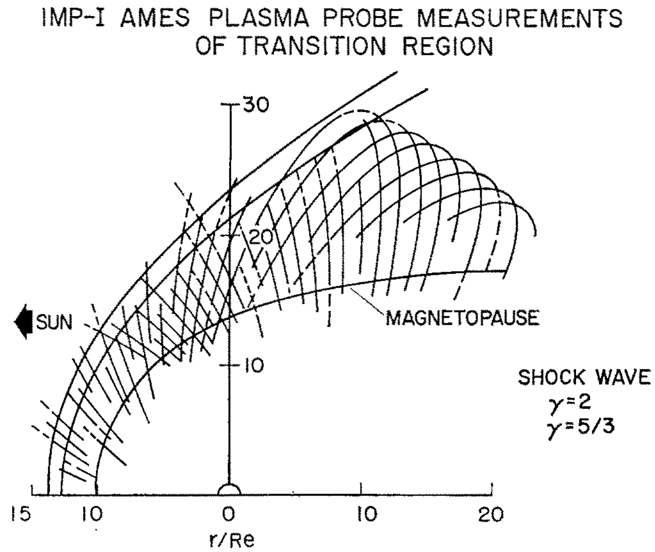

Fig. 14. The extent of the magnetosheath as determined by the IMP 1 electrostatic analyzer for the first 33 orbits, using the observational criteria of plasma thermalization at the shock transition and flow cessation at the magnetopause. The extent of the lines shown represent that portion of the IMP 1 trajectory over which the above criteria were satisfied in defining the magnetosheath. The dashed portions of the trajectories represent cases where the boundary criteria could not be applied due to the lack of resolution capability of the plasma probe or, more frequently, due to the apparent motion of these boundaries. The theoretical shock locations were taken from the calculations of Spreiter and Jones (1963). For details, see text.

(Wolfe *et al.*, 1966a). The lines shown represent that portion of the IMP 1 trajectory over which the above criteria were satisfied in defining the magnetosheath. The dashed portions of the trajectories represent cases where the boundary criteria could not be applied due to the lack of resolution capability of the plasma probe or, more frequently, due to the apparent motion of these boundaries. The theoretical shock locations were taken from the calculations of Spreiter and Jones (1963) for the ratios of the specific heats of the gas, $\gamma=2$ and $\frac{5}{3}$; a plasma convective velocity, $u=600$ km/sec; density, $n=2.5$ protons cm^{-3}; magnetic field, $B=5\gamma$; and a gas dynamic Mach number equated to an Alfvén Mach number, $M_A=8.71$.

The IMP 1 Faraday cup (Bridge *et al.*, 1965a) was similar to that flown on Explorer 10, with the exception that the energy windows on the IMP 1 instrument were differential rather than integral. Although this plasma probe produced a map of the shock and magnetopause locations that was quite similar in gross appearance with that obtained with the electrostatic analyzer, there were significant observational differences in most of the finer details of the plasma characteristics. Subsequent analysis (Vasyliunas, 1968; Olbert, 1968), however, has demonstrated the response of this cup to a variety of photoelectron effects and its spurious response to the superthermal electrons of the magnetosheath and outer magnetosphere. This has reconciled most of these observational differences.

The locations of the magnetopause as defined by the electrostatic analyzer results were compared on corresponding orbital passes to the observations of energetic electrons ($E>45$ keV) on the IMP 1 satellite as reported by Anderson *et al.* (1965). All of the early inbound passes reported (passes nearest the subsolar point) showed a good correspondence between the plasma flow cutoff and the beginning of a well-defined trapping region. Sporadic electron fluxes substantially above the interplanetary background (but well below the levels of the outer radiation zone) were also reported at locations both in and beyond the shock front location deduced from the plasma data. The above seemed true irrespective of the sun–earth probe angle; however, energetic electrons in and beyond the magnetosheath were more prominent at larger angles from the subsolar point. There seemed to be a fairly reasonable correspondence between the appearance of these energetic electron fluxes (reported also by Fan *et al.*, 1964) and a generally more disturbed appearance in the magnetosheath plasma. This provided arguments for the local acceleration of these electrons, of which only the high energy tail portion of the energy distribution was observed in the energetic electron detectors.

Although it seemed apparent that the mean shape of the shock front and magnetopause very closely resembled the calculated shape, in total, the IMP 1 results vividly revealed that the magnetosheath characteristics could, and frequently did, change significantly from one satellite pass to the next. The large differences in shock and magnetopause location ($>0.5\ R_E$) as defined by different instruments pointed to the complex nature of magnetosheath phenomena. In all likelihood, different instrument sampling periods and cycle times, different criteria imposed for the definition of a shock or magnetopause crossing, differences in data reduction technique, shock and magnetopause motion, and the observation of perhaps unrelated phenomena by different instruments probably all contributed in some way to the observational differences.

It seems fitting to close this section on early observations with the above discussion of the initial IMP 1 results. The IMP 1 results provide a firm foundation for consideration of the solar wind-geomagnetic field interaction from a more phenomenological point of view. In addition, subsequent to the IMP 1 flight, there was such a relatively high launch rate of spacecraft that provided observations pertinent to this review that the overlapping results do not easily lend themselves to a strictly historical treatment.

3. Sunward Interaction Region

A. SHOCK AND MAGNETOPAUSE MOTION

It was recognized in the early observations that the shock and magnetopause were capable of considerable gross motion. The extent and persistence of this motion, however, were not fully recognized. For Explorer 10 (Bonetti *et al.*, 1963) and Explorer 12 (Wolfe and Silva, 1965), the number of observations was limited. In the case of the IMP 1 satellite, the magnetopause and shock locations were observed to shift position on successive orbits (Ness *et al.*, 1964; Bridge *et al.*, 1965a; Wolfe *et al.*, 1966a); however, the motion of these boundaries was not obviously apparent on a single traversal. This is most easily explained by the high apogee (approximately 31 R_E), which resulted in a relatively large velocity of the spacecraft as it crossed the magnetosheath. In contrast to the IMP 1 findings, OGO 1 (launched September 5, 1964) and IMP 2 (launched October 4, 1964) frequently observed multiple shock and magnetopause crossings in a single orbital pass (Wolfe *et al.*, 1966b; Holzer *et al.*, 1966; Heppner *et al.*, 1967). The apogees of OGO 1 and IMP 2 were considerably lower than IMP 1, being 24.4 and 16.0 R_E geocentric, respectively. These spacecraft thus traversed the magnetosheath at a slower velocity and, on certain orbits, spent consider-

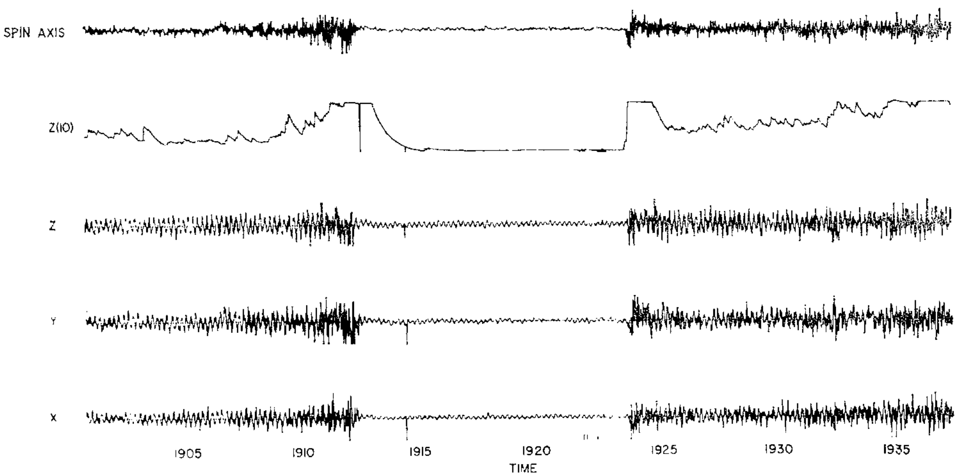

Fig. 15. An example of a double shock crossing observed by the OGO 1 triaxial search coil magnetometer. The lower three curves are the wave-form outputs from the three orthogonal search coil sensors with a 12-sec period modulation superimposed due to the spacecraft spin. The top curve is a linear combination of the three waveform channels, equivalent to the waveform output of a virtual sensor parallel to the spacecraft spin axis and, therefore, independent of rotation. The curve labelled Z (10) is the output of a passband channel from one axis with maximum transmission at 10 Hz. The double shock crossing is identified at 1912 and 1924 UT when the spacecraft was near 14 R_E.

ably more time near the boundaries, particularly in the vicinity of the shock front.

An example of a double shock crossing, observed by the OGO 1 triaxial search coil magnetometer (Holzer *et al.*, 1966), is shown in Figure 15. OGO 1, although designed to have three-axes stabilization, was forced into a spin stabilized configuration subsequent to a malfunction in the spacecraft attitude control system that occurred soon after launch. The resulting 12-sec period modulation on the waveform outputs from the three orthogonal search coil sensors due to the ambient dc magnetic field is evident on the three lower curves on Figure 15. The top curve in Figure 15 is a linear combination of the three waveform channels, equivalent to the waveform output of a virtual sensor parallel to the spacecraft spin axis and, therefore, independent of rotation. The curve labelled $Z(10)$ is the output of a passband channel from one axis with maximum transmission at 10 Hz. The data in Figure 15 were obtained near 14 R_E, and the double shock crossing is identified at 1912 and 1924 UT. The observation of relatively high magnetic noise at frequencies generally less than 300 Hz in the magnetosheath as compared to the magnetosphere or interplanetary space (see next section) was utilized in determining the magnetopause and shock traversals. From the above criteria, as many as 15 identifiable magnetopause crossings were observed on a single OGO 1 pass. Using a statistical approach, Holzer *et al.* (1966) estimated that the oscillatory motion of the shock front had an average amplitude, period, and mean velocity of 1.5 R_E, 60 min, and 10 km/sec, respectively; and for the magnetopause, 0.25 R_E, 20 min, and 10 km/sec, respectively. Heppner *et al.* (1967), utilizing the results from the OGO 1 triaxial fluxgate magnetometer, estimated from a somewhat more detailed statistical approach that the motion of the shock front had an average velocity of about 8 km/sec and an average amplitude of approximately 0.45 R_E. They also determined that the velocity of the magnetopause must have been, in general, considerably less than, or at most equal to, the velocity of the satellite, i.e., approximately 100 km/min. This was concluded from the fact that even when two or three magnetopause crossings were observed, the time required for the spacecraft to cross the boundary was not substantially different from those passes where only a single crossing was observed. Although the search coil and fluxgate observations led to somewhat different results with respect to boundary motion, the reconciliation of these differences does not seem warranted, due to the great variability in boundary motion that has been reported and the generally poor statistics. In any event, these results certainly indicated the general gross motion that the shock and magnetopause could undergo.

Shock and magnetopause motion have been observed on almost all spacecraft that have traversed the magnetosheath since the launch of OGO 1. These observations have been reported by numerous investigators, using a variety of detectors. For example, during the outbound trajectory of Mariner 4, Siscoe *et al.* (1967), using results from the helium magnetometer experiment, reported the possibility of as many as seven traversals of the shock front. Anderson *et al.* (1968) reported that observations on IMP 2 (Explorer 21) with several detectors showed that the magnetopause was found to be almost always in motion. The amplitudes of the motion were determined to vary from pass to pass from about 0.2 to 2.2 R_E. In addition, they found that the motions were sometimes periodic, with characteristic times on the order of 3–15 min. These results further indicated that the magnetopause motions were apparently coherent over distances of the order of 10 R_E, since the bow shock motions measured on the same satellite pass were found to have well-correlated amplitudes and characteristic times. Cummings and Coleman (1968) and Freeman *et al.* (1968) have reported the observation of multiple magnetopause crossings as detected by the ATS 1 satellite when the magnetopause was greatly depressed so as to be below the 6.6 R_E distance of the synchronous equatorial orbit.

The examples cited above clearly show that the location of the shock and the magnetopause cover a considerable range in geocentric distance from one observation to the next, and, in addition, these boundaries portray great variability in their motional behavior. On the other hand, the mean boundary positions, in the daytime hemisphere at least, determined from OGO 1 results (Holzer *et al.*, 1966; Heppner *et al.*, 1967), IMP 2 (Binsack, 1968), IMP 3 (Ness, 1967), and Vela 2 (Gosling *et al.*, 1967) all indicate approximate correspondence with the earlier Explorer 12 and IMP 1 results. One would expect, however, that if the shock and magnetopause shape and location are controlled by the solar wind, then the symmetry line of these boundaries should be misaligned with the earth–sun line by some 3° to 6° in the direction toward the West limb of the sun. This misalignment is expected from the aberration effect apparent in the mean solar wind flow direction caused by the orbital motion of the earth around the sun. This indeed has been observed by OGO 1 (Holzer *et al.*, 1966; Heppner *et al.*, 1967), which was able to map the magnetosheath from the dusk to dawn meridian in the daytime hemisphere. The Vela 2 satellites were particularly well suited for this observation, since their orbits are approximately 17 R_E circular, with high inclination (ecliptic latitudes up to $\pm 63°$) and they frequently provided two diametrically opposed magnetosheath traversals on a single orbit. Gosling *et al.* (1967) report the Vela 2 observation of a 2° to 4° East–West tilt in the symmetry line of the shock and magnetopause in substantial agreement with the expected aberration effect. This East–West asymmetry is even more apparent from results obtained from spacecraft observations taken in the far geomagnetic tail (see Section 4.B).

An obvious question is: what is the cause of the shock and magnetopause location variability and oscillatory behavior? In this regard, attempts were made to correlate these phenomena with the geomagnetic disturbance index, K_p, and thereby presumably also with the solar wind velocity (Neugebauer and Snyder, 1966). Gosling *et al.* (1967) cite evidence from Vela 2 observations that the average positions of the shock and magnetopause appear to be related to K_p and that gross motions in these boundaries were observed, coincident with sudden changes in plasma pressure within the magnetosheath. Heppner *et al.* (1967) and Holzer *et al.* (1966), on the other hand, did not detect any significant correlation of shock and magnetopause positions with K_p, although the latter did indicate that the magnetopause tended to be closer to the earth for high K_p values when K_p was within the range 0–3. Binsack (1968), utilizing the IMP 2 Faraday cup plasma probe data, observed that the shock and magnetopause boundaries tended to be extremely responsive to solar and geomagnetic activity. In addition, even during relatively quiet periods, the boundaries appeared to remain in motion, although on a smaller scale than that observed during more disturbed times. Afforded the opportunity of simultaneous IMP 1, IMP 2, and OGO 1 Faraday cup plasma probe observations, Binsack and Vasyliunas (1968) have been able to show that the large-scale motions of the shock that occur during geomagnetic storms result from an overall compression of the entire magnetosphere-magnetosheath system in response to the enhanced solar wind dynamic pressure. Using the initial IMP 1 results to provide the surface shape of the shock, they derived an expression for the expected instantaneous location of the shock observed by one satellite, based on the free-stream solar wind dynamic pressure observed by another satellite. Figure 16 shows the shock

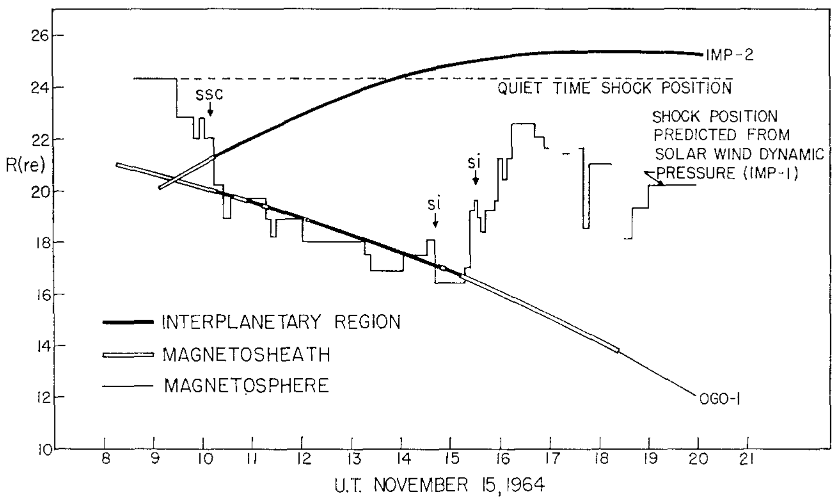

Fig. 16. Shock position and solar wind pressure observations by the Faraday cup plasma probe during the November 15, 1964, geomagnetic storm. The trajectories of the IMP 2 and OGO 1 spacecraft are shown, together with the calculated shock position based on simultaneous IMP 1 measurements.

position and solar wind pressure observations during the November 15, 1964, geomagnetic storm. The trajectories of the IMP 2 and OGO 1 spacecraft are shown as indicated in the figure, together with the calculated shock position based on the simultaneous IMP 1 measurements. In order to correspond to the predictions, the satellites should be located in the interplanetary medium when their trajectories lie above the calculated shock position shown in Figure 15 and within the magnetosheath when they lie below it. The actual observed positions of the two spacecraft with respect to the magnetosheath boundaries are shown as indicated in the figure legend. Even a cursory inspection of Figure 16 shows the excellent agreement between the predicted and observed positions. Although the responses of the geomagnetic cavity to changes in solar wind dynamic pressure were generally assumed, the above represents the first quantitative verification and thus provides direct insight into the question of shock and magnetopause dynamic behavior.

B. WAVES IN THE MAGNETOSHEATH

Results from the OGO 1 search coil magnetometer (Holzer *et al.*, 1966; Smith *et al.*, 1967) show the presence of 3–300 Hz magnetic noise throughout the entire magnetosheath with higher amplitudes near the boundaries, especially the shock. Broadband signals within this frequency range were found to be continuously present, relatively intense, and highly variable on a time scale of tens of seconds. The persistent feature of this magnetic noise within the magnetosheath as compared to the interplanetary or magnetosphere observations was used to identify the extent of the magnetosheath as discussed in the previous section. Representative power spectral density estimates within this frequency range revealed an inverse cube dependence on frequency. The results reported by Smith *et al.* (1967) extend, up to 300 Hz, previous estimates for the fluctuating magnetic fields in the magnetosheath. Their results indicated an apparent change in the frequency dependence of the power spectral density somewhere between 0.1 and 1 Hz. The above is quite evident in the composite power spectral density spectrum shown in Figure 17 (after Smith *et al.*, 1967) from OGO 1 data (Holzer

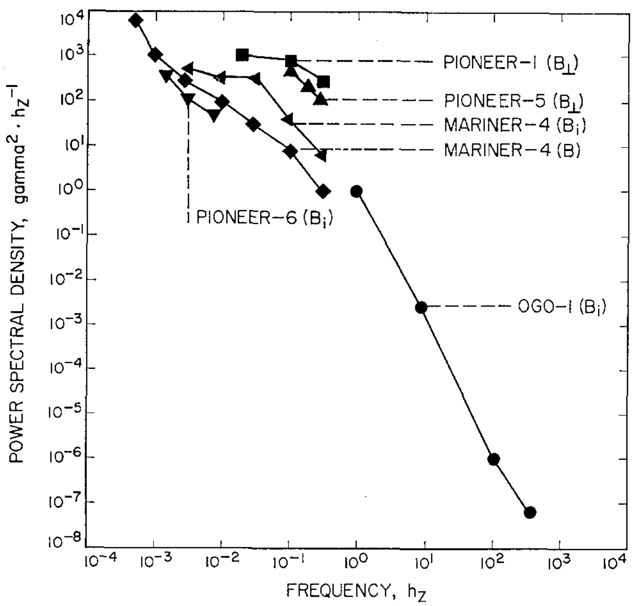

Fig. 17. Composite magnetosheath magnetic field power spectral density spectrum. (See note added in proof, p. 593.)

et al., 1966), Pioneer 1 (Sonett and Abrams, 1963), Pioneer 5 (Coleman, 1964), Pioneer 6 (Ness *et al.*, 1966), and Mariner 4 (Siscoe *et al.*, 1967). The spectra provided by Pioneer 1 and 5 are seen to be significantly higher. The Pioneer 1 data, however, were obtained near the subsolar point (see Figure 1), and the Pioneer 5 data were obtained during a geomagnetic disturbance. The other spectral estimates are seen to agree reasonably well. Smith *et al.* (1967) concluded that the apparent change in slope near 1 Hz was likely to be caused in part by the disappearance of the Alfvén wave contribution above the ion cyclotron frequency and was perhaps strongly influenced by wave generation or amplification (ion gyroresonance) near this frequency. It is cautioned, however, that these results were susceptible to Doppler shifting, since the waves were propagating in the streaming plasma of the magnetosheath and observed in the relatively stationary spacecraft frame of reference. The above, together with effects due to the irregular time varying character of the magnetosheath magnetic field, would tend to smear somewhat the observed spectra (Smith *et al.*, 1967; Siscoe *et al.*, 1967).

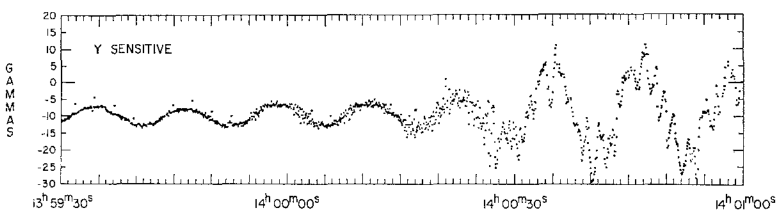

Fig. 18. Waveform output from one axis of the OGO 1 fluxgate magnetometer obtained during an inbound shock traversal. Rapid fluctuations, $f > 3$ Hz, are seen to appear at the shock (located near 1400-30 UT) and in the interplanetary field near the shock. Coherent oscillations near 1 Hz appear at the shock and in the magnetosheath in several groups of 3–6 cycles. The 12-sec period OGO 1 roll modulation is evident in the data, together with a 9 γ offset due to the spacecraft bias field.

Complementary to, and consistent with, the search coil results cited above, the OGO 1 fluxgate magnetometer results reported by Heppner *et al.* (1967) showed the presence of coherent, circularly polarized waves in the frequency range 0.5–1.5 Hz and unresolved fluctuations at frequencies greater than 7 Hz generated near the shock front. The former was identified as whistler mode waves with relatively sharp frequency cutoffs, and the latter, although not identified, seemed consistent with the higher frequency measurements provided by Smith *et al.* (1967). Figure 18 shows the waveform output from one axis of the magnetometer for a particularly striking inbound shock traversal. For this case, the rapid fluctuations, $f > 3$ Hz, appear at the shock (located near 1400-30 UT) and in the interplanetary field near the shock, whereas the coherent oscillations near 1 Hz appear at the shock and in the magnetosheath in several groups of 3–6 cycles. The 12-sec period spacecraft roll modulation is evident in the data, together with a 9 γ offset due to the spacecraft bias field. Siscoe *et al.* (1967) reported for the Mariner 4 magnetosheath traversal the presence of compressional fluctuations in the magnetic field in the frequency range 0.2–1 Hz, which were approximately constant in amplitude across the magnetosheath with a slight increase near the shock. Transverse fluctuations were also observed in the same frequency range that had smaller amplitudes near the magnetopause but increased greatly as the spacecraft approached the shock front.

Included among the total complement of experiments carried aboard the OGO 5 satellite (launched March 4, 1968) was a vlf plasma wave experiment. This experiment contained both electric dipole and magnetic loop sensors whose outputs were monitored through broadband analog and narrowband filter channels over the frequency range from approximately 0.56 to 70 kHz. The preliminary results from this experiment, reported by Fredricks *et al.* (1968), indicated the presence of significant electric field turbulence in the shock layer. Figure 19 presents a time sequence of approximate electric field power spectra derived from passband channel outputs for an outbound OGO 5 shock crossing on March 12, 1968. Shown in the small insets are simultaneous measurements of one component of the magnetic field detected by the UCLA fluxgate magnetometer, which, in this case, was sensitive over the frequency interval from 0 to 2.5 Hz. Upstream in the free streaming solar wind (top of Figure 19), the magnetic field was quiet, and the electric field spectrum contained a significantly high

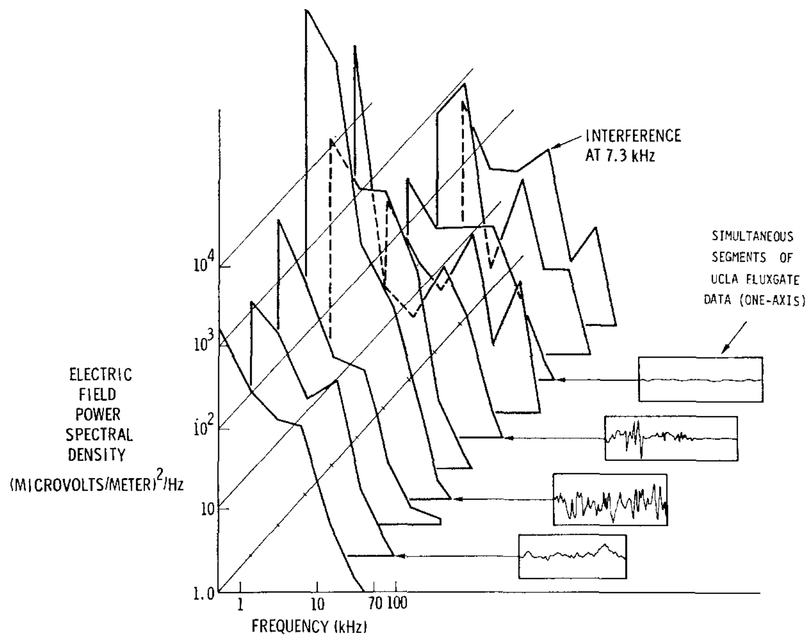

Fig. 19. Time sequence of approximate electric field power spectra derived from passband channel outputs from the OGO 5 electric field detector for the outbound shock crossing on March 12, 1968. Shown in the small insets are simultaneous measurements of one component of the magnetic field detected by the OGO 5 fluxgate magnetometer. Spectra near the top of the figure are in the free-streaming solar wind. The shock front is located here somewhere between the 5th and 6th spectrum from the top.

frequency component, which Fredricks *et al.* (1968) proposed to be near the local electron plasma frequency. At the shock front (fifth to sixth spectrum down from the top in Figure 19), the high frequency amplitude is significantly reduced, and the low frequency (0.56–3.0 kHz) components are enhanced approximately two orders of magnitude above their upstream amplitudes. The low frequency components are observed to relax within the magnetosheath to amplitudes that are above the upstream levels.

It was thus concluded that the high frequencies were quenched near the shock, while the lower frequency waves were greatly enhanced at the shock with downstream dissipation. It should be noted that no significant magnetic noise was observed at these frequencies during the entire sequence of Figure 19, thus indicating the electrostatic character of these waves. In addition, Fredricks *et al.* (1968) found that, in general, the electric field turbulence correlated with gradients in the dc magnetic field rather than the amplitude of the field itself. The above, together with the consistent absence of correlated magnetic fluctuations of 0.56 kHz, led to the tentative identification of the electric field turbulence production via a current driven instability, perhaps of the ion acoustic wave, with broadband spectra being explained by Doppler shifting.

C. UPSTREAM PHENOMENA

Numerous investigators, from theoretical as well as observational considerations, have speculated on the existence of wave and particle phenomena associated with the shock interaction yet situated in the interplanetary solar wind in the upstream region. Smith *et al.* (1967), e.g., report the frequent OGO 1 search coil observations of sporadic noise bursts in the 10–100 Hz range far upstream from the shock front. These waves were identified as being generated at the shock front and propagating upstream parallel to the interplanetary field lines in the whistler mode. The observed high frequency cutoff was consistent with the expected local electron gyrofrequency, and the low frequency cutoff with the frequency at which the whistler wave velocity could be expected to just exceed the solar wind convective velocity. Also on OGO 1, Heppner *et al.* (1967) reported the observation of coherent magnetic field oscillations in the frequency range 0.5–1.5 Hz and higher frequency noise, probably greater than 7 Hz (beyond the Nyquist frequency limit for the fluxgate magnetometer), which reached maximum amplitude immediately adjacent to the shock front. Both the coherent oscillations as well as the higher frequency noise were observed on occasion to extend into the interplanetary medium upstream from the shock, where their amplitudes diminished with increasing distance. As previously noted in Section 3.B, Figure 18 illustrates an example (Heppner *et al.*, 1967) of rapid, unresolved fluctuations at the shock and on the interplanetary side of the shock, with the coherent waves near 1 Hz at the shock and on the magnetosheath side of the shock. Siscoe *et al.* (1967) reported results similar to those of OGO 1 for the single Mariner 4 traversal. Here, however, the situation was somewhat clouded by the possibility of multiple shock crossing.

Dissipation of the upstream magnetic wave energy may be responsible, at least in part, for the upstream solar wind ion heating in the immediate vicinity of the shock front observed during the unusually quiet outbound shock traversal of Pioneer 6 (Wolfe and McKibbin, 1968). Figure 20 shows 12 solar wind ion spectra (peak flux per E/Q window) bracketing the shock transition that was observed by Pioneer 6 at 1711-42 UT. Inspection shows that steady interplanetary spectra were not observed until 1715-06 UT, some $3\frac{1}{2}$ min after the shock traversal. Consideration of the subsequent interplanetary spectra and the relative spacecraft velocity led to the conclusion that minor solar wind ion heating was taking place some 450–600 km upstream from the shock. This upstream ion heating could also result, in part, from wave-particle interactions associated with electric field oscillations. Figure 19 shows the presence of significantly high frequency electric field wave energy ahead of the shock as indicated in the top four spectra (Fredricks *et al.*, 1968).

Fairfield (1968a), using Explorer 34 fluxgate magnetometer results, reported the frequent observation of transverse waves with 20–100 sec periods in the interplanetary medium between the shock front and the spacecraft apogee at 34 R_E. It was concluded that the waves that were observed were associated with the shock front itself, as evidenced by the fact that they were usually only observed when the projection of the interplanetary field at the position of the spacecraft intersected the shock front. The

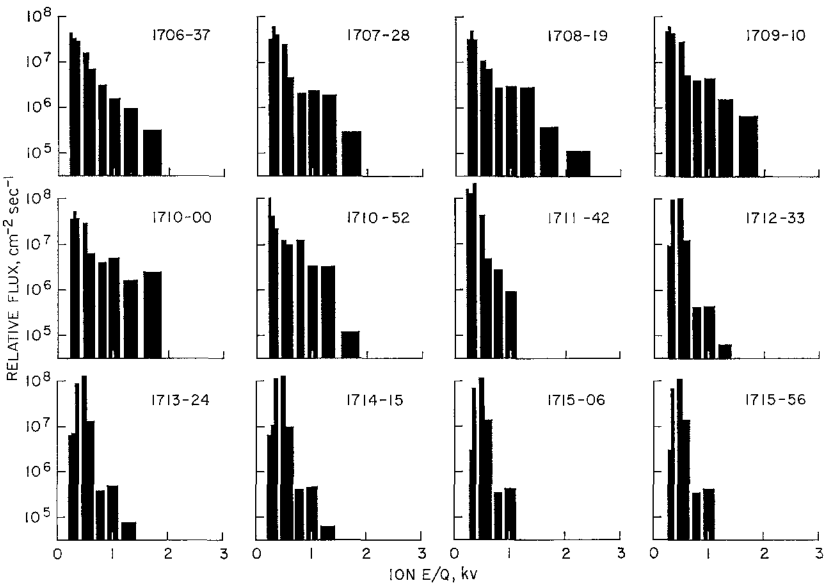

Fig. 20. Twelve consecutive Pioneer 6 electrostatic analyzer plasma probe peak flux ion spectra, which bracket the shock transition associated with the ion density pulse observed in the spectrum taken at 1711–42 UT.

waves were observed to have typical amplitudes of several gamma in the 4–8 γ ambient interplanetary fields and, in addition, were observed to diminish by only about a factor of 2 when the spacecraft was 15 R_E upstream from the shock. Two alternatives were suggested for the upstream presence of these waves. The first concerned wave generation at the shock front with upstream propagation parallel to the interplanetary field via the whistler mode. The large Doppler shifts required to bring the expected whistler mode waves into the frequency range observed by Explorer 34, however, seemed much greater than would normally be expected. A more attractive possibility was the local generation of Alfvén waves through the mechanism of a two stream instability between solar wind ions and ions moving back upstream from the earth's shock front along the interplanetary field lines. The above seems consistent with the observations of upstream flow of high energy solar wind particles (Asbridge *et al.*, 1968; Frank and Shope, 1968) presumably accelerated at the shock front with propagation upstream along the interplanetary field lines with low pitch angles.

Greenstadt *et al.* (1968), comparing simultaneous Vela 3 magnetic field and plasma results, reported the presence of 20–60 sec period magnetic oscillations in the solar wind outside the shock. The magnetic oscillations were more or less regular in nature with generally less than 5γ amplitudes, and, in addition, the direction of flow of the solar wind ion flux peaks were found to oscillate in close correlation with the magnetic waves. It is not certain that these observations are associated with those reported later by Fairfield (1968), since the Vela 3 upstream oscillations were most persistently observed only when the spacecraft was in the immediate vicinity of the shock front.

With regard to shock associated upstream particle phenomena, it is not clear whether the deviations in interplanetary particle distributions result from local wave energy dissipation or whether charged particles, accelerated at the shock, propagate upstream along interplanetary magnetic field lines. Jokipii (1968) and Anderson (1968), e.g., report the observation of energetic electrons of an impulsive nature present in the interplanetary medium beyond the shock front. The evidence, however, is unfortunately not adequate as to which of the above two mechanisms is predominantly responsible for these upstream electrons. Although the present picture of upstream phenomena seems nebulous at best, it is clear that consideration of the earth's bow shock, in the classical sense of a surface upstream from which information regarding the presence of the earth cannot be transmitted, is not strictly applicable. This should not be surprising, however, since we are dealing here with a magneto-ionic medium and would expect from theoretical considerations alone that waves such as those in the whistler mode can propagate with group velocities that are significantly greater than the solar wind velocity. In any event, from an observational point of view, the unique identification of the particular waves and wave-particle interactions remains somewhat obscured by interplanetary fluctuations, unknown Doppler shifting, and unsteady shock front behavior.

D. SHOCK STRUCTURE

The phenomena elucidated in the previous sections are all apparently associated with the shock interaction, but they do not, however, shed light on the nature of the shock transition itself. On the contrary, phenomena such as the spatially transient behavior of the shock front tend to mask the observation of its structure when viewed on a single satellite pass. Some ground has been gained in the past few years by observation of the mean or persistent appearance of the shock transition resulting from the accumulation of data from many satellite passes. In addition, there have been a few fortuitous observations of shock traversals under extremely quiet conditions.

Using OGO 1 fluxgate magnetometer data, Heppner *et al.* (1967) examined numerous OGO 1 shock crossings and concluded that of all crossings reported, probably one-half or more had a similar average total field profile. This examination led to the model profile, reproduced in Figure 21, of the average magnetic field apparent during the 'most typical' crossings. The model profile is characterized by three times or time intervals. The time t_0, at which the average field level first deviates from the interplanetary value, is identifiable within 2 sec. The time interval $|t_0 - t_1|$, over which the

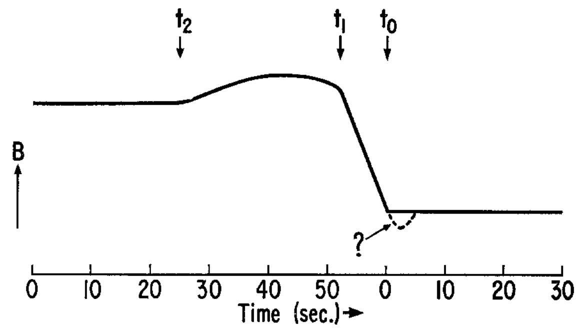

Fig. 21. Model profile of the average magnetic field apparent during the 'most typical' shock crossings, as determined by the OGO 1 fluxgate magnetometer. The model profile is characterized by three times or time intervals. For details, see text.

field intensity rapidly changes its level, was usually a well-defined characteristic of the shock. The time interval $|t_0 - t_2|$, between the break at t_0 and the time t_2 when the field 'overshoots' and relaxes back to a new average level in the magnetosheath, seemed to be the most poorly defined characteristic. This was due both to the difficulty in accurately determining the time t_2 and to the fact that the overshoot or bump in the field profile did not always occur on the magnetosheath side of the sharp change in field level. The dashed line and question mark in Figure 21 indicate that a slight decrease in field intensity was sometimes observed on the interplanetary side of the sharp field change. This slight decrease was not considered a typical characteristic, but it was observed often enough that its existence could not be ignored in the model presented by Heppner *et al.* (1967). Of necessity the profile characteristics shown in Figure 21 are given in terms of time rather than distance. Employing a statistical approach with regard to the motional behavior of the shock front with respect to the spacecraft, various characteristic thicknesses were estimated. The sharp field change onset time, $t_0 \pm 2$ sec, correspond to less than 20 km, whereas the rise time, $|t_0 - t_1|$, corresponded to approximately 50–100 km. The time interval, $|t_0 - t_2|$, corresponding to the interval required for the field to change from its initial interplanetary level to the final magnetosheath level, was about 250 km.

Superimposing now the magnetic wave observations discussed in Sections 3.B and 3.C on the shock transition profile of Figure 21 gives the bow shock appearance classification depicted in Figure 22 (Heppner *et al.*, 1967). Although the shock appearance seemed to vary from one case to the next, it was possible to classify a large variety of observations into the relatively small number of types shown in this figure. The classification adopted by Heppner *et al.* (1967) was based on whether or not wave phenomena were observed at the shock, and if so, what types of waves were the most dominant feature. In Figure 22 three principal types are presented. The first, marked (a), depicts a shock without the presence of waves and is similar to the mean profile discussed in Figure 21. The second classifies the appearance of the shock transition with coherent waves with frequencies near 1 Hz, with the waves being mainly associated with the sharp rise as in (b), or packets of these coherent oscillations spreading out on both sides of the shock as in (b′). The third type shown in Figure 22 illustrates the shock profile with the superposition of high frequency fluctuations ($f > 3$ Hz)

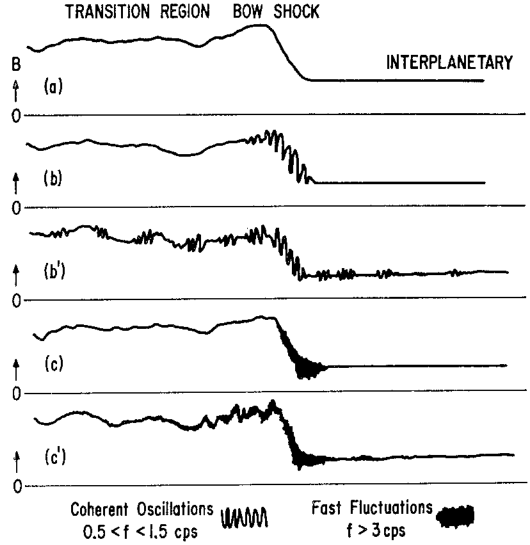

Fig. 22. Superposition of various magnetic wave observations on the shock transition profile of Figure 21.

existing at the sharp rise of the dc field as in (c) or extending on either side of the shock as in (c′). It is clear that these higher frequency fluctuations are those observed by the OGO 1 search coil (Holzer *et al.*, 1966; Smith *et al.*, 1967) in the 3–300 Hz range. Various combinations of shock appearance are also possible, such as high frequency noise dominant upstream from the shock and lower frequency oscillations dominant on the magnetosheath side (see Figure 18).

Plasma structure in the shock transition is not as clearly understood as the magnetic structure. This is due primarily to the relatively long time interval required to obtain a complete set of plasma parameters. On spinning spacecraft, e.g., plasma detectors view the gas flow only once per vehicle revolution; thus to completely scan the incident distribution function and thereby obtain a complete set of plasma parameters normally requires several tens of seconds. The plasma observations are thus much more susceptible to the detrimental effects of shock motion. Nonetheless, the existence of unique plasma structure within the shock transition has been successfully demonstrated. Comparison of Vela 3 magnetic field and plasma data (Greenstadt *et al.*, 1968) revealed non-magnetosheath, non-solar wind ion spectra of irregular shape with occasional large flux peaks. These plasma observations were found to correspond to the appearance of large amplitude (10–25 γ) irregular magnetic oscillations of 4–30 sec periods in the vicinity of the shock front. The intermediate form ion spectra and large flux peaks were identified with localized transient accelerations and decelerations of the bulk of the solar wind protons presumably associated with the shock structure. Although the resulting spectra were undoubtedly highly time aliased, the existence of unique plasma structure within the shock transition seemed well founded. Results quite similar to the above were also reported by Binsack (1967) from IMP 2 Faraday cup observations.

Perhaps the greatest insight into the plasma structure within the shock transition was provided by the single magnetosheath traversal of Pioneer 6, which occurred under unusually quiet conditions. Pioneer 6, launched December 16, 1965, traversed

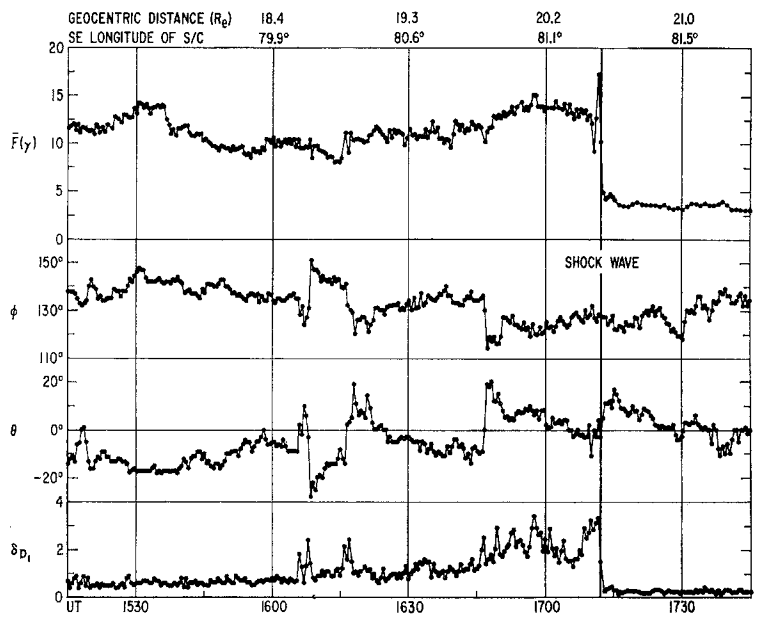

Fig. 23. Magnetic field observations during the Pioneer 6 shock traversal. The values shown are 30-sec averages of the field amplitude, $\bar{F}$, and the angular orientation of the field vector, θ and ϕ in spacecraft coordinates. The bottom curve is the rms deviation (in gamma) over the 30-sec period for one component of the field.

the shock near local sunset a few degrees below the plane of the ecliptic (see Figure 1). At this time, interplanetary conditions, as determined by subsequent flight data, were extremely quiet with $K_p = 0$ for many hours prior to, during, and subsequent to the entire magnetosheath traversal. The Pioneer 6 Ames Research Center plasma probe results (which had three component plasma vector distribution resolution capability) were compared across the magnetosheath and shock traversal by Wolfe and McKibbin (1968), with the simultaneous magnetic field data reported by Ness *et al.* (1966).

Figure 23 shows the magnetic signature across the shock transition (Ness *et al.*, 1966) in terms of the field amplitude, $\bar{F}$, and the angular orientation of the field vector, ϕ and θ (spacecraft coordinates). The values shown are 30-sec averages, and the bottom curve is the rms deviation (in gamma) over the 30-sec period for one component of the field. As the shock front was approached, the magnetic field first decreased from 13 to approximately 9 γ, then rose sharply to approximately 18 γ, with a final sharp decrease to an interplanetary value of about 3 γ. The pulse-shaped profile is seen to be quite similar to that observed by Heppner *et al.* (1967), with the exception of a tendency for downstream ringing in the field amplitude.

The detailed comparison of the Pioneer 6 magnetic field and plasma data on December 16, 1965, is shown in Figure 24 (Wolfe and McKibbin, 1968), plotted as a function of time in UT and geocentric distance in earth radii. The bottom curve is the average vector magnitude of the magnetic field in gammas, as reported by Ness *et al.* (1966), with the outer portion identical to that shown in detail in Figure 23. The sec-

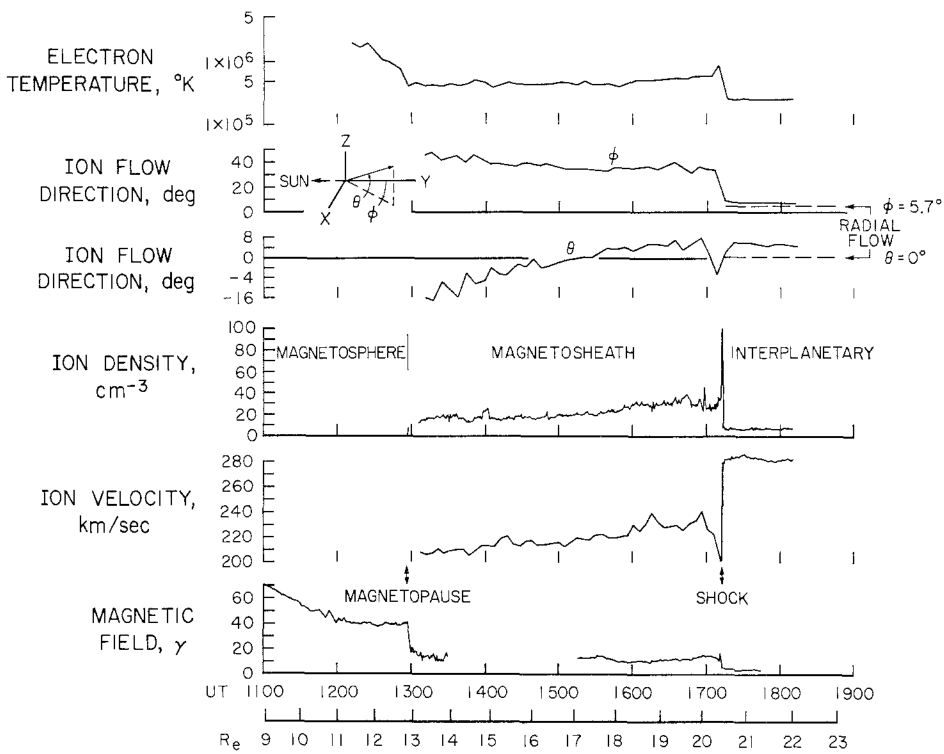

Fig. 24. A detailed comparison of the Pioneer 6 magnetic field and electrostatic analyzer plasma data during the magnetosheath traversal of December 16, 1965. The bottom curve is the average vector magnitude of the magnetic field in gamma, with the outer portion identical to that shown in detail in Figure 23. The second curve from the bottom shows the spectral peak ion velocity in km/sec, and the third curve from the bottom gives the density in ions per cm^3. The fourth and fifth curves from the bottom show the solar wind direction latitude and longitude, respectively, as defined by the coordinate system shown in the inset, and the top curve gives the electron temperature. The magnetopause and shock boundaries are located as indicated.

ond curve from the bottom in Figure 24 shows the spectral peak ion velocity in km/sec. Due to the somewhat variable nature of the ion spectra within the magnetosheath, the velocities shown were the averages of 8 values obtained over an interval of approximately 400 sec. The steady-state conditions observed in the interplanetary medium allowed the velocity values obtained from each interplanetary spectrum (approximately 50 sec intervals) to be plotted. The maximum difference between the velocity shown and the true plasma convective velocity was estimated to be less than approximately 10%. Within the magnetosheath, however, this difference was estimated to be less than about 20%. The ion density in ions per cm^3 is plotted in the third curve from the bottom in this figure. The density measurements required a knowledge of the complete energy-angular distribution of the plasma ion flow and could be uniquely obtained only from the full E/Q angular scan of the plasma probe (called the full scan mode, which required approximately 400 sec to complete). Smaller time interval values of the density were obtained, however, by plotting the spectral area of each peak flux E/Q spectrum acquired approximately every 50 sec (called the maximum flux mode), normalized to the full scan mode density values obtained approximately every 400 sec. This, in effect, assumed that there were no significant changes in the angular distribution of the plasma ions over the interval required to collect full scan mode data. The justification of this assumption was verified by the lack of significant discontinuities in the resulting density values between successive full scan mode measurements. The maximum cumulative error in the density values shown was estimated to be less than 50%. This error included the lack of knowledge of the relative abundances of various ion charge species within the magnetosheath.

The fourth and fifth curves from the bottom on Figure 24 are the spacecraft centered solar oriented ecliptic latitude and longitude of the ion vector velocity flow direction. These angles are defined as shown, where the ecliptic is the XY plane, Z is in the direction of the North ecliptic pole, and the sun is along the $-Y$ axis. The estimated maximum cumulative error for the flow directions in the magnetosheath was $\pm 3°$ in θ and $\pm 5°$ in ϕ. The error in θ and ϕ in the interplanetary medium was estimated to be approximately 50% less than that given above for the magnetosheath. The lower error in the interplanetary medium was due primarily to the Maxwellian character, much lower temperature, and steady behavior of the plasma ion velocity distribution that was observed there as compared to that in the magnetosheath. For reference purposes the expected angular components for solar radial flow are also shown. Solar radial flow in the interplanetary medium would correspond to $\theta = 0°$, and the expected aberration angle for a 280 km/sec solar wind speed would correspond to $\phi = 5.7°$ in the moving frame of reference of the spacecraft. The top curve in Figure 24 is a plot of the electron temperature in K. A preliminary estimate of the error involved in the electron measurements indicated an absolute accuracy in the electron temperature of approximately a factor of 2. The principal difficulty encountered in the electron observations was the presence of what appeared to be a substantial vehicle surface potential with respect to the plasma caused by the solar uv flux incident on the highly insulating surfaces of the spacecraft. The resulting photoelectron flux and the apparent effective plasma probe aperture were taken into consideration in only a preliminary manner in the calculation of the electron temperatures shown here.

Coincident with the magnetic field pulse was a spike in the ion number density to a value of approximately 110 ions per cm^3. The density spike occurred at 1711-42 ± 25 sec UT, at which time the spacecraft was located at a geocentric distance of 20.44 R_E. At the time of this density spike, the spectral peak E/Q dropped to the lowest window of the plasma probe. The flow velocity in the spike could have been no larger than approximately 200 km/sec. The velocity then jumped to an interplanetary value of about 280 km/sec, and the ion density dropped to approximately 11 per cm^3. Figure 24 also shows a large change in the ion flow direction and a spike in the electron temperature associated with the magnetic field and ion density pulses. The interplanetary flow direction seemed to be upward by approximately 5° with respect to the ecliptic at a longitude of $+6°$. The interplanetary electron temperature was approximately 2×10^5 K. Relatively steady conditions in interplanetary space were then observed to prevail in all parameters subsequent to the shock passage.

From Figure 20 it is observed that the density pulse at 1711-42 UT is due primarily to the large flux increase in the four lowest energy channels. In addition, the spectrum associated with the density pulse indicates a significant absence of a high energy tail such as that observed in the previous spectrum at 1710-52 UT. It should also be noted that steady interplanetary spectra were not observed until 1715-06 UT, some $3\frac{1}{2}$ min upstream from this density pulse, as discussed previously in Section 3.C. With the exception of minor differences, the downstream spectral characteristics were fairly constant and were typical of those obtained prior to 1700-00 UT.

Assuming that the shock structure is stationary in a solar ecliptic coordinate system and considering the spacecraft velocity and the obliquity of the traversal, the magnetic pulse shape and thickness agree quite well with those proposed by Heppner *et al.* (1967). Based on the Pioneer 6 magnetic field data (Ness *et al.*, 1966), the rise time of the shock pulse upstream and total width corresponded to a distance of 130 ± 60 km and 190 ± 60 km, respectively. Since the corresponding density pulse was observed in only one 50-sec scan period of the plasma probe, the pulse rise must have been less than 105 km, and the overall width must have been less than twice this, or 210 km. The corresponding thicknesses for the shock profile reported by Heppner *et al.* (1967) were 50–100 km for the pulse rise and approximately 250 km for the pulse width. The general agreement of the Pioneer 6 and OGO 1 observations lends support to the argument that the shock observed by Pioneer 6 was stationary.

The shock transit of Pioneer 6 revealed that, with the possible exception of the ion temperature (the interplanetary solar wind ion temperature was approximately 2 to 3×10^4 K, and the magnetosheath temperature was on the order of 5.0 to 7.5×10^5 K, with a 17% energy density non-thermal high energy tail that remained approximately constant across the entire magnetosheath), all plasma and field parameters experienced an overshoot or partial reversal as the solar wind passed through the shock transition. In addition, the magnetic field (Ness *et al.*, 1966) continued to ring downstream from

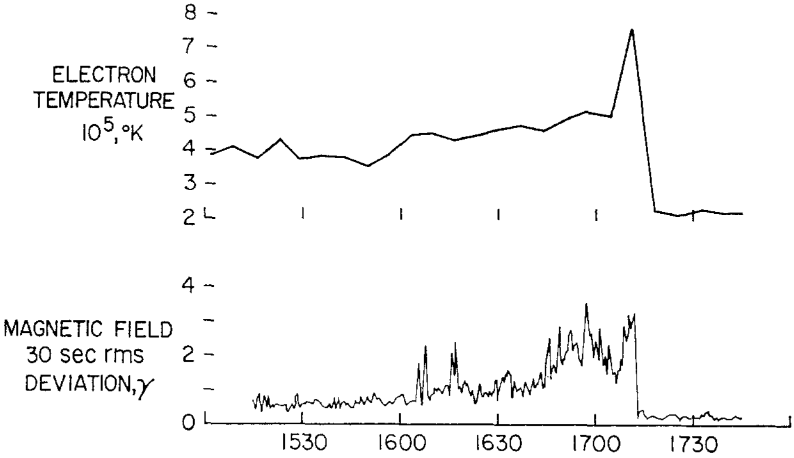

Fig. 25. A detailed comparison of the Pioneer 6 electron temperature and variations in the magnetic field in the vicinity of the shock front plotted as a function of UT. The lower curve is the 30-sec rms deviation of one component of the magnetic field, and the upper curve is the electron temperature in K.

the initial shock pulse similar to the October 7, 1962, interplanetary shock observed by Mariner 2 (Sonett *et al.*, 1964).

The true shock thickness observed by Pioneer 6 was difficult to determine, not only from the point of view of instrument time resolution but also from the indication that the changes in the various plasma and field parameters could have been occurring over different scale lengths and at slightly different locations across the entire shock transition. Within the instrument time resolution limitations, however, the data indicated that the peak in the magnetic field pulse and the ion density pulse were coincident. The density pulse, however, could have been significantly narrower. Inspection of the ion spectra taken across the shock transition (see Figure 20) further shows that although minor ion heating was taking place from 450 to 600 km upstream from the density pulse, the significant ion heating occurred between 25 and 150 km downstream from the pulse. The data further indicated that within the cycle period of the plasma probe (corresponding to approximately ± 150 km) the position of the pulse was coincident with the electron temperature increase and the destruction of the ion thermal anisotropy observed upstream. The electron shock heating and downstream cooling are perhaps more dramatically seen in Figure 25, which shows the detailed comparison of the electron temperature variations and the variance of the magnetic field in the vicinity of the shock front. The lower curve in this figure is the 30 sec rms deviation of one component of the magnetic field as reported by Ness *et al.* (1966), and the upper curve is the electron temperature. The electrons are observed to be heated from an interplanetary temperature of 2×10^5 K to over 7×10^5 K at the shock (approximately 1711 UT). The electron temperature is then seen to immediately relax to 5×10^5 K followed by a further gradual decrease to a temperature of 3.5 to 4.0×10^5 K. Comparison with the magnetic field variance indicates a similarity in the time profile.

The characteristics of the plasma heating (both ions and electrons) in the vicinity of the shock as well as upstream and downstream from the shock are certainly related to the magnetic fluctuations (Smith *et al.*, 1967; Heppner *et al.*, 1967) observed in this region of space and the electric field oscillations (Fredricks *et al.*, 1968) observed in the vicinity of the shock layer. In addition, the differences in the location and spatial extent of the plasma ion and electron heating and the correspondingly different spatial dominance of the various magnetic and electric field oscillations further indicate that the wave dissipation affects the various plasma species differently. The precise mechanisms and correspondence, however, for the various wave-particle interactions are not as yet certain. In any event, a somewhat clearer picture of the structure of the shock transition is now beginning to emerge. The results discussed thus far indicate that the boundary between the magnetosheath and the free streaming solar wind is suggestive of a standing wave which has steepened into a true shock transition while retaining partial reversibility. The identification of this wave is not yet clear but the indications are that it is of the magnetosonic mode. Higher frequency magnetic and electric field oscillations are generated in the vicinity of the shock transition and subsequently propagate and dissipate upstream as well as downstream from the shock. These waves might be triggered by plasma instabilities with the upstream waves resulting as a consequence of their group velocities exceeding the local solar wind convective velocity. Under certain favorable conditions, the back streaming of charged particles accelerated or reflected at the shock transition should also be considered. It seems likely that the shock structure can undergo great variability over the shock face due to differing external field orientations and, in addition, can change drastically in overall appearance due to changing interplanetary conditions.

E. THE MAGNETOSHEATH FLOW FIELD

Subsequent to the launch of the IMP 1 satellite, some confusion appeared in the literature with regard to the plasma flow in the magnetosheath. Bridge *et al.* (1965a,b), using the initial results from the IMP 1 Faraday cup plasma probe, reported the observation of an essentially omnidirectional plasma ion flux within the magnetosheath. In contrast, Wolfe *et al.* (1966a), although conceding broad angular distributions, reported IMP 1 electrostatic analyzer results consistent with flow around the geomagnetic cavity boundary. Measurements of magnetosheath plasma since that time (see, e.g., Wolfe *et al.*, 1966b; Coon, 1966; Argo *et al.*, 1967; Gosling *et al.*, 1967; Binsack, 1968; Wolfe and McKibbin, 1968; and others) have all been consistent with solar wind flow deflection at the shock front with magnetosheath flow around the magnetopause away from the subsolar point. Recent reevaluation of the IMP 1 Faraday cup data by Olbert (1968) has shown that the apparent omnidirectional magnetosheath ion fluxes actually resulted from the cup response to the hot magnetosheath electrons. Thus the gross features of the magnetosheath plasma flow seem well established.

A more detailed illustration of the ordered magnetosheath flow pattern is evident in the Pioneer 6 traversal data shown in Figure 24. Within the magnetosheath near the magnetopause the ion density is approximately 14–15 ions per cm^3 with a peak velocity of 205–210 km/sec. The ion velocity vector shows a longitude of about 45° which should be expected for tangential flow along the magnetopause. The latitude, however, indicates a downward flow with respect to the ecliptic of almost 18°. Figure 24 indicates that as the magnetosheath was traversed by the Pioneer 6 spacecraft, a gradual increase was evident in the ion density, ion velocity, and electron temperature associated with a gradual change in flow direction. The parameters near the outer boundary of the magnetosheath are $B \simeq 13\,\gamma$, $u = 225$–240 km/sec, $n = 25$–35 cm^{-3}, $\theta = 3$–$6°$, $\phi = 30$–$35°$, and $T_e \simeq 5 \times 10^5$ K. It was suggested that the downward flow near the magnetopause and the gradual change to slightly upward flow near the shock was probably due to a gradual increase in the controlling influence of the magnetosheath magnetic field configuration as the flow proceeded inward across the magnetosheath.

It is cautioned that the gradual and well-defined changes in the plasma and field parameters across the magnetosheath for the Pioneer 6 traversal may have been so clear only because of the extremely quiet conditions that prevailed at the time. During somewhat more disturbed periods, the wave phenomena discussed in Section 3.B are expected to play a significant role in the magnetosheath flow field. A case in point is evident in Figure 26. Four magnetosheath spectra taken over a 48-hour period of moderate geomagnetic activity ($K_p = 3$–5) are shown at widely scattered locations (Wolfe *et al.*, 1966b). The corresponding solar ecliptic longitudes and geocentric

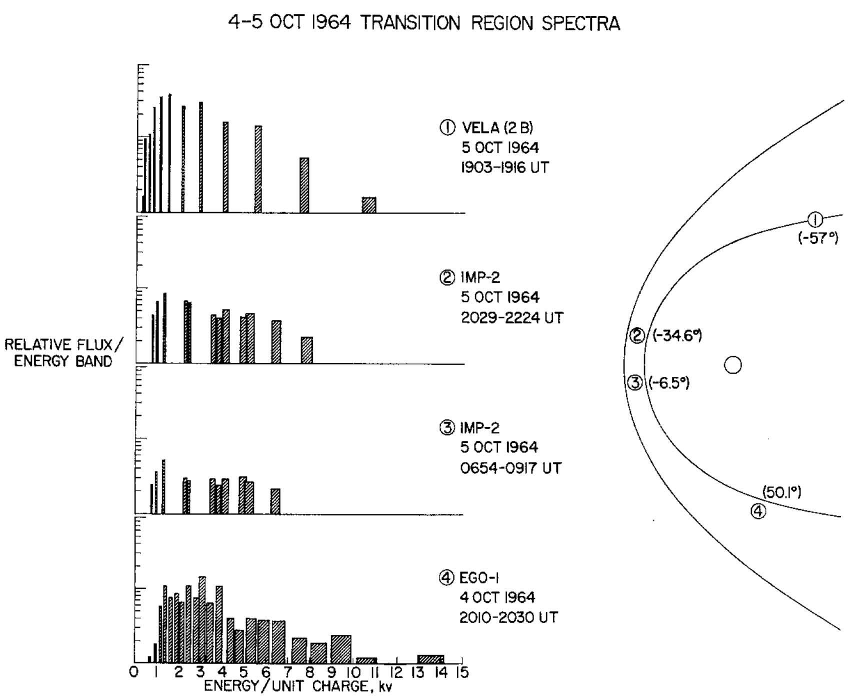

Fig. 26. Four magnetosheath spectra taken over a 2-day period at widely scattered locations, indicating the general homogeneity of the magnetosheath. The corresponding solar ecliptic longitude of the four spectra are superimposed on the approximate mean magnetopause and shock positions, and the solar ecliptic latitude at each point is shown.

radial distances of the locations of the four spectra are shown superimposed on the approximate mean magnetopause and shock positions with the solar ecliptic latitudes indicated at each point. The strong similarity of these four widely separated spectra together with their highly non-thermal character clearly indicates the general homogeneity of the moderately disturbed magnetosheath. This case thus illustrates the difficulty in separating the spatial and temporal features of the flow field even when the magnetosheath is only modestly perturbed.

A more long-term observation of the plasma flow in the magnetosheath near the shock was provided in the Explorer 34 plasma detector results reported by Burlaga and Ogilvie (1968). Their results are shown in Figure 27. The curves represent the

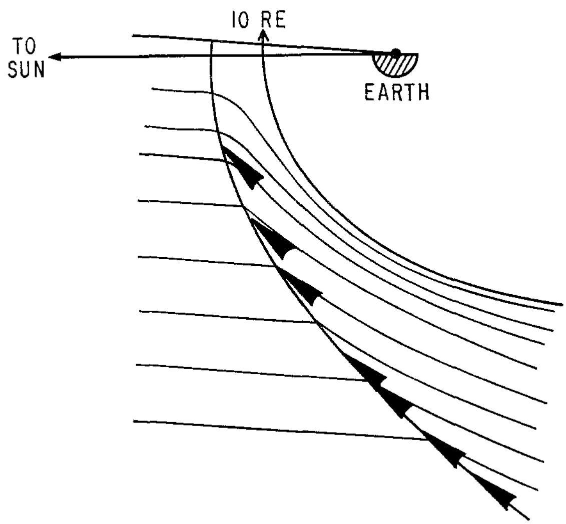

Fig. 27. Plasma flow directions in the magnetosheath near the shock as observed by the Explorer 34 plasma detector. The solid curves represent the aberrated interplanetary solar wind flow and the resultant theoretical magnetosheath stream lines and magnetosheath boundaries. The observed plasma flow directions were into the solid angular sectors shown along the magnetosheath side of the shock front.

aberrated interplanetary solar wind flow and the resultant theoretical magnetosheath streamlines and magnetosheath boundaries as determined by Spreiter *et al.* (1966). The observed plasma flow directions were into the solid angular sectors shown along the magnetosheath side of the shock front. Note that these angular sectors were moved slightly in each case so that they fell on the theoretical shock location. The data were selected, however, such that the shock locations actually observed by Explorer 34 were in most cases within 1 R_E of the theoretical shock position. As expected, the flow was observed to be highly directional and generally in good agreement with flow around the geomagnetic cavity.

Fairfield (1967), comparing interplanetary field discontinuities observed by the IMP 1 and IMP 2 satellites, found a one-to-one correspondence of discontinuities at the two satellites persisted, even when one of the satellites was located within the magnetosheath. It was thus demonstrated that the interplanetary field lines are convected through the shock by the solar wind into the magnetosheath. Detailed analyses of the directional distributions of magnetosheath fields and their relation to simultaneously measured interplanetary fields revealed that as the magnetosheath fields are convected around the magnetopause by the solar wind they undergo distortion

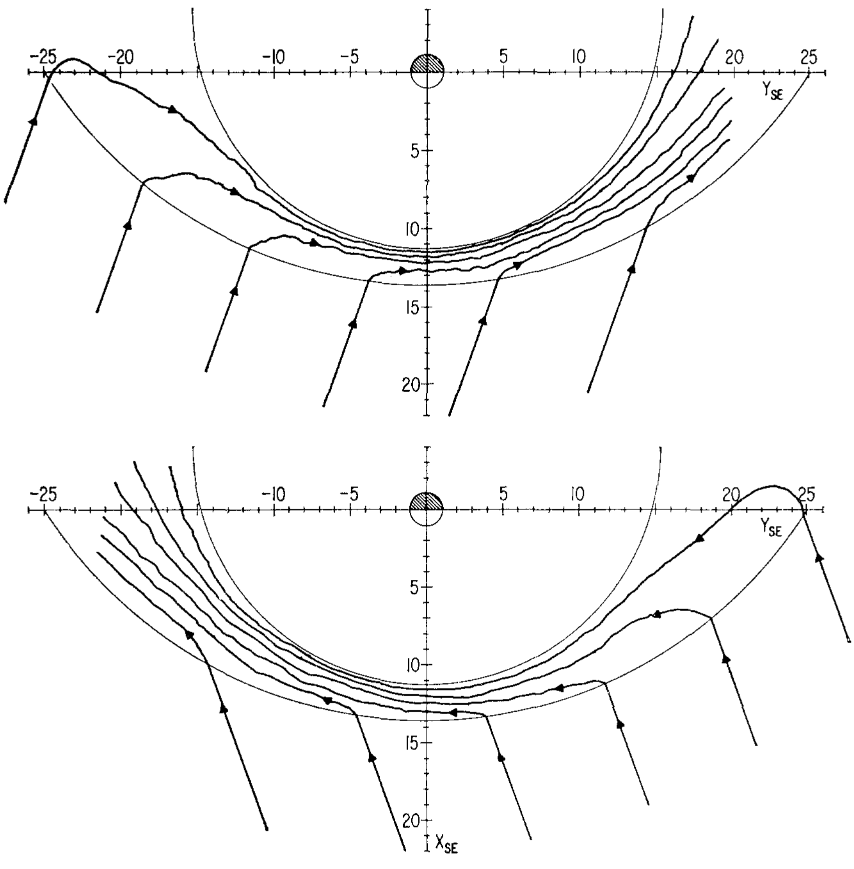

Fig. 28. A schematic representation of magnetic fields in the vicinity of the earth as observed by the IMP 2 magnetometer. The field lines drawn are illustrative of the behavior of the data and show how the magnetic field lines cross the shock, with their direction in the magnetosheath being determined by whether the interplanetary field has a component pointing in the general direction of the dawn or dusk meridian.

from their original interplanetary directions until they are aligned tangent to the magnetopause.

A schematic representation of magnetic fields in the vicinity of the earth is shown in Figure 28 (Fairfield, 1967). The figure is illustrative of the behavior of the data and shows how the magnetic field lines cross the shock with their direction in the magnetosheath being determined by whether the interplanetary field has a component pointing in the general direction of the dawn or dusk meridian. Comparison of the upper and lower portions of Figure 28 indicates that small changes in the interplanetary field azimuth (40° in the case shown here) can completely alter the appearance of the magnetosheath fields. It should be noted that the apparent dawn-dusk asymmetry in field magnitude is a result of the schematic representation in the plane of the ecliptic and not necessarily a real effect. It is resonable to assume that the magnetosheath field lines slip around the polar regions of the geomagnetic cavity and ultimately return to the interplanetary medium after convection through the distant magnetosheath.

We are thus left with the overall picture of the magnetosheath flow field consistent with the flow of the post shock plasma around the geomagnetic cavity carrying with it the embedded and distorted interplanetary magnetic field. The above must, of necessity, be valid even during disturbed periods, although at such times the magnetosheath is evidently copiously filled with a variety of instabilities leading to waves and wave-particle interactions that grossly distort the quiet time flow field.

F. COMPARISONS WITH THEORY

Since the early suggestion by Chapman and Ferraro (1931) that the earth's magnetic field could be confined by corpuscular radiation of solar origin, numerous investigators have refined the theoretical picture of the solar wind-geomagnetic field interaction region. These theoretical studies mainly involved the extension of the concept of the Chapman-Ferraro sheath and the continuum fluid theory (see, e.g., Beard, 1960; Spreiter and Briggs, 1962; Axford, 1962; Kellogg, 1962; Spreiter and Jones, 1963; Mead and Beard, 1964; and others). Obayashi (1964) compared magnetic field and plasma data reported since the flight of Pioneer 1 with the fluid model and was able to demonstrate reasonable agreement for the shock and magnetopause locations for calculations based on a solar wind density of 5 per cm^3, convective speed of 400–600 km/sec, magnetic field level of 10 γ, and a gas dynamic Mach number of 3–4. Dryer and Faye-Petersen (1966) extended the fluid model of Spreiter and Jones (1963) for an assumed teardrop shape for the geomagnetic cavity. They were able to obtain a qualitative fit to the magnetic field changes observed across the magnetopause on IMP 1 (Ness *et al.*, 1964). The fit was less than satisfactory, however, perhaps due to an unrealistic boundary shape, unknown magnetosheath field orientation, and less appropriate values for the ratio of specific heats and magnetoacoustic Mach number.

The IMP 1 results (Ness *et al.*, 1964; Bridge *et al.*, 1965a; Wolfe *et al.*, 1966a) gave magnetopause and shock locations that had excellent qualitative fit to these boundaries based on the Spreiter and Jones (1963) model. Using shock and magnetopause position information up through the Pioneer 6 launch, Dryer and Heckman (1967) were also able to demonstrate reasonable agreement with continuum fluid theory.

With regard to the theoretical and observed jump conditions across the shock, Argo *et al.* (1967), using Vela 3 satellite data from 13 magnetosheath traversals, showed that the ratios of the velocities and densities on the two sides of the shock front were in close agreement with the theoretical predictions provided by the gas dynamic calculations of Spreiter *et al.* (1966). The ratios of the temperatures, however, were approximately twice the calculated values. Spreiter *et al.* (1968) were able to show that most of this discrepancy could be attributed to the arbitrary selection by Argo *et al.* (1967) of the free stream Mach number. Calculations based on the actual Mach number determined from the measured solar wind speed and temperature by the Vela 3 spacecraft resulted in substantially better agreement between the measured and computed temperature ratios across the shock. Using a reduced set of magnetohydrodynamic jump conditions, Ogilvie *et al.* (1968) were able to obtain a fairly good fit between the computed and measured solar wind velocity ratios from the Explorer 34 plasma and magnetic field observations of only 30 out of 100 shock crossings.

The extremely quiet conditions that prevailed during the single shock crossing by Pioneer 6 provided the opportunity to consider the measured plasma and field quantities with regard to the MHD Rankine-Hugoniot relations for an over-determined case (Mihalov *et al.*, 1969). This was possible since the vector magnetic field variations (Ness *et al.*, 1966) and vector plasma variations were both available for the shock transit. Reasonable agreement was obtained between the measured and computed downstream ion density, thermal pressure, and speed only when a 1 γ change was made to one component of the reported downstream magnetic field. The computed upstream thermal pressure, however, was only 10% of the experimentally determined value. Disagreements were probably due to the use of the magnetic coplanarity theorem in establishing the coordinate system for the shock calculations. When plasma velocity coplanarity was used to establish the shock normal, excellent agreement with the continuum fluid model (Spreiter *et al.*, 1966) was obtained. The discrepancy between magnetic and velocity coplanarity was perhaps due to the extreme sensitivity of magnetic coplanarity to small errors. For the Pioneer 6 traversal, the angle between the upstream and downstream field orientation was only about 6°, and the determination of the plane defined by the cross product of these two vectors was therefore susceptible to error. Velocity coplanarity, on the other hand, is dependent only on the change in the velocity vector across the shock and, therefore, is better suited for the computation of the shock normal, since Δv is much less susceptible to measurement error. The results (Mihalov *et al.*, 1969) also suggested that a disagreement between computed and measured upstream thermal pressures might be due to the neglect in the computation of terms involving pressure anisotropy and magnetic turbulence.

It seems that comparisons between the measured magnetosheath flow field and the flow field expected on the basis of the continuum fluid model yield more satisfying results than those involving the shock jump conditions. This is probably the result of a fact that the measured magnetosheath flow field represents long-term observations, and the fluctuations are thereby averaged out. This is borne out by the good agreement of the mean magnetosheath field configuration (Fairfield, 1967) and the mean magnetosheath plasma flow streamlines (Burlaga and Ogilvie, 1968) with those computed from the fluid model (Spreiter *et al.*, 1966). The fortuitously quiet magnetosheath traversal of Pioneer 6 also verified the more satisfactory agreement for measured and computed magnetosheath flow field results for a single transit. Figure 29 (Spreiter and

Alksne, 1968) shows the comparison with theory of various measured and computed plasma and magnetic field parameters for the Pioneer 6 traversal of Figure 24. Inspection shows that the agreement is very satisfactory, and this conclusion applies not only to the entire run of values for the velocity, density, and magnetic field intensity, but also to the location of the virtually discontinuous changes in values at the magnetopause and shock as well.

Although comparisons of experiment and theory based on the continuum fluid

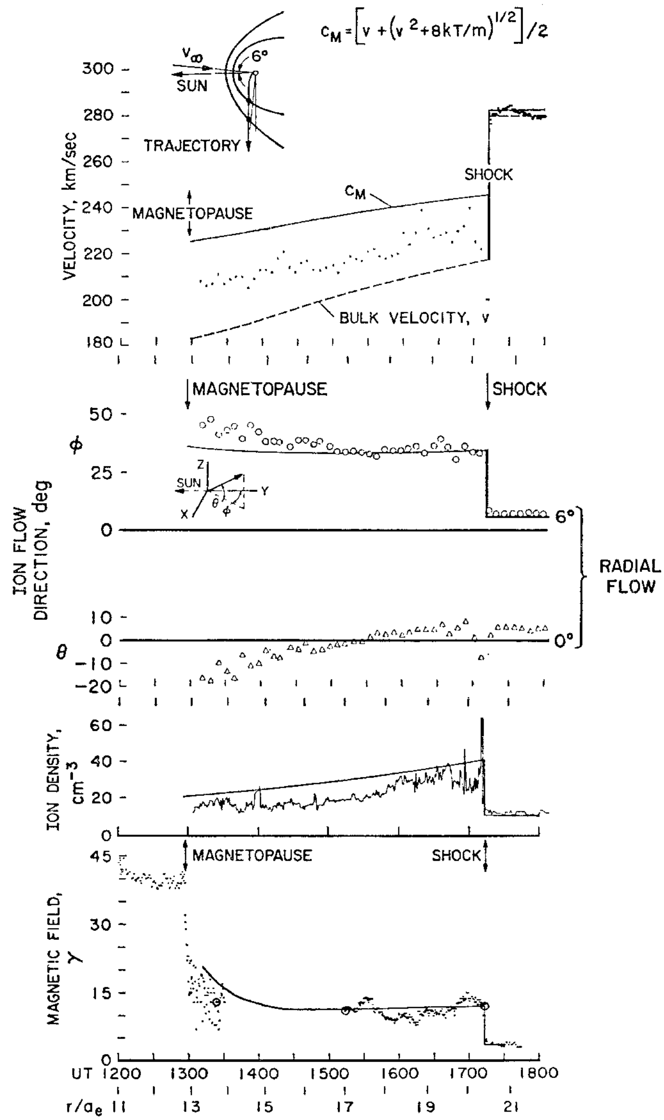

Fig. 29. Comparison of theoretical results based on fluid continuum theory with data from Pioneer 6 during the magnetosheath traversal of December 16, 1965.

model and MHD relations give, in general, satisfactory agreement, it is cautioned that, for the most part, this macroscopic theoretical approach provides insight only into the gross features of the solar wind-geomagnetic field interaction. The wave-particle interaction from a microscopic point of view (see, e.g., Tidman, 1967; Kennel and Sagdeev, 1967) will have to be examined more closely before the detailed physics of the interaction region can be adequately understood.

4. The Geomagnetic Tail

A. TOPOGRAPHY, NEAR EARTH

There has been considerable interest in predicting and measuring the characteristics of

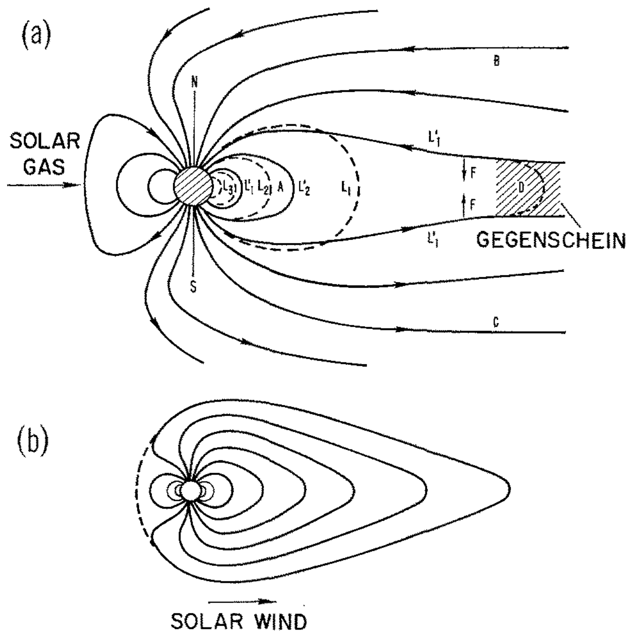

Fig. 30. Early models of the geomagnetic tail. (a) Diagram of the geomagnetic field during the transition from the sudden commencement to the main phase of a storm. (Piddington, 1960), showing lines of force drawn out to form the magnetic tail in the antisolar direction. The tail is composed of two bundles of lines of force (B and C), which are oppositely directed. – (b) Teardrop model (Johnson, 1960) for magnetosphere, showing a 'closed' geomagnetic tail in the antisolar direction.

Fig. 31. First experimental evidence for geomagnetic tail. (a) Disturbance field measured by Explorer 6 on August 9, 1959. The disturbance field F (solid line) is equal to $B - G$, where B is observed magnetic field and G (dashed line) is the extrapolated geomagnetic dipole field. B is obtained by transforming the measured field parameters $|B_\perp|$ and ϕ into geomagnetic coordinates, assuming there is no component of F perpendicular to the magnetic meridian plane (the plane containing the dipole field line and the center of the earth). F is shown at selected positions on the Explorer 6 trajectory, as viewed from a direction perpendicular to the local magnetic meridian plane. – (b) Disturbance field measured by Explorer 10. Data are plotted here in a manner similar to (a). Both figures show a tendency for F to rotate counterclockwise and be radial at large distances.

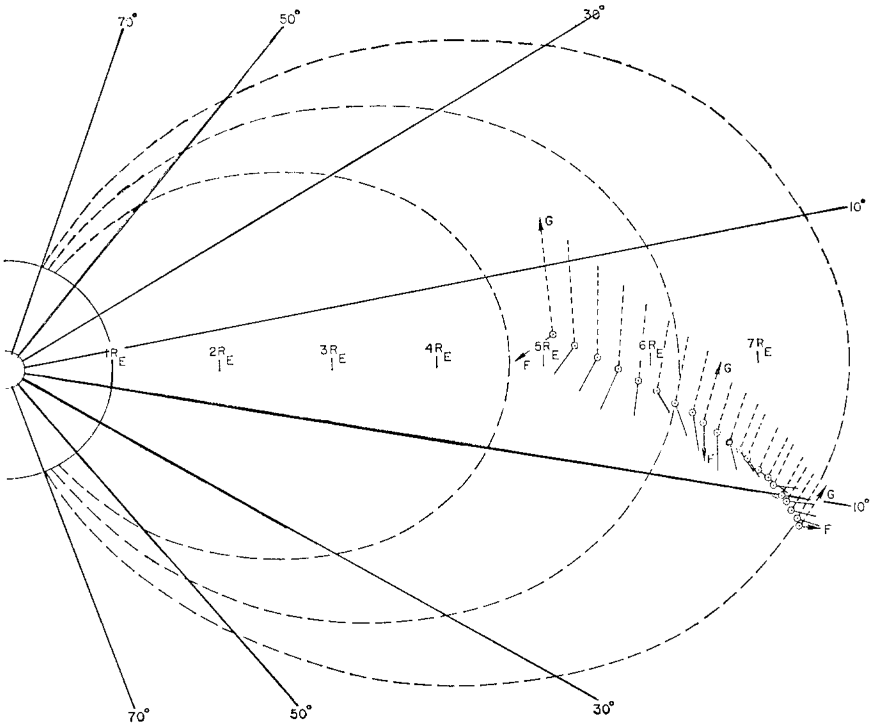
70°
50°
30°
10°
R_E
$2R_E$
$3R_E$
$4R_E$
$5R_E$
$6R_E$
$7R_E$
G
F
10°
30°
50°
70°

(a)

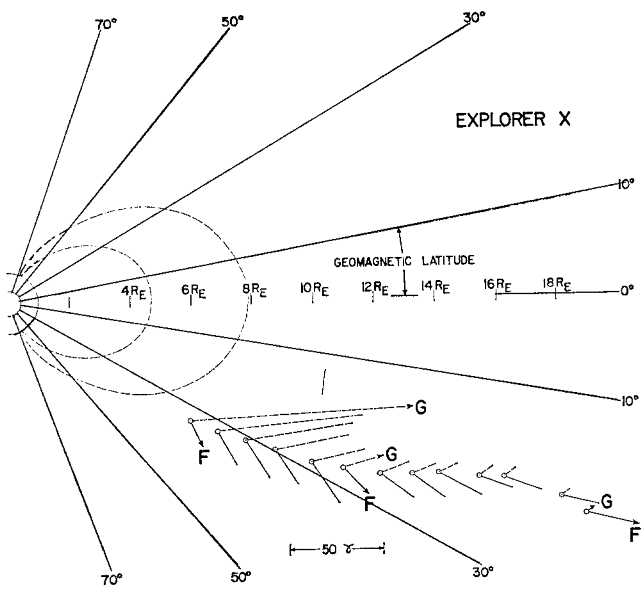
70°
50°
30°
EXPLORER X
10°
GEOMAGNETIC LATITUDE
$4R_E$
$6R_E$
$8R_E$
$10R_E$
$12R_E$
$14R_E$
$16R_E$
$18R_E$
0°
10°
G
F
50 γ
70°
50°
30°

(b)

the magnetosphere in the antisolar direction. Figure 2 shows the magnetosphere with the lines of force extending out in the antisolar direction to form the geomagnetic tail, analogous to a comet tail. The existence of the geomagnetic tail and its configuration were discussed first by Piddington (1960) and Johnson (1960). Piddington associated the existence of the geomagnetic tail with geomagnetic storms. Figure 30a is a reproduction of Piddington's diagram of the geomagnetic field during the transition from the sudden commencement to the main phase of a storm. The figure shows how lines of force from high latitudes are drawn out to form the magnetic tail in the antisolar direction. Also note that the magnetic tail is composed of two bundles of lines of force (B and C) that are oppositely directed. Johnson suggested that the geomagnetic field was confined by the solar wind into a teardrop shape (Figure 30b) and that it might play a role in auroral phenomena and the formation of the ionospheric F region. Johnson noted that, in addition to specifying the distance from the earth, the sun–earth–vehicle angle is important when presenting experimental data and should also be specified.

Since 1960 there have been a number of spacecraft that have explored the tail in cislunar space out to distances of approximately 60 R_E. It has been found that the geomagnetic tail at these distances is well ordered and well defined. Recently, Explorers 33 and 35 have extended measurements of the near-earth tail out to a distance of 80 R_E, and these measurements show that the tail at these distances is still well ordered and well defined.

In this section we will summarize some of the experimental results that have added to our knowledge of the topography of the near-earth geomagnetic tail. For additional information on some of the early spacecraft prior to and including Explorer 18 (IMP 1), the reader is referred to Section 1 and Figure 1. Hess (1968) and Ness (1969) also discuss the geomagnetic tail.

The first real observational evidence of the existence of the geomagnetic tail was made by Smith (1962). Smith compared Explorer 6 and 10 magnetometer data and found that each spacecraft measured a large deformation of the geomagnetic field even on quiet days in the antisolar direction. Figure 31 shows a comparison of Explorer 6 and 10 data (Smith, 1962). The top figure (31a) is the disturbance field measured by Explorer 6 on August 9, 1959. The disturbance field F (solid line) is equal to B-G, where B is the observed magnetic field and G (dashed line) is the extrapolated geomagnetic dipole field. Using a suggestion of Leverett Davis, Smith (1962) obtained B by transforming the measured field parameters $|B_\perp|$ and ϕ into geomagnetic coordinates, assuming there was no component of F perpendicular to the magnetic meridian plane (the plane containing the dipole field line and the center of the earth). In the figure, F is shown at selected positions on the Explorer 6 trajectory as viewed from a direction perpendicular to the local magnetic meridian plane. The bottom figure (Figure 31b) shows the disturbance field measured by Explorer 10 in March 1961. The geomagnetic field vector G and the component of the disturbance field F (B-G) are shown projected into the local magnetic meridian plane. Both the top and bottom figures show a tendency for F to rotate counterclockwise and to be radial at large geocentric distances. Smith (1962), of course, interpreted these data as being evidence for the existence of the geomagnetic tail.

Explorer 14 (Cahill, 1965, 1966) confirmed the Explorer 6 and 10 results on the existence of the geomagnetic tail. Figure 32 is a composite of two figures from Cahill

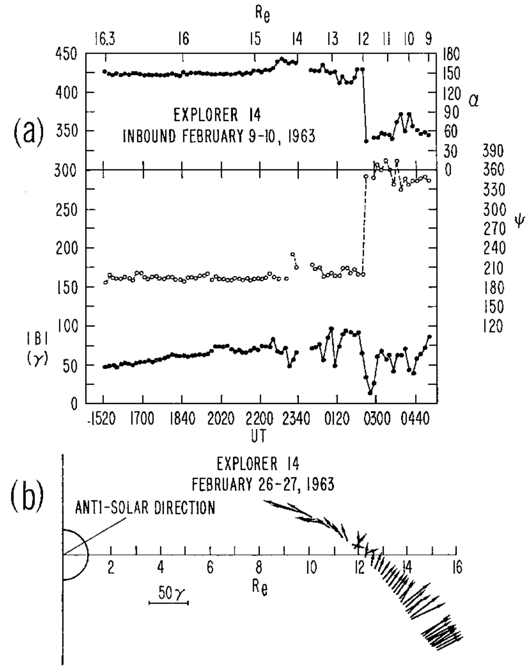

Fig. 32. Explorer 14 mapped geomagnetic tail out to $\sim 16\ R_E$. (a) Measurements taken on February 9–10, 1963, showing the magnitude of the field $|B|$ and the orientation, α and Ψ, in spacecraft coordinates (see Cahill and Amazeen, 1963). – (b) Measurements taken on February 26–27, 1963, showing projections of the magnetic field vector into the local magnetic meridian plane. Vectors plotted are the sums of the B_r and B_θ components of the magnetic field in geomagnetic, spherical coordinates, with the end points of the vectors lying at the location of the spacecraft.

(1965). He found that the magnitude of the measured magnetic field was greater than that predicted for a dipole beyond 8 R_E. There were also indications that at 10 R_E the field lines still formed closed loops between the two hemispheres. The top figure shows the measurements taken on February 9–10, 1963. The magnitude of the field $|B|$ and the orientation, α and Ψ (spacecraft coordinates; see Cahill and Amazeen, 1963) are plotted. From the angles shown, Cahill (1965) concluded that the orientation of the field for this inbound pass was quite constant in the antisolar direction until a distance of about 14.5 R_E. At about 12 R_E a field reversal was observed. The bottom figure shows the measurements obtained on February 26–27, 1963, presented in a different form. Here the magnetic field vector is shown projected on the local magnetic meridian plane. The vectors plotted are the sums of the B_r and B_θ components of the

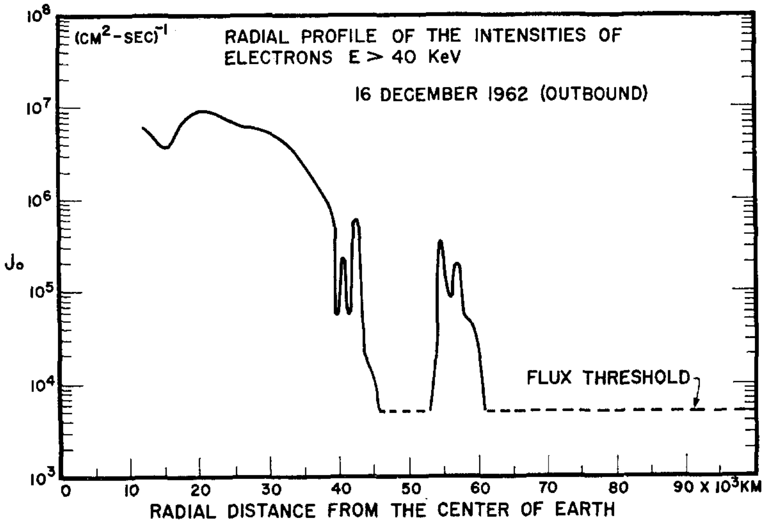

(CM²-SEC)⁻¹
RADIAL PROFILE OF THE INTENSITIES OF ELECTRONS E > 40 KeV
16 DECEMBER 1962 (OUTBOUND)
FLUX THRESHOLD
J₀
RADIAL DISTANCE FROM THE CENTER OF EARTH
90 X 10³KM

(a)

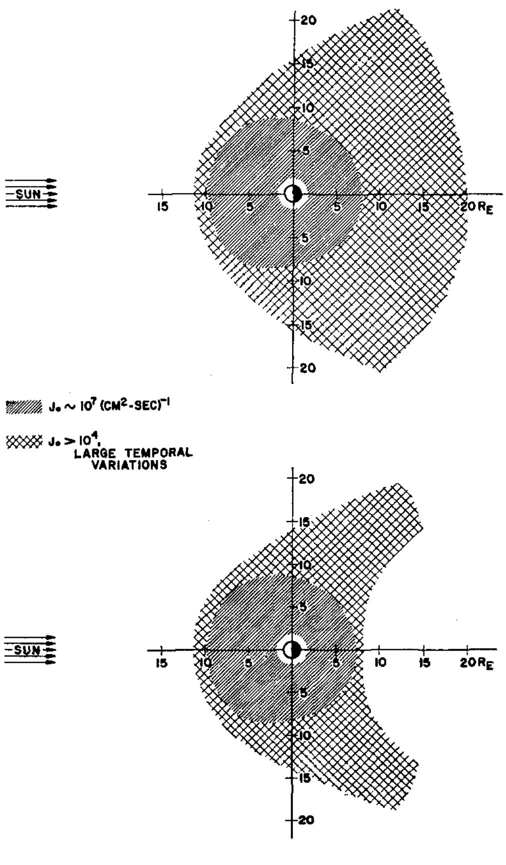

SUN
20 R_E
J₀ ~ 10⁷ (CM²-SEC)⁻¹
J₀ > 10⁴, LARGE TEMPORAL VARIATIONS

(b)

magnetic field in geomagnetic, spherical coordinates. The end points of the vectors lie at the location of the spacecraft. Note the change in orientation (antisolar to solar) of the vectors as the spacecraft passes into the northern hemisphere, obviously implying the crossing of a field reversal region. The antisolar direction varies on this

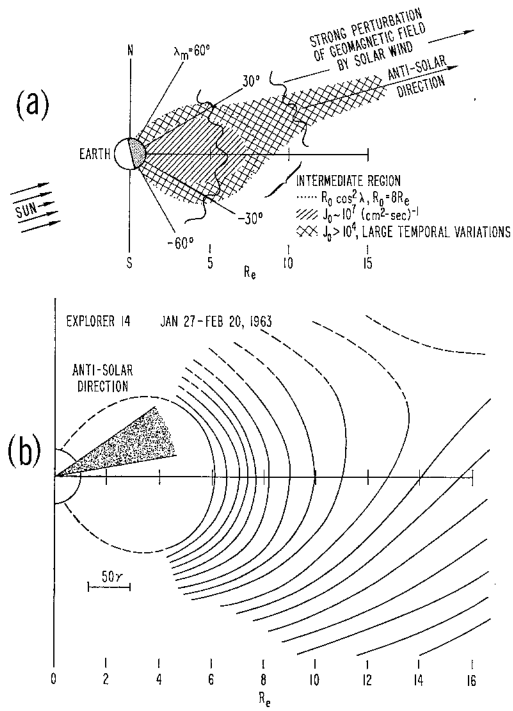

Figure 34. Summary of Explorer 14 electron and magnetic field data in the tail. (a) Schematic of electrons measured on Explorer 14, showing 'hard core' steady electron intensities ($\sim 10^7$ cm^{-2} sec^{-1}) extending to $\sim$ 8 R_E. The more variable and less intense 'tail' electrons extending beyond 10 R_E are confined near the ecliptic plane. – (b) Schematic diagram of the magnetic lines of force as derived from vector magnetic measurements on Explorer 14. Within $\sim$ 8 R_E, the field is similar to that of predicted dipole; beyond $\sim$ 10 R_E, it is drawn out to form the geomagnetic tail. The field reversal region can also be seen.

plot in the magnetic meridian plane due to the wobble of the magnetic dipole axis.

Freeman (1964) reported the observation of electrons with energies between 0.2 and 40 keV in the tail on Explorer 12. Fluxes of 10^8–10^9 cm^{-2} sec^{-1} were measured. Frank (1965) reported the measurement of electrons with energy $E>40$ keV on Explorer 14 with the SUI Geiger-Muller tubes. He found a 'hard core' of steady electron

---

Fig. 33. Explorer 14 electron data in the tail. (a) Typical radial profile of electrons ($E>40$ keV) near local midnight. – (b) Spatial distribution of $E>40$ keV electrons. The top diagram shows distribution in the ecliptic plane; the lower diagram at an ecliptic latitude of $\sim$ $-30°$ as seen looking down along north ecliptic pole.

fluxes between ~ 2 and $8\ R_E$ near the magnetic equatorial plane. The intensities here were $\sim 10^7$ electrons $cm^{-2}\ sec^{-1}$. An extended region of smaller and more variable electron fluxes was observed beyond $10\ R_E$ confined near the ecliptic plane. Figure 33 is a composite of two figures from Frank (1965). The top portion shows a typical radial profile of the intensities of electrons near local midnight. The spatial distribution of the $E > 40$ keV electrons is summarized in the bottom set of diagrams in this figure. The top diagram in the bottom set shows the distribution in the ecliptic plane, and the lower one for an ecliptic latitude of $> -30°$ as seen looking down along the north ecliptic pole. Serlemitsos (1966) studied ~ 100 keV electrons measured on Explorer 14 in the tail and found that they are essentially isotropic, that they appear in pulse-like events clustered around the geomagnetic equatorial plane (at least up to $16\ R_E$), and that the frequency of their occurrence decreases with geocentric distance.

The electron and magnetic field results on Explorer 14 are summarized in Figure 34,

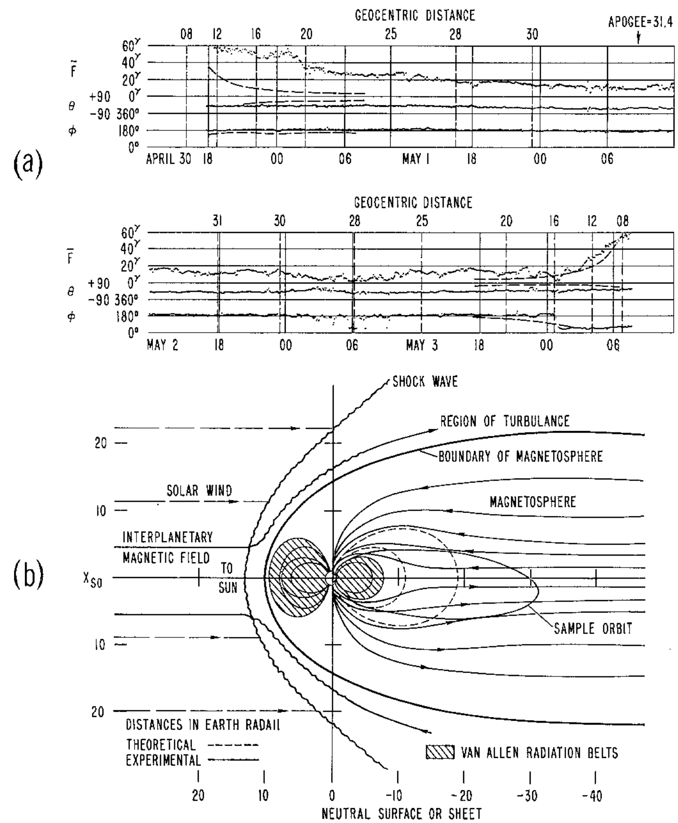

Fig. 35. Magnetic field measurements of the geomagnetic tail out to 31 R_E from IMP 1. (a) The first series of data is from orbit 41 outbound, the second from the same orbit inbound. Dashed lines indicate the values for the extrapolated geomagnetic dipole field. There is a neutral sheet crossing at $\sim 16\ R_E$ in the inbound pass. – (b) Illustration of the interpretation of the IMP 1 magnetic field topology within the magnetosphere in the noon-midnight meridian plane. A sample IMP 1 orbit is indicated, and the relative position of the neutral sheet and the tail field lines are also shown.

taken from Frank (1965) and Cahill (1965). The top figure is a schematic of the measured electrons, showing the hard 'core' steady electron intensities ($\sim 10^7$ cm^{-2} sec^{-1}) extending to $\sim 8\ R_E$ and then the more variable and less intense 'tail' electron intensities extending beyond 10 R_E and confined near the ecliptic plane. The bottom figure is a schematic diagram of the magnetic lines of force as derived from vector magnetic measurements on Explorer 14. Note the similarity of the field within $\sim 8\ R_E$ to that of the predicted dipole and then its distortion beyond $\sim 10\ R_E$ where it is drawn out to form the geomagnetic tail. The similarity between the top and bottom drawings in this figure is obvious and striking, and illustrates the existence of the geomagnetic tail out to a distance of $\sim 16\ R_E$ or greater.

Experiments on the IMP 1 spacecraft extended our knowledge of the topography of the geomagnetic tail out to distances of about 31 R_E. Figure 35 combines two figures from Ness (1965). Each series of plots presents the magnitude and the solar ecliptic θ and ϕ orientation of the magnetic field. The first series (the outbound pass) displays data obtained in the magnetic tail on orbit 41. The apogee of this orbit occurs at a geocentric distance of 31.4 R_E and at a sun–earth–probe angle of 181°. The magnitude of the field can be seen to vary from $\sim 60\,\gamma$ near 12 R_E to 10–20 γ beyond. In general, the θ and ϕ orientation of the field is quite steady ($\phi \sim 180°$ is antisolar); however, it is clear that there are some fluctuations in magnitude and orientation (e.g., May 2, $\sim$04 hour). The lower plot is taken from the same orbit inbound (May 2–4, 1964). These data show the magnitude of the field in the geomagnetic tail varies from $\sim 20\,\gamma$ to very low values. It can be seen that the orientation of the field is initially quite steady in the antisolar direction, although there are some fluctuations in magnitude and orientation also evident. At a distance of 16 R_E the ϕ orientation of the field changes from antisolar (180°) to solar (0°) and the magnitude approaches zero. This abrupt directional change in the earth's magnetic field is similar to that seen on Explorer 14 by Cahill (1965) and was identified by Ness (1965) as the first experimental detection of a neutral sheet in the geomagnetic tail. Ness summarized the physical characteristics of the neutral sheet as follows:

"The neutral sheet is evidenced by both the magnetic field topology within the magnetic tail of the earth and by its position in the magnetic tail. It has been uniquely observed on 14 of the orbits 31 through 47 and is identifiable on the basis of a very weak or zero magnetic field measured while the field orientation changes from an anti-solar to a solar direction. The satellite is moving northward with respect to the solar ecliptic pole at approximately 0.5 km/sec when the abrupt change occurs in the direction of the field from the antisolar direction in the southern hemisphere to the solar direction in the northern hemisphere. This velocity, multiplied by the time over which the direction changes, yields a 'thickness' of approximately 600 km, which is of the order of a proton gyroradius for a 1-keV particle. This describes a 'thin' sheet and is representative of several of the traversals of the neutral sheet."

In Figure 35b, Ness (1965) illustrates the interpretation of the IMP 1 data within the magnetosphere in the noon-midnight meridian plane.

Speiser and Ness (1967) discussed the neutral sheet observed on IMP 1 in more detail. The neutral sheet is described as the relatively narrow region of field reversal found within the broader plasma sheet (5–10 R_E) characterized by magnetic field depression and high intensity electron fluxes (see below, also Anderson and Ness, 1966). The neutral sheet often appears to be moving relative to the spacecraft with a maximum velocity of a few km/sec. On many orbits multiple neutral sheet crossings occurred. The formation of the sheet was found to begin near the magnetic equatorial plane at a geocentric distance of 10 ± 3 R_E. "The sheet thickness appears to be larger close to the Earth and the dawn side of the tail and smaller farther away and toward the noon-midnight meridian. At its thinnest region the sheet appears to be about 500 km thick and about 5000 km at the thickest part. The normal component of magnetic field within the sheet appears from these measurements to be 1 to 4 gammas toward the dawn side of the tail and less than 1 gamma near the noon-midnight merian plane" (Speiser and Ness, 1967).

Energetic electron measurements ($E > 45$ keV) were also made on IMP 1. Figure 36 is a composite of several figures from Anderson (1965). *Electron island fluxes* were observed on IMP 1 and found to be impulsively injected and characterized by a fast rise and a slow decay. This fast-slow behavior is illustrated in detail in Figure 36a, in which data from both the beta counter and the ion chamber are plotted. Both detectors indicate the fast buildup of the counting rate followed by its slower decrease. Figure 36b indicates the termination of the trapping region at 9 ± 1 R_E, the *cusp* extending to 14 or 15 R_E with a sharp outer boundary and then the electron island fluxes. Anderson notes that the island fluxes exhibit a marked tendency to have the same peak flux of electrons above 45 keV. An outbound pass near the dawn meridian is shown in Figure 36c. This illustrates the *skirt* region that begins ~ 6 R_E. The radiation in this region is soft as can be seen by comparing the simultaneous counting rates of the beta counter (higher rate) to that of the ion chamber. The skirt radiation is not as smooth in appearance as that of the trapping region. In this example the skirt is confined within the magnetopause that terminates at about 12 R_E.

Figure 37a is also taken from Anderson (1965) and summarizes the approximate locations of the energetic electron island fluxes, the cusp, and the skirt regions in the ecliptic plane. Figure 37b is from Anderson and Ness (1966) and presents simultaneous IMP 1 energetic electron and magnetic field data. Note the electron island fluxes at $\gtrsim 15$ R_E, the neutral sheet crossing at ~ 20 R_E, and the cusp region between ~ 15 R_E and ~ 9 R_E.

McDiarmid and Burrows (1965) detected high latitude electron spikes ($E > 40$ keV) on the Alouette 1 satellite at 1000 km, just outside the high latitude boundary of the outer radiation zone. The spikes had high intensities ranging up to 10^9 cm^{-2} ster^{-1} and occurred mainly on the night side of the earth on lines of force presumably connected with the geomagnetic tail. It was also found that the high latitude spikes occurred at times of moderately high magnetic ground activity (as indicated by the K_p index) and at times when enhanced electron fluxes were observed in the outer radiation zone.

Konradi (1966) reported observations of both electron and proton islands on the

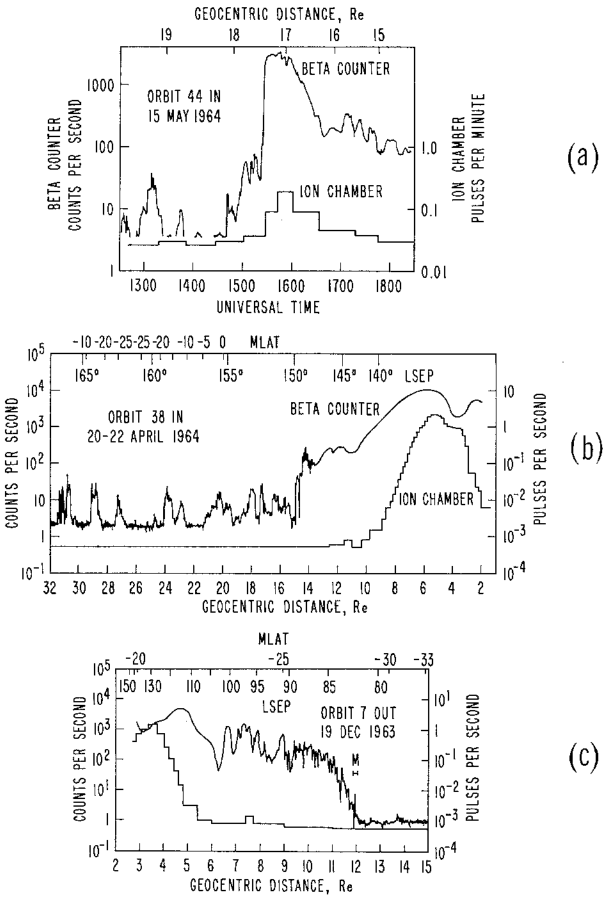

Fig. 36. Energetic electron measurements from IMP 1. (a) *Electron island fluxes.* Note the fast injection and slow decay. – (b) *Cusp.* Note the termination of the trapping region at 9 ± 1 R_E and the cusp extending to 14 to 15 R_E with a sharp outer boundary and then the electron island fluxes. – (c) *Skirt.* Note that it begins at ~ 6 R_E and is characterized by soft radiation.

night side of the magnetosphere from the ion–electron detector flow on Explorer 14 by Davis and Williamson. He reported electron fluxes that had a fast-slow behavior similar to that reported by Anderson (Figure 36a). In addition, proton fluxes were observed to be associated with the electron fluxes. While he found a softening with time of the electron spectrum, there was no clear-cut change with time observed for the proton spectrum. Konradi (1966) noted the similarity of the spectra and intensities of both electrons and protons in the islands and the aurora and suggested that a common accelerating mechanism was responsible for their production.

The Vela satellites have also made particle observations in the night side of the magnetosphere (Bame *et al.*, 1966, 1967; Montgomery *et al.*, 1965; Montgomery, 1968). The observations of low energy electrons (350 eV – 20 keV) and protons ($E > 100$ eV) show that a sheet of plasma with enhanced energy density extends across

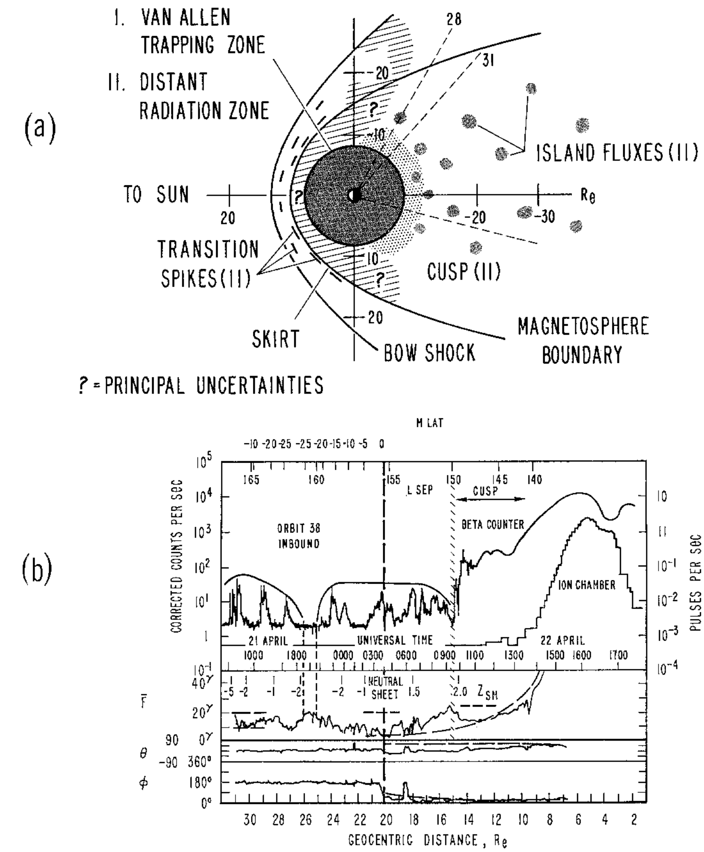

Fig. 37. (a) Schematic diagram summarizing approximate locations in the ecliptic plane of energetic electron island fluxes, cusp, and skirt. – (b) Simultaneous IMP 1 energetic electron and magnetometer data. Note the electron island fluxes at >15 the central sheet crossing at ~ 20 R_E, and the cusp region between 15 and 9 R_E.

the earth's magnetotail in the vicinity of the neutral sheet, as indicated in Figure 2. The plasma sheet has been observed at all geocentric distances probed by the Vela satellites from 15.5 to 20.5 R_E. Both the location and thickness of the plasma sheet have been seen to vary from time to time. Near the midnight meridian at ≈ 17 R_E, the sheet is often ~ 4 to 6 R_E thick, while toward the dusk and dawn boundaries, it flares out to about twice this thickness. Bame *et al.* (1967) summarize the physical characteristics of the plasma sheet in the following manner:

"The plane of symmetry of the sheet lies above or below the solar magnetospheric equatorial plane depending on whether the geomagnetic dipole axis tilts toward or away from the sun. The plasma is located in the vicinity of the 'neutral sheet' region of magnetic field reversal; inside the plasma sheet the measured kinetic energy densities of the electrons are comparable to the expected magnetic field energy densities, while outside the sheet the kinetic energy densities are much lower. The energy spectrums are quasi-thermal in character, having average energies extending from $\sim$200 eV to about 12 keV; omnidirectional fluxes extend to above 10^9 cm^{-2} sec^{-1}. Both rapid (100–200 sec) and slower changes occur in the average energies of the plasma sheet electrons, resulting in large variations in the flux of energetic electrons ($E>45$ keV). The plasma sheet boundaries, which are frequently in motion, are clearly defined by large changes in the electron flux. The average energy of the electron population is higher on the dawn side of the magnetotail than the dusk side, resulting in a more frequent appearance of energetic electrons on the dawn side."

Montgomery *et al.* (1965) and Montgomery (1968) reported Vela observations of electrons of energies $E>45$ keV similar to the measurements of Frank (1964, 1965) and Anderson (1965). Apparently the intensities of the energetic electrons depend strongly on the average energy of the entire electron population. The spatial distributions of the energetic electrons show a dawn-to-dusk asymmetry where the electrons in the plasma sheet on the dawn side of the tail are hotter than those of the dusk side. Montgomery (1968) believes it plausible that the presence of a high energy electron tail in the magnetotail is due to a 'local' acceleration of a small fraction of the low energy electron population.

Hones *et al.* (1967) reported that hot plasma containing energetic electrons ($E>45$ keV) often arrives suddenly in the plasma sheet at the Vela orbit of $\sim 17\ R_E$ at the peak or during the recovery phase of a negative magnetic bay in the auroral zone. It was also found that if the spacecraft happened to be in the plasma sheet at the time a negative bay starts, it is likely to detect a decrease in the intensity and/or average energy of the plasma sheet electrons as the depth of the bay increases. Hones *et al.* (1967) suggest that a contraction of the plasma sheet occurs during the development of a bay and that a sudden expansion occurs later at the beginning of the bay recovery. Hones *et al.* (1967) conclude that the bursts of hot plasma in the magnetotail derive their energy from processes occurring inside the Vela orbit.

Murayama (1966) analyzed the spatial distribution of electrons with energy $E>30$ keV in the geomagnetic tail and in the magnetosheath surrounding the tail on IMP 1 from the solid-state detector in the experiment of Fan *et al.* (1964). A multiple correlation analysis was made and some of the main conclusions are:

(a) The counting rates in the tail depend strongly on the distance from the neutral sheet, so that most of the electrons are confined within a few earth radii from the sheet.

(b) There is no significant dependence of the counting rates on geocentric distance. (This result is contrary to the findings of Anderson, 1965.)

(c) The counting rates have a dawn-dusk asymmetry in the tail, with those on the dawn side of the magnetosphere being higher than those on the dusk side.

(d) There is no clear discontinuity of the electron counting rates near the intersection of the neutral sheet and the dawn side boundary of the tail.

Murayama (1966) points out that this last result is important in connection with the problem of the origin of energetic electrons in the tail, since it suggests that electrons can flow into the tail via the neutral sheet as pointed out by Jokipii (1966).

Gringauz *et al.* (1966) reported the observation of electron fluxes ($E>70$ eV) in the earth's magnetic tail based on measurements performed on Luna 10 (launched March 31, 1966). This extended the IMP 1 observations of the tail out to the lunar orbit.

The Low-Energy Proton and Electron Differential Energy Analyzer (LEPEDEA) flow on OGO 3 measured low energy electrons in the energy range extending from ~ 100 eV to 50 keV in the dark hemisphere of the magnetosphere from 8 to 20 R_E (Frank, 1967a). It was found that as the geocentric radial distance of the observation decreases, electron differential energy spectra typically harden for $E \gtrsim 5$ keV, broaden, and are characterized by a peak in intensities that, in an average sense, occurs at higher energies. Frank (1967a) states that these results suggest that the process for accelerating these electrons is effective over a region in the magnetospheric tail extending from at least ~ 10–20 R_E. The radial profile of the electron ($E > 280$ eV) energy densities provided further information concerning the nature of the spikes of electron intensities. According to Frank (1967a):

"(1) the peak energy density is $\sim 10^{-9}$ erg/cm^3 (equivalent diamagnetic effect, $\Delta B = (8\pi \bar{E})^{1/2} \simeq 15\gamma$), (2) there is a notable relative absence of peaks in the energy density in the range 5×10^{-12} to 2×10^{-10} erg/cm^3, and (3) there is an absence of a strong radial dependence in the energy densities in these spikes within a factor 2 beyond ~ 13 R_E. In view of these results it is certain that the distribution of electrons substantially distorts the geomagnetic field beyond 8 R_E, and it is probable that the persistent peak energy densities $\sim 10^{-9}$ erg/cm^3 beyond ~ 13 R_E reflect a saturation limit of the magnetic field in these regions beyond which the tail field can no longer support the pressure due to the electrons. The relative absence of energy density peaks of smaller amplitude would appear to indicate that the acceleration mechanism drives the electron intensities to this saturation point. It is of further interest to note that the electron energy density peak at ~ 19.5 R_E was observed while the spacecraft was ~ 12 R_E above the neutral sheet ($\theta_{sm} \simeq 0°$ [Ness, 1965]). Thus large intensities of low energy electrons do appear within the earth's magnetic tail at large distances above the neutral sheet (in fact, for this observation, near the midpoint between the position of the neutral sheet and the presumed location of the northern magnetopause in the meridional cross section of the magnetosphere (Ness, 1965). Consideration of these large intensities of electrons at large distances from the neutral sheet in the earth's magnetic tail is important in constructing auroral theories and for analyzing the topology of the magnetic field in the tail region."

The first simultaneous observations of proton and electron differential energy spectra over the energy range extending from ~ 200 eV to 50 keV in the late evening sector of the earth's magnetic tail were made on OGO 3 by Frank (1967b). A comparison showed that the proton spectrum was significantly broader than the simultaneously measured electron spectrum. There was also a noncoincidence of the differential intensity peaks in the protron and electron spectra. For example, the proton and electron intensity peaks were found at ~ 1.5 keV and $\sim$ 700 eV, respectively. In addition, the proton intensities were not consistently occurring at higher energies than the peak in electron intensities, but also could occur at lower energies. The energy spectra showed energy densities of protons (190 eV $\leqslant E \leqslant$ 48 keV) and electrons (170 eV $\leqslant E \leqslant$

46 keV) were each $(4 \pm 2) \times 10^{-9}$ erg cm^{-3}. The number densities were 1 ± 0.5 cm^{-3}.

Vasyliunas (1968) reported the results of electron measurements made on the OGO 1 and OGO 3 satellites with the M.I.T. Faraday cup detectors that confirm the earlier measurements of Gringauz *et al.* (1960a, b). OGO 1 measurements were made of electrons having energies between 125 eV and $\sim$2 keV and on OGO 3 for electrons with energies ranging from $\sim$40 eV to $\sim$2 keV. The intense electron fluxes observed are confined to a spatial region, the plasma sheet, which is an extension of the plasma sheet measured by the Vela satellites.

Figure 38 is a composite of two figures from Vasyliunas (1968). The top sketch shows the electron distribution in the equatorial region, viewed from above the North pole. The intense low energy electron fluxes of the plasma sheet are observed across the entire magnetospheric tail at distances near 17 R_E. At closer distances it extends at least from close to the midnight meridian to past the dusk meridian. The figure shows that the radial extent of the plasma sheet is bounded on the outside by the magnetopause and on the inside by a sharp, nearly circular "inner boundary at $\sim$11 R_E, which is close to the outer boundary of the high energy trapped radiation zone" (Frank,

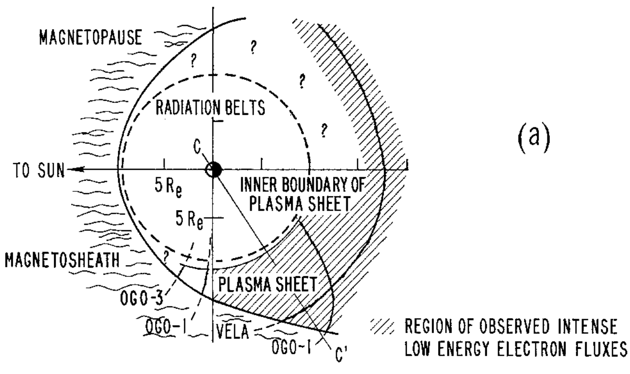

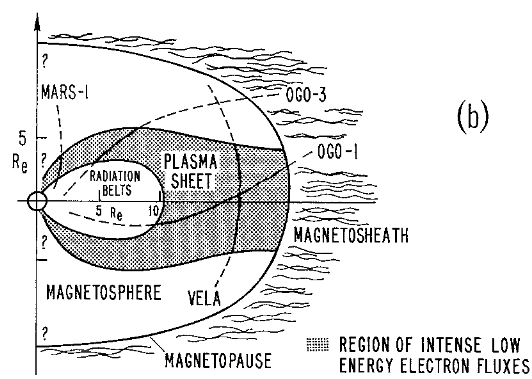

Fig. 38. (a) Spatial distribution of low energy electrons. Equatorial cut of the magnetosphere (viewed from above the North Pole), showing schematically the principal features of the low-energy ($\sim$ 100–1000 eV) electron population. – (b) Meridian cut (late evening plane) of the magnetosphere, along the line CC' of Figure 38a.

1965), which may or may not be related. The bottom figure is a meridian plane sketch, taking a cut through the magnetosphere along the line CC' in the top figure. It can be seen that the plasma sheet is confined to within several R_E of the equatorial region, and Vasyliunas (1968) emphasizes that it does *not* extend along the magnetopause to high latitudes. Allowing for significant distortions, the inner boundary approximates a magnetic shell. Unfortunately, at present there is little information available about the plasma sheet at very high latitudes. The only observations (Gringauz *et al.*, 1964; Vernov *et al.*, 1966) seem to indicate that the plasma sheet extends down to or near the auroral zones in the horn-like fashion illustrated.

Vasyliunas (1968) also studied the effect of magnetic storms on the spatial distribution of electrons. Figure 39 is from Vasyliunas (1968) and illustrates the changes in the spatial distribution of low energy electrons in the evening side of the magnetosphere that occur during magnetic storms. During a magnetic storm the plasma sheet extends considerably closer to the earth than during quiet periods. This could be the result of an inward motion of the plasma caused by an electric field across the tail. There appears to be a correlation between the onset time of a bay and the beginning of an inward motion. Freeman and Maguire (1967) have measured intense fluxes of positive

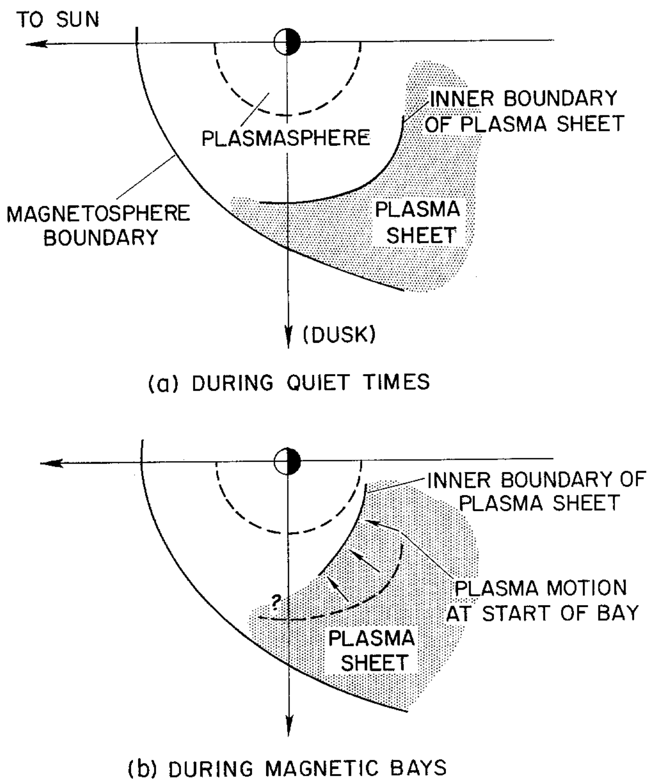

Fig. 39. Sketch of changes in the spatial distribution of low-energy electrons in the evening side of the magnetosphere that occur during magnetic bays.

ions on the ATS satellite at $\sim 6.6\ R_E$ during magnetically disturbed periods, and they also interpret their observations in terms of the inward motion of plasma from the magnetic tail. It appears, therefore, that at times of magnetic bays, the plasma sheet moves inward over the entire dark hemisphere and is closest to the earth in the midnight-to-dawn quadrant.

Figure 40 is a composite of several figures from Vasyliunas (1968). These figures explore the spatial dependence and/or a correlation with geomagnetic activity of the observed electron densities and mean energies. The first three figures present the observed densities and mean energies of electrons within the plasma sheet as a function of solar magnetospheric coordinates. The first three figures show respectively the *XSMS*, the distance down the tail, coordinate dependence; the *YSMS*, the distance across the magnetosphere, dependence; and the *ZSMS*, the height above the equa-

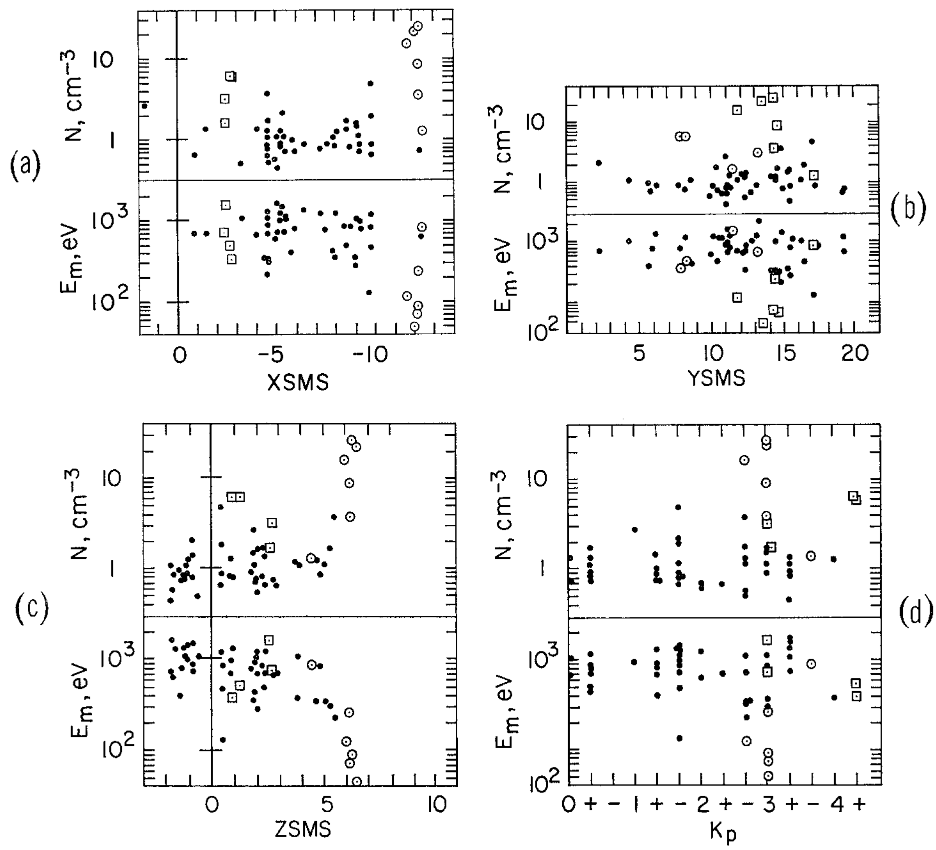

Fig. 40. Electron densities and mean energies in the plasma sheet. (a) Electron densities and mean energies vs. solar magnetospheric X coordinate. Points enclosed in circles and squares here (and in Figures 40b, c, and d) refer to measurements during the October 3, 1964, magnetic storm and the November 15, 1964, magnetic storm, respectively. – (b) Observed densities and mean energies vs. the solar magnetospheric Y coordinate. – (c) Observed densities and mean energies versus the solar magnetospheric Z coordinate. – (d) Observed densities and mean energies versus K_p.

torial plane, dependence. In the fourth figure the mean electron energies and densities are plotted as a function of K_p. In all the figures, points enclosed in circles refer to measurements made during the October 3, 1964, magnetic storm. Points enclosed in squares refer to measurements made during the November 15, 1964, storm. It is clear that most of the low energies and high densities occur during storms. However, there does not appear to be any other significant trend in the four figures, implying that although there is considerable scatter among the points, there is no evidence for any gross self-evident systematic dependence on spatial position or K_p.

Typical proton energy spectra are shown in Figure 41 (Frank, private communi-

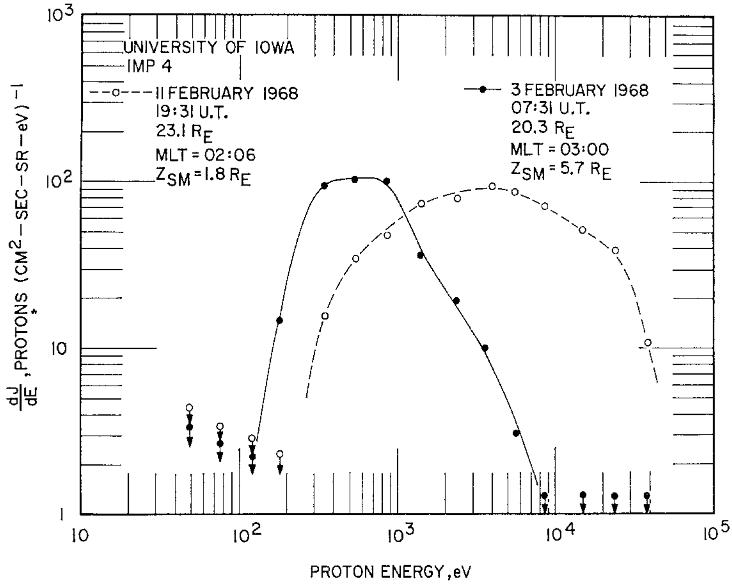

Fig. 41. Typical proton energy spectra. Data presented from February 3, 1968, were obtained in the magnetic tail but not near the plasma sheet. Data from February 11, 1968, were measured in the plasma sheet.

cation). The data presented from February 3, 1968, were obtained in the magnetic tail but not near the plasma sheet. The data from February 11, 1968, were taken in the plasma sheet. The differences in shape and peak energy of the two spectra are clear: the tail spectrum peaks at a lower energy and has a lower temperature (narrower spectral width) associated with it than the plasma sheet spectrum. There is also a higher proton number density in the plasma sheet. A plot of the average proton energies at a geocentric distance of 25 R_E in the magnetic tail from January to April 1968 is presented in Figure 42 (Frank, private communication). This is reminiscent of the data plotted in Figure 40 (Vasyliunas, 1968) where there was a large scatter and no clear relation between particle energies and *ZSMS*.

Murayama and Simpson (1968) studied the distribution, intensity, and energy spectra of electrons near and within the neutral sheet by using the simultaneous measurements of the University of Chicago Au-Si surface barrier detector ($E > 160$ keV) and the University of California detector ($E > 45$ keV) on IMP 1. They find that within the geomagnetic tail, there is a tongue-like region distributed 5 R_E above and below the neutral sheet, which is populated by an intense plasma (plasma sheet) and islands of electrons extending in energy above 200 keV. The tongue is

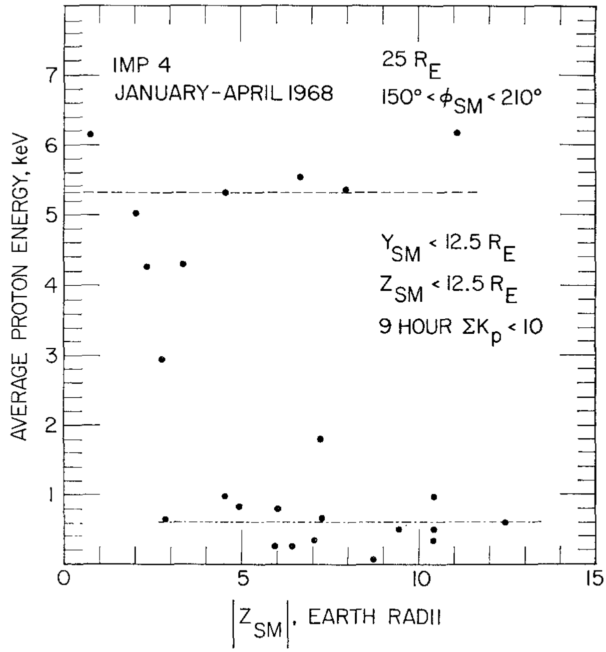

Fig. 42. Average proton energies at a geocentric distance of 25 R_E in the magnetic tail for January to April 1968.

spread out in longitude from the dawn-to-dusk boundaries of the tail and extends radially outward to $\sim 80\ R_E$, where a thin neutral sheet has again been detected by the Explorer 33 magnetometers (see below). Within the neutral sheet there is an ever present (to $\sim 31\ R_E$) but highly variable (in intensity) energetic electron flux with energies extending to ~ 200 keV. The neutral sheet thickness exceeds the gyroradius of 200 keV electrons by a factor of 5. Figure 43 is from Murayama and Simpson (1968) and summarizes the electron observations in the tail by superposing them on a drawing by Speiser and Ness (1967) of magnetic fields in the noon-midnight meridian plane. This figure shows a possible neutral sheet location in the tail when the magnetic moment vector of the earth's dipole is tilted through the angle X_{ss}. Murayama and Simpson conclude that the present evidence for neutral sheet electrons indicates that either the neutral sheet is well connected to a region of electron acceleration in the magnetosphere and behaves like a corridor or channel for electron escape or, alternatively, that the electrons are accelerated within the neutral sheet itself.

Lin and Anderson (1966) and Lin (1968) have examined the behavior of solar flare electron events in the geomagnetic tail to investigate the connection of geomagnetic tail lines to the interplanetary field lines. Figures 44a and 44b are from Lin (1968) and show two solar electron events observed in the tail: in Figure 44a data from both IMP 4 and AIMP 2 are shown. Both satellite records are shown in the same format. The upper curve in each plot is the open Geiger-Müller detector count rate × 10. This

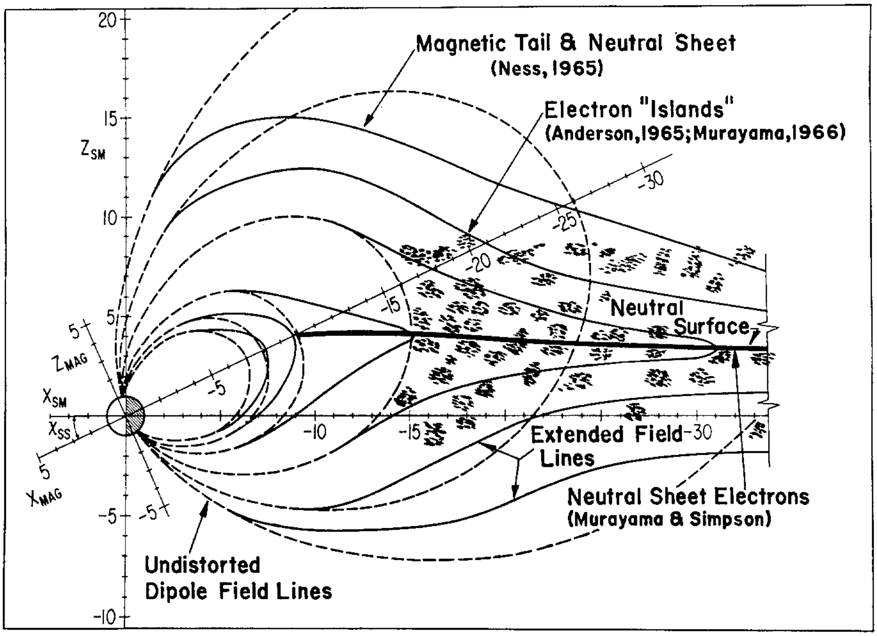

Fig. 43. Schematic drawing in the meridian plane of overall distribution of high-energy electrons in geomagnetic tail. The magnetic field configuration is from Speiser and Ness (1967).

detector measures electrons with $E > 22$ keV and protons with $E > 300$ keV. The lower curve shows the scatter GM detector count rate, detecting electrons only with $E > 45$ keV. In Figure 44b, data from September 18, 1967, on AIMP are shown. The dotted line indicates when both counters are observing only cosmic-ray backgrounds. The locations of the AIMP2 spacecraft during the decreases in the electron flux are marked on the orbit diagrams shown at the right. These are drawn on a moon-centered solar ecliptic coordinate system where the X_{LSE} axis points from the moon to the sun and the negative Y_{LSE} axis lies parallel to the ecliptic plane and points in the direction of the moon's orbital motion around the sun.

In the first event the open counter shows a substantial decrease when the satellite is in front of the moon with respect to the sun and earth and close to the neutral sheet ($Z_{sm} \lesssim 1\ R_E$). The large electron flux increases that are also seen are tail electron island fluxes discussed earlier. The two decreases shown in Figure 44b were also obtained in front of the moon but away from the neutral sheet ($Z_{sm} = 3$–$6\ R_E$). In Figure 44a and 44b the portion of the orbit over which the decrease was observed had a spatial extent that was within 200 km of the lunar diameter. The 200 km corresponds to one 20-keV electron gyrodiameter. Lin (1968) states that these observations indicate that the solar flare electrons enter the tail beyond $\sim 64\ R_E$ and then stream along the tail toward the earth. Lin (1968) also notes that so far AIMP 2 has recorded no evidence for magnetic shadows for the tail electron island fluxes.

Recently Anderson and Lin (1969) have studied more solar electron data in the

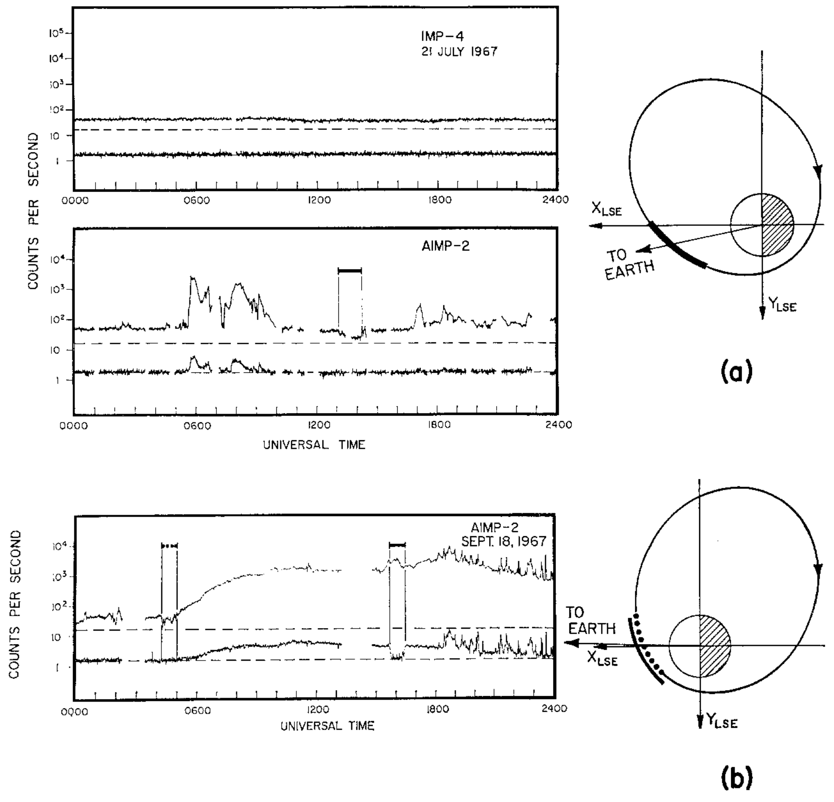

Fig. 44. Solar electron observations in the geomagnetic tail and their implications. (a) Solar flare electron fluxes are observed by AIMP 2 and IMP 4 while AIMP 2 is in the geomagnetic tail. Both satellite records are shown in the same format. The upper trace in each plot is the open GM counter (> 22 keV electrons and > 300 keV protons) count rate × 10. The lower curve is the scatter GM counter (> 45 keV electrons only) count rate. The large rapid electron flux increases that are superimposed on the steady solar electron component are the tail island fluxes. The location of the AIMP 2 spacecraft during the decreases in the electron flux are marked on the orbit diagrams drawn at the right (see text). – (b) Solar flare electron fluxes observed by AIMP 2 in the geomagnetic tail in the same format as Figure 44a.

magnetotail and have further developed the 'method of large absorbers' to identify the topology of field lines by means of the shadow pattern cast by the moon. Figure 44c is from Anderson and Lin (1969) and distinguishes between three types of field lines: type one is an interplanetary field line, type two is a geomagnetic dipole field line, and type three is a field line resulting from the connection of the first two types. The interplanetary field line originates at the sun, is convected out by the solar wind, and possibly extends to distances as far as tens of astronomical units. The geomagnetic dipole field line originates from currents inside the earth and closes in the vicinity of the earth. As the interplanetary field line convects past the earth, it connects with a

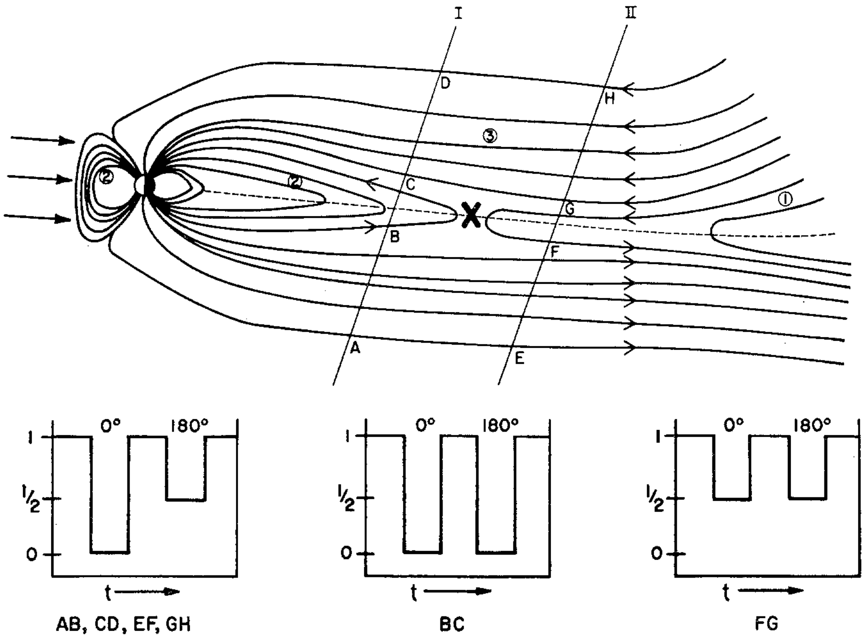

Fig. 44c. This figure shows how the magnetotail may be composed mostly of type 3 field lines, which are formed by the connection of interplanetary (type 1) and geomagnetic (type 2) field lines. See text for further explanation.

geomagnetic field line (Dungey, 1961). The resulting field line (type three) continues to be convected away from the sun until it reconnects with a similar type three field line associated with the other hemisphere of the earth (Dungey, 1961). When reconnection takes place, the type one (interplanetary) and type two (geomagnetic dipole) field lines are reformed. The forming of type three lines and then the reforming (reconnection) of the type one and type two lines from these type three lines is a dynamic process that is thought to be always occurring but at varying rates of reconnection (Dungey, 1961; see also Section 4.C). In Figure 44c the magnetotail is composed mostly of type three field lines. If one were to traverse the magnetosphere in the tail region along path I (*ABCD*) in Figure 44c, only type two and type three field lines would be encountered. On the other hand, if one were to traverse the magnetosphere in the tail region along path II (*EFGH*) only type one and type three field lines would be encountered. Therefore, field line reconnection is taking place at the neutral line X someplace between paths I and II. Anderson and Lin (1969) point out that the moon, or other large absorbers, will shadow energetic solar particles in differing ways, depending on which type of field line it is on. Various shadow patterns are illustrated along the bottom of Figure 44c (Anderson and Lin, 1969). From the study of these shadow patterns, Anderson and Lin (1969) conclude that most of the magnetotail field lines at 60 R_E connect to the interplanetary field (i.e., they are type three field lines). On one occasion, interplanetary field lines were found near the neutral sheet in the magnetotail. This supports the existence of reconnection (Dungey, 1961) and places the neutral line on this particular occasion at a geocentric distance $<60\ R_E$.

Dungey and Speiser (Speiser, 1968) have suggested that there may be magnetic field noise in the magnetotail associated with processes near the neutral sheet (e.g., acceleration of electrons giving rise to two stream cyclotron instabilities). The OGO 1 triaxial search coil magnetometer of Holzer and Smith measures magnetic field frequencies from dc to 900 Hz. Characteristic frequencies in the magnetotail are listed in Figure 45 (Brody, private communication). These observations (Brody *et al.*, 1968)

Proton gyro $\frac{1}{2\pi}\frac{eB}{m_p c}$	.08 — .50 Hz
Electron gyro $\frac{1}{2\pi}\frac{eB}{m_e c}$	140 — 980 Hz
Lower hybrid $\frac{1}{2\pi}\frac{eB}{c\sqrt{m_p m_e}}$	3 — 23 Hz
Ion plasma $\frac{1}{2\pi}\sqrt{\frac{4\pi ne^2}{m_p}}$	66 — 209 Hz
Spinning Search Coil OGO-1	0 — 900 Hz

n_e .1 - 1 electrons/cc

B 5 - 35 gamma

Fig. 45. Characteristic frequencies in the magnetotail plasma.

indicate that in the magnetotail magnetic noise in the 5–900 Hz range is moderate ($\sim 0.3\ \gamma$) and rather infrequent in occurrence but that it is correlated with a proximity to the neutral sheet.

Brody *et al.* (1968) have found that the magnetic noise bursts tend to occur together as a collection of two or more events with a typical duration of each event of 15 sec. After the group of events has occurred, usually long intervals of $\frac{1}{2}$ hour to hours follow in which no spectrum analyzer activity is observed. Figure 46 (Brody, private communication) presents examples of three magnetic noise bursts. The outputs of 12 of the spectrum analyzers are labeled along the ordinate and are plotted against universal time in hours and minutes. The first and third magnetic noise bursts are examples of typical broadband noise whose power spectral density falls off as $1/f^2$. The second magnetic noise burst is a nearly monochromatic signal at ~ 30 Hz.

Figure 47 (Brody, private communication) illustrates the magnetotail morphology and also the occurrence of noise bursts. The top curve in Figure 47 is the direction in degrees (with respect to some arbitrarily chosen direction) of the component of the

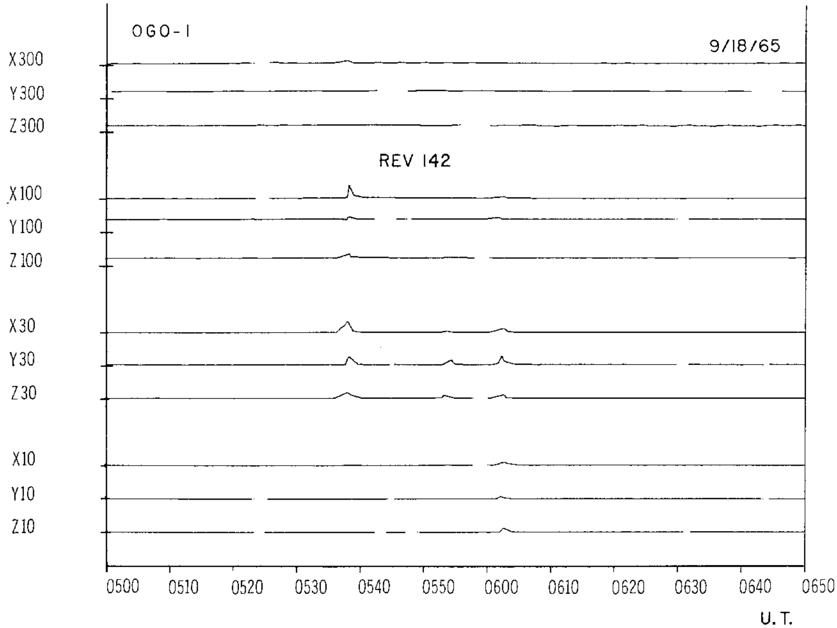

Fig. 46. Three magnetic noise bursts from OGO 1. The outputs of 12 of the spectrum analyzers are labelled along the ordinate and are plotted against universal time in hours and minutes. The first and third magnetic noise bursts are examples of typical broadband noise whose power spectral density falls off as $1/f^2$. The second magnetic noise burst is a nearly monochromatic signal at $\sim$ 30 Hz.

dc field measured in a plane perpendicular to the spin axis. The bottom curve is the magnitude of this component measured in gamma plotted as a function of universal time. The geocentric radial distance of the spacecraft in earth radii is indicated at the very bottom of the figure. There is a *depressed field sheet* ($\sim$ 18–17 R_E) that lies in the vicinity of the geocentric solar magnetospheric equator and is part of the plasma sheet. Within this region there are partial and complete crossings of the neutral sheet characterized by a sharp decrease in field magnitude and change in orientation. The vertical arrows indicate the occurrence of one or more magnetic noise bursts. It can be seen that inside the depressed field sheet there are three magnetic noise bursts.

Recently, Explorer 33 and 35 (Mihalov and Sonett, 1968; Behannon, 1968) have extended measurements of the near-earth geomagnetic tail out to a distance of ~ 82 R_E. These results show that even at this distance, the tail is still well ordered and well defined.

Explorer 33 was launched July 1, 1966, and has a particularly suitable orbit for studying the geomagnetic tail and the tail field gradient. Sonett *et al.* (1968) reported that the field remained regular out to distances greater than 82 R_E and that the average field values were in the neighborhood of 10–20 γ with the field values varying (for $K_p \leqslant 2^+$) from a low of 4 γ to a high of 40 γ.

A general tendency of the field direction to lie toward the sun in the northern half of the tail and away from the sun in the southern half of the tail was noted by Sonett *et al.* (1968), Behannon (1968), and Mihalov *et al.* (1968). Projections of the average

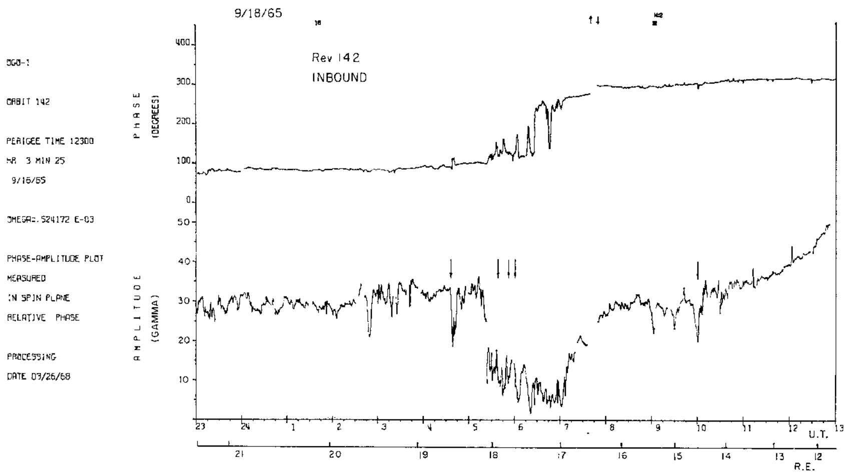

Fig. 47. Magnetotail morphology and the occurrence of noise bursts. The top curve is the direction in degrees (with respect to some arbitrarily chosen direction) of the component of the dc field measured in a plane perpendicular to the spin axis. The bottom curve is the magnitude of this component measured in gamma and plotted as a function of universal time. The geocentric radial distance of the spacecraft in earth radii is indicated at the very bottom of the figure. The *depressed field sheet* ($\sim$ 18 to 17 R_E), which lies in the vicinity of the geocentric solar magnetospheric equator and is part of the plasma sheet, is also shown. Within this region there are partial and complete crossings of the neutral sheet characterized by a sharp decrease in field magnitude and change in orientation. The vertical arrows indicate the occurrence of one or more magnetic noise bursts. It can be seen that inside the depressed field sheet there are three magnetic noise bursts.

magnetic fields North and South of the neutral sheet are shown in Figure 48, which is a composite of two figures from Mihalov *et al.* (1968) and Sonett *et al.* (1968). The tail fields North of the neutral sheet are shown in the top figure as projections on the solar-magnetospheric XY plane of 3-hour average magnetic field vectors. Similarly, the projections on the solar magnetospheric XY plane of the 3-hour average tail magnetic field vectors measured South of the neutral sheet are displayed in the bottom plot of Figure 48. These data show the well-ordered and regular extensions of the tail to a geocentric distance of $\sim$82 R_E and a lateral extension of the tail at these distances of $\sim$40 R_E. In addition, Sonett *et al.* (1968) and Mihalov *et al.* (1968) reported a distinct skewing of the field lines away from the solar-antisolar direction. They point

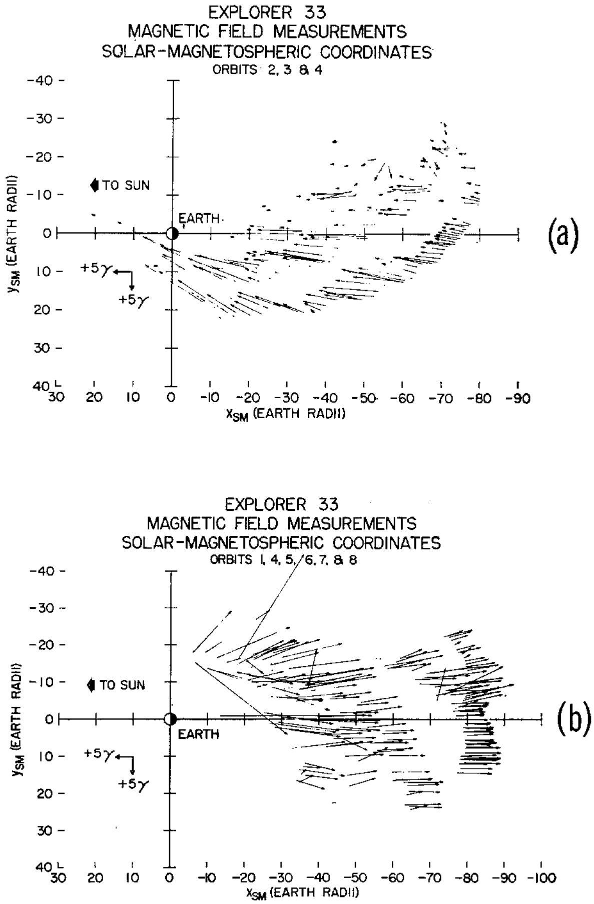

Fig. 48. Projections on the solar magnetospheric *X-Y* plane of 3-hour average magnetic field vectors measured in the earth's magnetic tail. (a) The data are from orbits 2, 3, and 4 of Explorer 33 and were taken at times during July 14 to August 26, 1966, when the spacecraft was in the Northern half of the tail. – (b) The data are from orbits 1, 4, 5, 6, 7, and 8 of Explorer 33 and were taken at times during July 1 to November 10, 1966, when the spacecraft was in the Southern half of the tail.

out that examination of the top plot in Figure 48 shows that the tail field direction tends to skew away from the antisolar direction in the dusk quadrant and that it is not likely that this result is an unexplained offset in one or more magnetometer sensors, since such a bias would affect the larger near-earth values less. They find the skewing is such that an added component of the magnetic field is present on both sides of the neutral sheet, with the skewing largest near the neutral sheet.

An example of the relation of K_p to the magnitude of the tail field is shown in Figure 49 (Mihalov *et al.*, 1968; Sonett *et al.*, 1968). One-hour average tail magnitudes (in gamma) from Explorer 33 for geocentric distances $>70\ R_E$ are plotted against K_p. The crosses indicate data from the northern section of the tail (solar pointing), and the dots indicate data from the southern part of the tail. By chance, higher values of K_p occurred while the spacecraft was in the southern part of the tail. In choosing the data, regions near the neutral sheet were eliminated to obtain a more representative view of the core of the tail in both the northern and southern sections. While there is a general trend to encounter higher tail fields with larger values of K_p, the spread of values shows that the relation in not obvious. Inspection of Figure 49

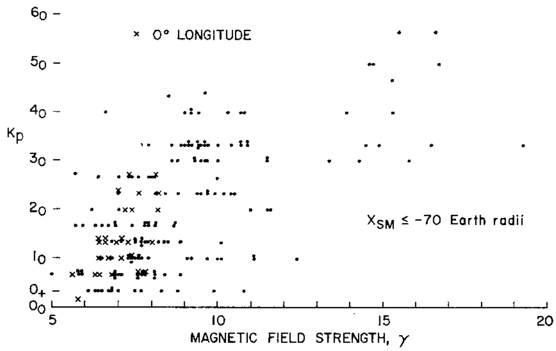

Fig. 49. 1966 Explorer 33 1-hour average geomagnetic tail field magnitudes with the component of the spacecraft location along the earth–sun line, X, more than 70 R_E behind the earth, plotted against K_p. The dots indicate antisolar-oriented field vectors (Southern hemisphere); the crosses indicate solar-oriented field vectors (Northern hemisphere). The number of individual magnetic field samples averaged during each 1-hour period ranges from 331 to 587.

shows that the largest tail magnitude ($\sim 20\gamma$) occurs for $K_p = 3+$ and that when K_p is largest ($K_p = 6$), the field magnitude is 17γ. Previously, Behannon and Ness (1966) had reported positive correlation of increased tail field magnitude with K_p.

Additional tail magnetometer data from Explorer 33 are presented in Figures 50 and 51 (Behannon, 1968). Figure 50 is a composite of three figures from Behannon (1968). The first displays the projection of hourly average field vectors onto the plane perpendicular to the solar magnetospheric equatorial plane from July to November 1966. The hourly averages were linearly computed from 82-sec averages of the magnetic field components. To avoid overlapping, not all the hourly vectors are shown. The middle plot shows the $X_{sm}Y_{sm}$ plane projection of the hourly average tail field vectors at distances $Z_{sm} \geqslant 3$ R_E above the solar magnetospheric equatorial plane. Similarly, the bottom figure shows the $X_{sm}Y_{sm}$ plane projection of the hourly average tail field vectors at $Z_{sm} < 3$ R_E. The neutral sheet was generally found to lie approximately at $Z_{sm} = 3$ R_E with the solar directed fields seen above it and the antisolar directed fields below it. If the base of the neutral sheet lies near the geomagnetic equatorial plane (Speiser and Ness, 1967), then the neutral sheet would be expected to lie above the solar magnetospheric plane in August as observed by Explorer 33 (Behannon, 1968).

The commencement of the September 14, 1966, magnetic storm in the geomagnetic tail at a distance of 73.8 R_E is shown in the magnetometer data in Figure 51. It can be seen that an increase of 10γ in the field magnitude, as well as changes in orientation, occurred. The storm began at 1522 ± 2 UT at the spacecraft, but field variations also occurred before the storm (~ 1009 UT).

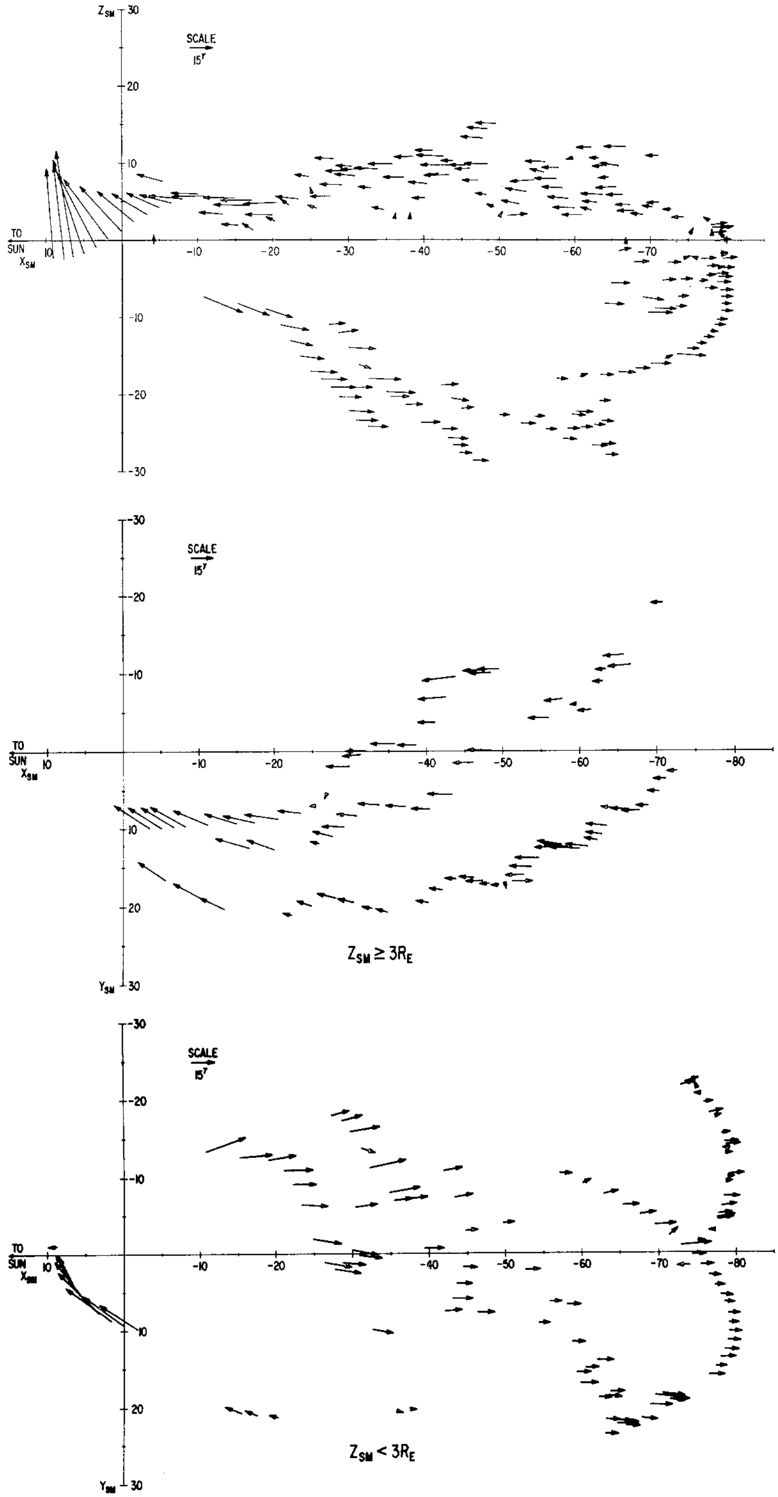

Z_{SM}
SCALE
15γ
TO SUN
X_{SM}
Y_{SM}
$Z_{SM} \geq 3R_E$
$Z_{SM} < 3R_E$

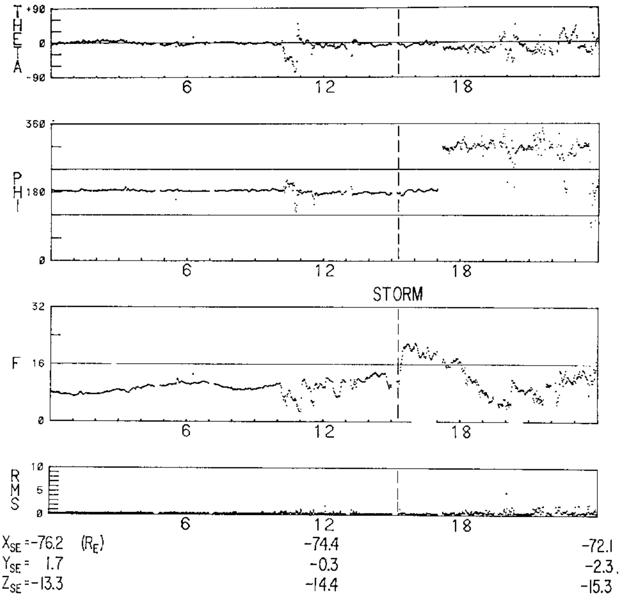

Fig. 51. Magnetic field data from September 14, 1966, illustrating the commencement of the September 14, 1966, magnetic storm in the geomagnetic tail beyond the lunar orbital distance.

The propagation of the sudden commencement of July 8, 1966, into the magnetotail was studied by Suguira *et al.* (1968). A sudden increase in the magnitude of the magnetic field was observed at the OGO 3 spacecraft within ~ 30 sec of the estimated onset at earth. By comparing the IMP 3 and Explorer 33 observations, Suguira *et al.* (1968) concluded that the observed magnetic field increase in the tail was unlikely to be due to an increased lateral pressure of the post shock solar wind gas from the sides of the tail. Using an idealized model, they concluded that the increase in the tail field was due mainly to a transfer of magnetic flux to the tail by the increased solar wind pressure exerted on the front and sides of the forward magnetosphere.

Data from both Explorer 33 and 35 were compiled by Mihalov and Sonett (1968) to determine the cislunar geomagnetic tail gradient in 1967. The average magnetic field strength (in gamma) is plotted in Figure 52 as a function of geocentric distance for intervals when $K_p \leqslant 2^+$. The solid symbols display solar-oriented fields. A multiple correlation analysis of hourly average magnetic field magnitudes in the geomagnetic tail was performed for 948 hours of data from April to August 1967 (Explorer 33) and for 142 hours of data from July and August 1967 (Explorer 35). The heavy line gives the radial part of the multiple correlation analysis, using all values of K_p for all 1967 tail field magnitudes from April to August, irrespective of geocentric distance. The

Fig. 50. Average vector magnetic field observed in the geomagnetic tail by Explorer 33 during July–November 1966. The uppermost figure shows the projection on the noon-midnight plane in solar magnetospheric coordinates, the lower two figures show the projections on the equatorial plane for data obtained above and below the plane $Z_{sm} = 3R_E$, respectively.

light solid line and the dashed line give the radial components of similar fits for all values of K_p for 1967 and 1966, respectively, for only geocentric distances of less than 58 R_E. Recently, Mihalov (private communication) reported that, based on 13 traversals of the Explorer 35 spacecraft into and out of the magnetic tail, the average dia-

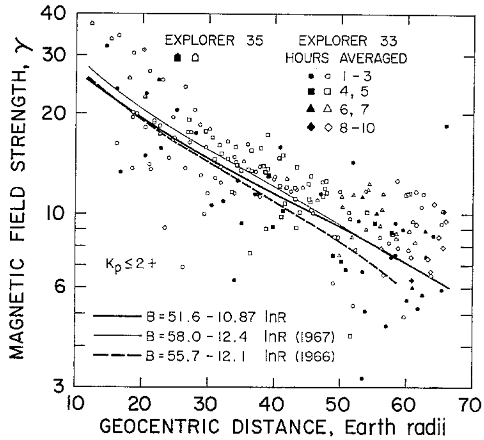

Fig. 52. Average geomagnetic tail field magnitudes B measured in 1967 by Explorers 33 and 35 for $K_p \leqslant 2+$. Symbols distinguish Explorer 35 data from Explorer 33 data. The number of hours of Explorer 33 data averaged for each plotted point are also indicated by symbols. Solid and open symbols represent solar and antisolar directed tail fields, respectively. The heavy line gives the radial part of a multiple correlation analysis, using all values of K_p of all 1967 tail-field magnitudes from April to August. The light solid and dashed lines give the radial parts of similar fits for 1967 and 1966, respectively, using all values of K_p but with geocentric distances of less than 58 R_E only.

meter of the magnetotail is 50 R_E at the mean crossing distance of the lunar orbit (57 R_E).

Armstrong and Krimigis (1968) measured protons ($E > 0.31$ MeV) out to geocentric distance of ~ 80 R_E on Explorer 33. Small proton fluxes ($\lesssim 5$ cm^{-2} sec^{-1} ster^{-1}) were measured in the tail and were usually anisotropic, with the largest flux apparently flowing down the tail away from the earth.

B. TOPOGRAPHY, EXTENDED REGION

There has been considerable interest in predicting the length of the geomagnetic tail. Dessler (1964) suggested that there could be a long geomagnetic tail extending for thousands of earth radii, perhaps to a distance of 20–50 AU from the sun. In Figure 53a Dessler's original sketch (Dessler, 1964) of this long magnetosphere is shown. Dungey (1961, 1963) suggested the reconnection model resulting in an open magnetosphere. Figure 53b is a reproduction of Dungey's drawing. In this model, lines of force that are carried along by the solar wind become distorted as they connect to a geomagnetic field line in flowing past the magnetosphere and then reconnect at approximately 1000 R_E downstream. At the point of reconnection there is a magnetically neutral point. (As discussed in Section 4.A the lines of force in the northern hemi-

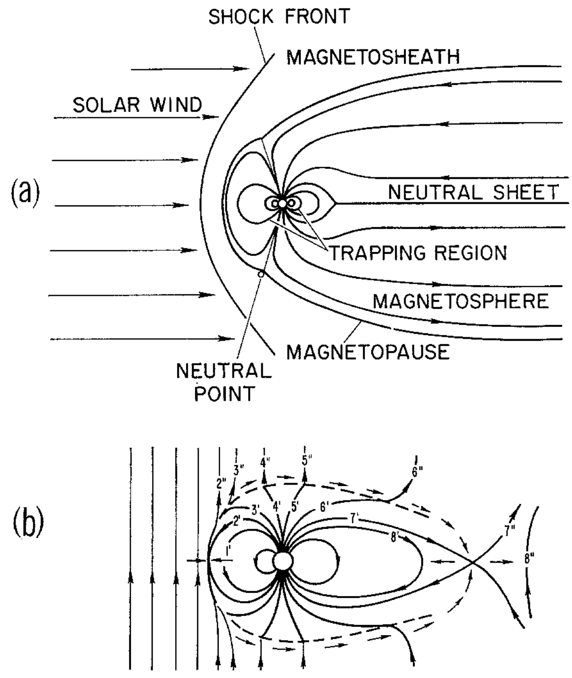

Fig. 53. (a) The long tail, closed magnetosphere model. – (b) The reconnection model for an open magnetosphere.

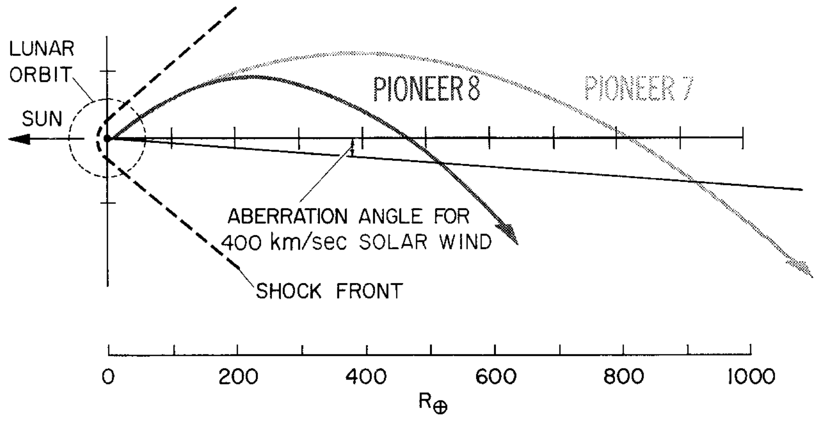

Fig. 54. Pioneers 7 and 8 trajectories. Ecliptic projection. Pioneer 7, launched August 17, 1966, went through the expected region of the geomagnetic tail at 1000 R_E in September 1966. Pioneer 8, launched December 13, 1967, went through the expected region of the geomagnetic tail at 500 R_E in January 1968. At a geocentric distance of 525 R_E, the Pioneer 8 spacecraft was 10.5 R_E above the ecliptic and at an ecliptic projection of the spacecraft–earth–sun angle of 185.5°. At a geocentric distance of 1059 R_E, the Pioneer 7 spacecraft was 28.7 R_E above the ecliptic at an ecliptic projection of the spacecraft–earth–sun angle of 189°.

sphere of the tail are solar pointing.) A further discussion of magnetospheric models is presented in Section 4.C, 'Comparisons with Theory', which also includes a discussion of magnetic merging and Dessler's (1968) revised model for the magnetosphere and its length.

Observational information on the extended nature of the geomagnetic tail was first obtained on the Pioneer 7 spacecraft by Ness *et al.* (1967) and Wolfe *et al.* (1967). Pioneer 7, launched August 16, 1966, went through the expected region of the geomagnetic tail at a distance of approximately 1000 R_E downstream from the earth (Figure 54). Wolfe *et al.* (1967) reported the observation of intermittent intervals of disturbed ion spectra. The changes in the spectra were so great that one would have expected them to have been associated with wide changes in geomagnetic activity (as indicated by the K_p index). Since during these intervals of observation of disturbed spectra there were no such changes, it was argued by Wolfe *et al.* (1967) that the observation was that of a more local 'geomagnetospheric wake.' On this spacecraft, Ness *et al.* (1967) reported magnetometer observations that could also be associated with an extended geomagnetic tail. Fairfield (1968) has compared Pioneer 7 magnetometer data with simultaneous magnetometer data from Explorers 33 and 28 and found

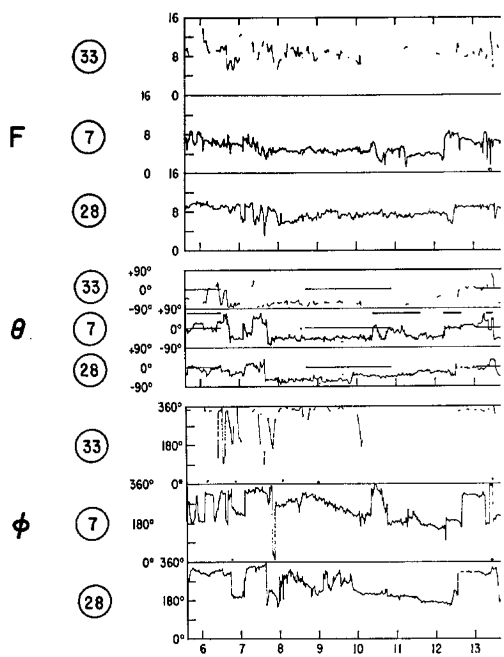

Fig. 55. Simultaneous magnetic field measurements at the Explorer 33, Pioneer 7, and Explorer 28 spacecraft. Field magnitude F, solar ecliptic latitude angles θ, and longitude angle ϕ are grouped together and marked with the number of the satellite. The time scale in hours UT on September 26, 1966, corresponds to the Explorer 28 data. Pioneer 7 data have been shifted 4 hours and 15 min to the left, and Explorer 33 data 25 min to the left, to make the field discontinuities correspond at the three spacecraft. Periods of probable tail observations at Pioneer 7 are designated by solid lines above the θ trace.

(after correcting for time delays) that there were intervals during which the observed magnetic field characteristics at Pioneer 7 were different from those observed at the other spacecraft (as illustrated in Figure 55). In this figure the black bar inserted over the Pioneer 7 θ magnetic field orientation data indicates Fairfield's identification of tail associated phenomena. Intriligator *et al.* (1968, 1969b) have compared simultaneous plasma and magnetic field data and found that there is no unique correspondence between changes in these parameters. Since Pioneer 7 seemed to have encountered features associated with an extended geomagnetospheric wake at 1000 R_E, the trajectory of the Pioneer 8 spacecraft was tailored so that it would pass through the expected region of the geomagnetic tail at a distance of about 500 R_E (Figure 54). Pioneer 8 was launched on December 13, 1967, and approximately one month later passed through this region about 500 R_E downstream from the earth. In Figure 54 the outbound trajectories of Pioneers 7 and 8 are shown. Intriligator *et al.* (1968, 1969a) have reported that the Pioneer 8 spacecraft also encountered phenomena associated with an extended geomagnetospheric wake, implying that between 80 R_E and 500 R_E, the geomagnetic tail undergoes significant changes, so that apparently it is no longer a well-defined and well-ordered tail such as that observed nearer earth.

Figure 56 is from Intriligator *et al.* (1968) and summarizes simultaneous Pioneer 8 data from the Ames Research Center plasma probe (Intriligator *et al.*, 1969a), the TRW Systems Group vlf electric field detector (Scarf *et al.*, 1968), and the Goddard Space Flight Center magnetometer (Ness *et al.*, 1967). The data were obtained from 0830 to 1030 UT on January 23, 1968, when the Pioneer 8 spacecraft was in the expect-

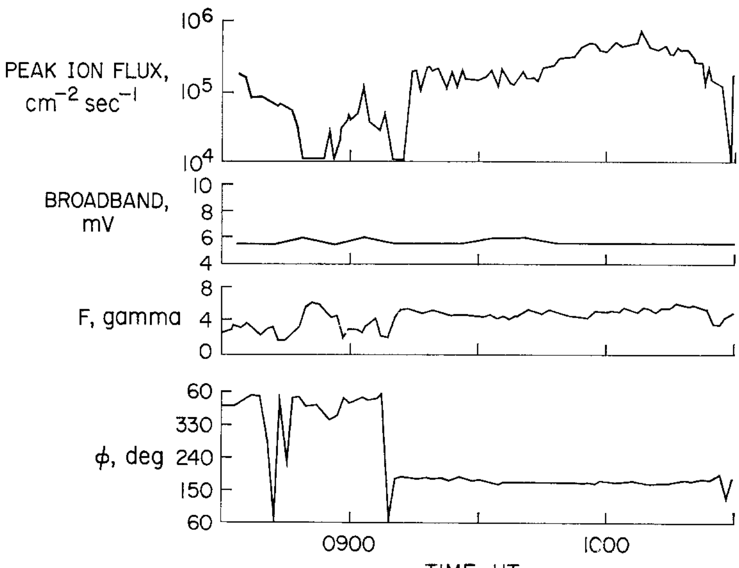

Fig. 56. Simultaneous plasma ion, electric field, and magnetic field measurements from the Pioneer 8 spacecraft in the expected region of the geomagnetic tail at a geocentric distance of ~ 500 R_E from 0830 to 1030 UT on January 23, 1968.

ed region of the geomagnetic tail at a geocentric distance of approximately 500 R_E. The top curve indicates the peak ion flux in the peak E/Q step; the second curve shows the broadband wave level; and the two bottom curves, the magnitude and ϕ orientation, respectively, of the magnetic field. Throughout this entire time interval, the spacecraft is most likely encountering tail associated phenomena. This is indicated by the low peak ion flux or absence of measurable ion flux; the low broadband wave level between 5.5 mV (threshold) and 6 mV; and the ϕ orientation of the magnetic field near 360° and 180°. To obtain more knowledge of the actual plasma ion characteristics, it is necessary to look at the individual ion energy/unit charge spectra. The spectra for the same interval of time as the summary curves presented in Figure 56 are presented in the three bottom series of spectra in Figure 57 (Intriligator *et al.*,

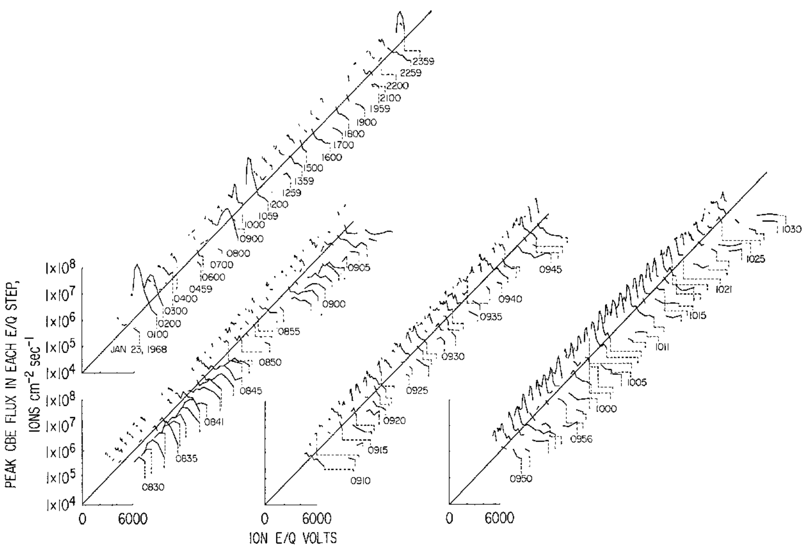

Fig. 57. Plasma ion spectra in the geomagnetospheric wake, showing the peak flux in each E/Q step obtained on the Pioneer 8 spacecraft on January 23, 1968. The series of 24 spectra on the upper left are the hourly spectra from 0000 to 2400 UT. Detailed spectra for the interval from 0830 to 1030 UT are shown in the series on the right. The spectra are often time aliased and 'ragged', indicating that the ion E/Q distribution is rapidly changing. The dashed lines extend across to indicate the time of the measurement.

1969a) and show each individual spectrum obtained. The series of spectra on the upper left of Figure 57 shows one ion E/Q spectrum for each of the 24 hours on January 23, 1968, as measured on Pioneer 8. In general, all the spectra shown in Figure 57 are 'ragged' and time aliased, indicating that the measurable plasma characteristics are rapidly changing. The figure illustrates that there are some intervals (e.g., 0910–0915 UT) when there is an absence of measurable plasma within the energy range of the detector and others (e.g., 0830–0845 UT) where the observed plasma has a relatively high energy distribution peaking between 3 and 4 kV. Intriligator *et al.* (1969a) conclude that the widely varying spectra or the absence of measurable plasma are indicative of geomagnetospheric wake associated phenomena.

In summary, then, the Pioneer 7 and 8 observations imply the existence of features associated with an extended geomagnetospheric wake. At this time, however, it is not possible to distinguish between several possibilities:

(1) If the earth's magnetosphere has closed between 80 and 500 R_E, then the observations could be those of the turbulent downstream wake.

(2) If the solar wind has not diffused into the geomagnetic tail, then the observations could be those of the tail flapping past the spacecraft.

(3) If, at these extended distances, the tail has a filamentary structure, possibly quite intertwined, then the observations could be those of the various filaments.

(4) If the tail has broken up into 'bundles' that are not connected to the earth, then the observations could be those of some of the bundles traveling past the spacecraft.

(5) If magnetic merging (Dungey, 1965) has taken place, then the observations could be those of the subsequent acceleration of pinched-off gas to near solar wind velocities.

It is anticipated that further analysis may shed light on the actual physical processes taking place at these distances. Recently McKibbin (private communication) has estimated, based on some Pioneer 7 data, that the total effective diameter of the tail at $\sim 1000\ R_E$ is 35 R_E.

In 1965 Mariner 4 passed through the expected region of the geomagnetic tail at a distance of 3300 R_E (~ 0.1 AU) downstream from the earth. No tail associated phenomena were observed (Van Allen, 1966; Coleman *et al.*, 1965). Recently, however, McKibbin *et al.* (1969) have shown, based on analysis of intervals of tail associated phenomena observed by the Pioneer spacecraft, that even if the geomagnetic tail did exist at 3300 R_E, the sampling frequency of Mariner 4 was such that it would not have been possible to identify such phenomena.

Krimigis *et al.* (1967) reported simultaneous observations of low energy protons ($E \sim 0.5$ MeV) from the July 7, 1966, solar flare on Explorer 33 and Injun 4. At this time the Explorer 33 spacecraft was outside the magnetosphere but in the immediate astronomical vicinity of the earth, while Injun 4 was in the magnetosphere over the earth's polar cap. The reconnection model (Dungey, 1961) for an open magnetosphere (Figure 53b) predicts that charged particles approaching the earth on interplanetary field lines have immediate access to points over the polar caps. On the other hand, the long tail model (Dessler, 1964) for the magnetosphere (Figure 53a) predicts that solar protons having energies $\lesssim 5$ MeV must diffuse into the very long tail of the magnetosphere and spread slowly from the auroral zone over the polar caps after a delay or 'diffusion time' of hours. Even if the tail length were only 1 AU, there should be a delay of more than a day between the time of arrival of a 0.5 MeV proton in the vicinity of the earth, but outside the magnetosphere and the time of arrival for this proton over the polar caps (Krimigis *et al.*, 1967).

Figure 58 is from Krimigis *et al.* (1967) and shows counting rate vs. time of the channel, $0.5 \leqslant E_p \leqslant 4.2$ MeV, from Explorer 33 (solid line) and the equivalent channel from Injun 4 (plotted points) obtained while the latter satellite (orbital inclination

81°) was moving over the earth's polar cap at an altitude ranging from 1300 to 2000 km. The solid curve uses $\frac{1}{2}$-hour averages of the Explorer 33 counting rate, while the plotted points represent 8–16 min averages of the Injun 4 counting rate. Since the unidirectional geometries of the two detectors differ by approximately a factor of 10,

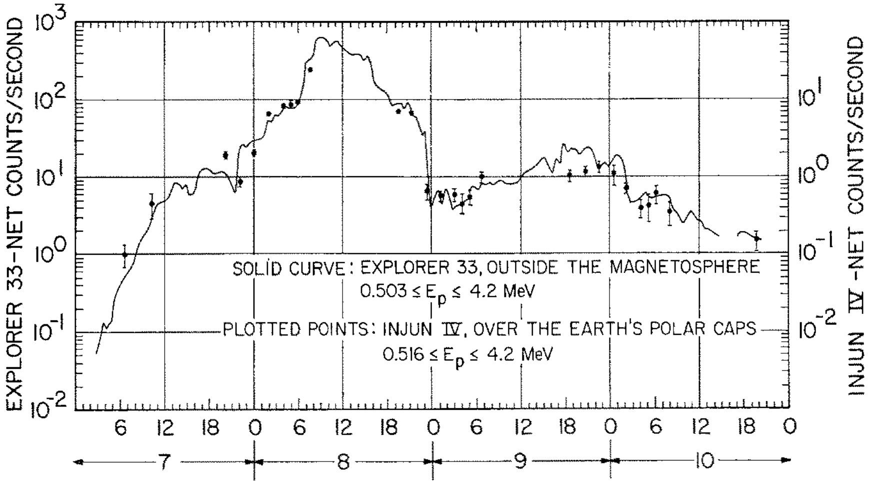

Fig. 58. Simultaneous observations of directional intensities of solar protons with Explorer 33 and Injun 4. The smooth curve is drawn through the half-hour averaged counting rates from Explorer 33. Each plotted point represents a polar-cap averaged counting rate for Injun 4. The respective sets of data are superimposed on the same absolute intensity basis (to within 25%) by displacing the count-rate scale of Injun 4 data upward by one decade.

the Injun 4 points were moved up one decade in logarithmic scale, so that the absolute values of the intensity at the two satellites could be compared directly in the figure. Comparison of the data shows that in interplanetary space and over the polar cap of the earth during the entire 4-day period of simultaneous observations, the absolute intensities of protons in identical energy channels are essentially the same moment-by-moment (within the uncertainties of statistics and the geometric factor).

Krimigis *et al.* (1967) conclude that low energy (~0.5 MeV) solar protons have full access to the earth's polar caps from the interplanetary medium with a delay of 0.5 hour or less. These observations provided a specific test of the diffusion calculation for solar protons with a long tail model of the magnetosphere and are in definite disagreement with its predictions and, therefore, favor an 'open' model of the magnetosphere.

C. COMPARISONS WITH THEORY

Since the initial discussions of the existence of the geomagnetic tail by Piddington (1960) and Johnson (1960) and the observations of the tail by Smith (1962), our observational knowledge of the geomagnetic tail has greatly increased, as outlined in Sections 4.A and 4.B above. A great deal of interesting theoretical work has also been done and much of this is quite controversial. Some aspects of these papers will be discussed in this section.

There are essentially three magnetospheric models that concern the geomagnetic tail: the closed magnetosphere (Figure 30b), the long magnetosphere (Figure 53a), and the reconnection model for an open magnetosphere (Figure 53b). In the closed magnetosphere model (Johnson, 1960), the lines of force from one hemisphere lead back to the earth in the other hemisphere. In the long tail model (Dessler, 1964), these lines of force are prevented from closing near the earth and are stretched out to distances of 20–50 AU, where they eventually close. In the reconnection model (Dungey, 1961), interplanetary field lines (that are southward pointing) are carried along by the solar wind and become distorted as they connect to geomagnetic field lines in flowing past the magnetosphere. The interplanetary field lines and the geomagnetic field lines are then each reformed when they reconnect downstream in the tail at the neutral point. In the reconnection model the length of the geomagnetic tail field line (such as line 6′ in Figure 53b), when it is connected to the interplanetary field line (such as line 6″ in Figure 53b), may be less than 100 R_E, but it will probably be stretched to more than 1000 R_E before it disconnects, such as line 7′ in Figure 53b (Dungey, 1968).

The basic question concerning the reconnection model for the magnetosphere vs. the closed model magnetosphere is whether, when you follow an auroral field line away from the earth, it eventually connects to an interplanetary field line or it eventually closes by leading back to the opposite hemisphere of the earth. A field line, of course, cannot be measured *per se*, it is just a conceptual convenience; however, if technically all that is required for a reconnection model magnetosphere is that one (a few) field line(s) from the earth connect to (an) interplanetary field line(s), then there is no question that the reconnection model has not only been verified but is usually appropriate. The solar electron data of Lin and Anderson (1966) and Lin (1968) (see Figures 44a and 44b) show that solar electrons (which are tied quite tightly to the lines of force) are at times definitely streaming down the tail lines toward the earth. There is evidence, therefore, for the validity of the reconnection model magnetosphere at these times.

With the reconnection model one would expect several branches of different ages within the tail that were formed from interplanetary field lines with different directions (Dungey, 1968). Parts of branch boundaries connected to the auroral ovals may be distinguished by energetic particles (Dungey, 1968). When a boundary moves past a spacecraft, a sharp particle spike should be detected, such as the electron spikes seen by Anderson *et al.* (1965). These particles ($E \sim 40$ keV) are travelling much faster than the solar wind and can cross the shock and travel upstream. Energetic particle spikes have been detected upstream by Anderson (1968), Frank and Shope (1968), and Jokipii (1968).

The assumption of a reconnection model (an open magnetosphere) or closed magnetosphere (Figures 53b and 30b, respectively), immediately leads to a number of other specific predictions concerning magnetospheric and tail phenomena, such as the length of the geomagnetic tail.

Johnson (1960) proposed a teardrop model of the magnetosphere (Figure 30b).

However, Johnson did point out that the action of hydromagnetic shock waves could force the tail open. Dessler (1964) argues that the hydromagnetic waves generated at the front of the magnetosphere through the action of radiation pressure could prevent the tail of the magnetosphere from closing near the earth. He predicted that the length of the geomagnetic tail may be 20–50 AU. Dessler's configuration (Dessler, 1964) for the tail fields is shown in Figure 53a. The tail would eventually close at such heliocentric distances in the charge-exchange boundary shell where the solar wind is terminated. Far down the tail from the earth, the tail plasma and field conditions might be such as to make them indistinguishable from those within the solar wind itself.

More recently Dessler (1968) proposed that the magnetic merging across the neutral sheet of the geomagnetic tail takes place very near the earth between ~ 10 and 30 R_E. Assuming that the plasma density in the near earth tail is low (because the supersonic solar wind leaves a rarefied wake region extending ~ 30 R_E behind the dipole-like magnetosphere), then magnetic merging takes place as it would in a vacuum where the plasma density is too low to form a current sheet of sufficient strength to prevent merging.

Dungey (1965, 1968), using his reconnection model for an open magnetosphere (Figure 53b), also estimated the length of the geomagnetic tail and found that it was approximately 1000 R_E. Dungey (1968) considers the history of a tail line as follows:

"Before its dayside reconnection it has been distorted by the shock in a way illustrated by Spreiter *et al.* (1966) (though they have no reconnection). It may be asked how far this distortion goes before reconnection occurs or more precisely, at the time of reconnection how far downwind are the points where the line of force crosses the shock. This is directly related to the time between the line first meeting the shock and its reconnection, but the order of magnitude may be discussed in relation to the speed of the free [solar] wind w. Thus $\bar{v} \sim 0.1\, w$ will be taken for a high rate of reconnection and $\bar{v} \sim 10^{-3}\, w$ would correspond to a very low rate. Taking the high rate then, the distance traveled by the wind during the time while the line of force is crossing the magnetosheath is $10 \times$ the thickness of the magnetosheath or tens of R_E .... The evidence for motion in the polar ionosphere suggests that the field line remains connected to a polar cap for hours (Dungey, 1965) and during this time the interplanetary part of the line is moving with the wind at ~ 200 R_E/hr. Thus, the length of the tail from P [a point on the polar cap] to S [a point on the shock surface], when it is first reconnected on the dayside, may be less than a hundred R_E, but it will be stretched to probably more than a thousand R_E before it disconnects."

Anderson and Lin (1969) have found that most of the field lines at 60 R_E connect to the interplanetary field (Figure 44c). This is in agreement with the reconnection model as discussed above. On one occasion Anderson and Lin (1969) found interplanetary field lines near the neutral sheet. This further supports the existence of reconnection and places the neutral line at a geocentric distance of less than 60 R_E on this particular occasion. Referring to Figures 53b and 44c, this model indicates that the tail merging on this particular occasion is taking place within 60 R_E.

Krimigis *et al.* (1967) observed solar protons ($E \sim 0.5$ MeV) simultaneously at

Explorer 33 and Injun 4 (Figure 58) and found that there was a delay of $\frac{1}{2}$ hour or less between the particle arrival times outside the magnetosphere (Explorer 33) and over the polar caps inside the magnetosphere (Injun 4). This also implies an open magnetosphere.

Piddington (1960) suggested that tangential stresses might stretch the geomagnetic tail and thus account for the main phase of magnetic storms. Axford and Hines (1961) suggested that viscous interaction could give rise to tangential stresses that produce internal convection within the magnetosphere. Dungey (1961) also considered convection within the magnetosphere but as a result of reconnection: the tail lines connect with the interplanetary field and are dragged by the solar wind, giving rise to tangential stresses that produce the convection. If there is an outward flow (away from the sun) over the polar caps, one must find a convective mechanism for carrying the field lines toward the sun in the magnetosphere.

Dessler and Michel (1966) and Michel and Dessler (1966) argue that the ionosphere over the polar caps is sufficiently hot that plasma (mainly ionized hydrogen) can escape from the two polar ionospheres and flow along the magnetic field lines into the tail and that the resulting flow of protons and electrons out of the ionosphere acts to limit the thermal plasma number density to $\sim 10^2$ cm^{-3} immediately above the polar ionosphere and to $\sim 10^{-1}$ cm^{-3} at a distance of $\sim 30\ R_E$ down the tail. The plasma flowing down into the tail is replaced by the ionization of the neutral atmosphere over the polar caps. They conclude that, unless they have overlooked some process that can condense plasma in the tail to a high density, the tail is filled principally with solar plasma with a number density no greater than ~ 10 cm^{-3}.

Recently, Spreiter and Alksne (1969) have studied the effects of neutral sheet currents on the shape and magnetic field of the geomagnetic tail. They present numerical results for several representative cases that show that there is an additional flaring out of the geomagnetic tail of the order of a few earth radii over a distance of several tens of earth radii. Associated with this increase in tail size is a decrease in magnetic field intensity resulting from the approximate conservation of total magnetic flux in each half of the tail cross section. Although the inclusion of the current sheet does have this considerable effect in enlarging the ultimate cross section of the geomagnetic tail, the principal changes are in the portion of the boundary that is deeply embedded in a highly supersonic flow. Spreiter and Alksne also compare the results of their calculations with the IMP 1 observations (Figure 14) of Wolfe *et al.* (1966a); the Explorer 33 observations of Behannon (1968); and the Explorer 33 observations of Mihalov *et al.* (1969) (similar to Figure 52). These comparisons show the substantial improvement in the agreement between the calculated and observed dimensions of the geomagnetic tail and the strength of the magnetic tail field provided by the simple modification of the theory to include the neutral sheet currents.

5. Summary and Conclusions

Beyond the protective envelope of the atmosphere, the single most important phenomenon that dominates the whole of the near earth environment is the interaction of the solar wind with the geomagnetic field. The present concept of this interaction has evolved rapidly in the last few years as the result of the rather intensive experimental probing by a variety of scientific spacecraft. It has been well established that the earth's magnetic field forms a cavity in the streaming solar wind. This cavity (the magnetosphere) has a generally well-defined boundary (the magnetopause) in the daylight hemisphere, but in terms of the exclusion of the solar wind plasma and the existence of an ordered geomagnetic field, the nighttime hemisphere is much less well defined.

The interaction region in the daylight hemisphere is dominated by a standing MHD shock wave located at about 15 R_E at the subsolar point, some 4–5 R_E beyond the mean geocentric distance of the magnetopause. Although the general features of the shock and downstream flow field (the magnetosheath) are predictable on the basis of MHD fluid theory, many of the details of the shock interaction do not lend themselves to the strict application of the gas dynamic analog. The solar wind plasma, convecting the interplanetary magnetic field, is deflected, slowed, and heated across the shock front. The resulting magnetosheath flow field configuration, in general, follows the expected streamlines around the geomagnetic cavity, with the imbedded and distorted interplanetary magnetic field becoming approximately tangent to the magnetopause. The shock structure is suggestive of a standing wave that has steepened into a true shock, yet retains partial reversibility. It is apparent that both magnetic and electric waves are generated at the shock front and that this wave energy can propagate and dissipate via wave-particle interactions, upstream as well as downstream. During even moderately disturbed times, the magnetopause and shock boundaries exhibit a high degree of motion, and the magnetosheath is apparently dominated by wave-particle interactions that grossly distort the magnetosheath flow field.

The dominant feature of the nighttime hemisphere is the geomagnetic tail. Within the tail there is imbedded a plasma sheet that is several earth radii thick and within which there exists a thin neutral sheet. The neutral sheet separates oppositely directed geomagnetic field lines that connect to the earth near the poles. This structure seems well defined out to a distance of at least 80 R_E but may extend to a considerably farther distance. The distorted geomagnetic tail has been observed out to distances as far as 1000 R_E, where it is apparently better classified as a wake rather than a tail. In all likelihood, the overall tail structure is quite comet-like in nature.

It is clear that there still are many uncertainties with regard to the details of the solar wind-geomagnetic field interaction and many questions have yet to be answered. For example, the stagnation point, where the magnetosheath plasma should become completely random, has not been observed. This is probably the result of the fact that any one satellite in its lifetime does not spend any significant time in the expected region of the stagnation point. The situation is further complicated by the motion of the magnetosheath boundaries. The neutral points in the daylight hemisphere and the geomagnetic tail between the lunar orbit and 500 R_E have not yet been explored. These regions are somewhat inaccessible from a spacecraft orbital mechanics point of view, yet they should be investigated since they may play a critical role with respect to magnetospheric structure and dynamics. The true nature of the shock transition and the identification of the various waves and wave-particle interactions is still uncertain. Although more sophisticated, high data rate satellite investigations will be helpful, the old problem of separating spatial from temporal phenomena can be answered adequately only by simultaneous observations from a network of satellites.

Note added in proof: It has recently been determined that an improper normalization factor was used in the computation of the power spectral density for Pioneer 1 (Sonett, private communication). Values quoted in Figure 17 should be reduced by approximately a factor of 10. The corrected Pioneer 1 spectral density now agrees much better with the values obtained from other observations.

Acknowledgments

The authors are grateful to Dr. L. A. Frank, University of Iowa, and Mr. K. I. Brody, UCLA, for permitting the use of unpublished data. We would also like to thank Mr. D. Stroud and Mr. W. Balandis for their efforts in the preparation of the figures. The authors appreciate the helpful comments and suggestions provided by J. D. Mihalov, D. S. Colburn, and J. M. Wilcox in their review of the text.

References

Anderson, K. A.: 1965, *J. Geophys. Res.* **70**, 4741.
Anderson, K. A.: 1968, *J. Geophys. Res.* **73**, 2387.
Anderson, K. A. and Lin, R. P.: 1969, *J. Geophys. Res.* **74**, 3953.
Anderson, K. A. and Ness, N. F.: 1966, *J. Geophys. Res.* **71**, 3705.
Anderson, K. A., Harris, H. K., and Paoli, R. J.: 1965, *J. Geophys. Res.* **70**, 1039.
Anderson, K. A., Binsack, J. H., and Fairfield, D. H.: 1968, *J. Geophys. Res.* **73**, 2371.
Argo, H. V., Asbridge, J. R., Bame, S. J., Hundhausen, A. J., and Strong, I. B.: 1967, *J. Geophys. Res.* **72**, 1989.
Armstrong, T. P. and Krimigis, S. M.: 1968, *J. Geophys. Res.* **73**, 143.
Asbridge, J. R., Bame, S. J., and Strong, I. B.: 1968, *J. Geophys. Res.* **73**, 5777.
Axford, W. I.: 1962, *J. Geophys. Res.* **67**, 3791.
Axford, W. I. and Hines, C. O.: 1961, *Can. J. Phys.* **39**, 1433.
Bame, S. J., Asbridge, J. R., Felthauser, H. E., Olson, R. A., and Strong, I. B.: 1966, *Phys. Rev. Letters* **16**, 138.
Bame, S. J., Asbridge, J. R., Felthauser, H. E., Hones, E. W., and Strong, I. B.: 1967, *J. Geophys. Res.* **72**, 113.
Beard, D. B.: 1960, *J. Geophys. Res.* **65**, 3559.
Behannon, K. W.: 1968, *J. Geophys. Res.* **73**, 907.
Behannon, K. W. and Ness, N. F.: 1966, *J. Geophys. Res.* **71**, 2327.
Binsack, J. H.: 1968, in *Physics of the Magnetosphere* (ed. by R. L. Carovillano *et al.*), D. Reidel Pub. Co., Dordrecht, Holland, p. 605.
Binsack, J. H. and Vasyliunas, V. M.: 1968, *J. Geophys. Res.* **73**, 429.
Bonetti, A., Bridge, H. S., Lazarus, A. J., Rossi, B., and Sherb, F.: 1963, *J. Geophys. Res.* **68**, 4017.
Bridge, H., Egidi, A., Lazarus, A., and Lyon, E.: 1965a, in *Space Research*, vol. V, North-Holland Pub. Co., Amsterdam, p. 969.

Bridge, H., Egidi, A., Lyon, E., Moreno, G., Olbert, S., and Rossi, B.: 1965b, *Trans. Am. Geophys. Union* **46**, 119.
Brody, K. I., Holzer, R. E., and Smith, E. T.: 1968, *Trans. Am. Geophys. Union* **49**, 280.
Burlaga, L. F. and Ogilvie, K. W.: 1968, *J. Geophys. Res.* **73**, 6167.
Cahill, L. J., Jr.: 1965, University of New Hampshire Preprint, UNH-65-4.
Cahill, L. J., Jr.: 1966, in *Space Research*, vol. VI, Spartan Books, Washington, D.C., p. 662.
Cahill, L. J. and Amazeen, P. G.: 1963, *J. Geophys. Res.* **68**, 1835.
Chapman, S. and Ferraro, V. C. A.: 1931, *Terr. Magnetism Atmos. Elec.* **36**, 77 and 171.
Coleman, P. J., Jr.: 1964, *J. Geophys. Res.* **69**, 3051.
Coleman, P. J., Jr., Sonett, C. P., Judge, D. L., and Smith, E. J.: 1960, *J. Geophys. Res.* **65**, 1856.
Coleman, P. J., Jr., Davis, L., Jr., Hones, D. E., and Smith, E. J.: 1965, *Trans. Am. Geophys. Union* **46**, 533.
Coon, J. H.: 1966, in *Radiation Trapped in the Earth's Magnetic Field* (ed. by B. M. McCormac), D. Reidel Publ. Co., Dordrecht, Holland, p. 231.
Cummings, W. D. and Coleman, P. J., Jr.: 1968, UCLA Preprint No. 654, Los Angeles, Calif.
Dessler, A. J.: 1964, *J. Geophys. Res.* **69**, 3913.
Dessler, A. J.: 1967, *Revs. Geophys.* **5**, 1.
Dessler, A. J.: 1968, *J. Geophys. Res.* **73**, 209.
Dessler, A. J. and Michel, F. C.: 1966, *J. Geophys. Res.* **71**, 1421.
Dryer, M. and Faye-Peterson, R.: 1966, *Am. Inst. Aeronaut. Astronaut. J.* **4**, 246.
Dryer, M. and Heckman, G. E.: 1967, *Planetary Space Sci.* **15**, 515.
Dungey, J. W.: 1961, *Phys. Rev. Letters* **6**, 47.
Dungey, J. W.: 1963, *Planetary Space Sci.* **10**, 223.
Dungey, J. W.: 1965, *J. Geophys. Res.* **70**, 1753.
Dungey, J. W.: 1968, *Earth Particle and Fields*, Reinhold Book Corp., New York, p. 385.
Fairfield, D. H.: 1967, *J. Geophys. Res.* **72**, 5865.
Fairfield, D. H.: 1968a, Goddard Space Flight Center, Preprint X-616-68-454, Greenbelt, Md.
Fairfield, D. H.: 1968b, *J. Geophys. Res.* **73**, 6179.
Fairfield, D. H. and Ness, N. F.: 1967, *J. Geophys. Res.* **72**, 2379.
Fan, C. Y., Gloeckler, G., and Simpson, J. A.: 1964, *Phys. Rev. Letters* **13**, 149.
Frank, L. A.: 1965, *J. Geophys. Res.* **70**, 1593.
Frank, L. A.: 1967a, *J. Geophys. Res.* **72**, 185.
Frank, L. A.: 1967b, *J. Geophys. Res.* **72**, 1905.
Frank, L. A. and Shope, W. L.: 1968, *Trans. Am. Geophys. Union* **49**, 279.
Fredricks, R. W., Kennel, C. F., Scarf, F. L., Crook, G. M., and Green, I. M.: 1968, *Phys. Rev. Letters* **21**, 1761.
Freeman, J. W., Jr.: 1964, *J. Geophys. Res.* **69**, 1691.
Freeman, J. W., Jr. and Maguire, J. J.: 1967, *J. Geophys. Res.* **72**, 5257.
Freeman, J. W., Van Allen, J. A., and Cahill, L. J.: 1963, *J. Geophys. Res.* **68**, 2121.
Freeman, J. W., Jr., Warren, C. S., and Maguire, J. J.: 1968, *J. Geophys. Res.* **73**, 5719.
Gosling, J. T., Asbridge, J. R., Bame, S. J., and Strong, I. B.: 1967, *J. Geophys. Res.* **72**, 101.
Greenstadt, E. W., Green, I. M., Inouye, G. T., Hundhausen, A. J., Bame, S. J., and Strong, I. B.: 1968, *J. Geophys. Res.* **73**, 51.
Gringauz, K. I., Kurt, V. G., Moroz, V. I., and Shklovskiy, I. S.: 1960a, *Doklady AN SSSR* **132**, 1062.
Gringauz, K. I., Kurt, V. G., Moroz, V. I., and Shklovskiy, I. S.: 1960b, *Astron. Zh.* **37**, 716.
Gringauz, K. I., Bezrukikh, V. V., Balandina, S. M., Ozerov, V. D., and Rybchinsky, R. E.: 1963, in *Space Research*, vol. III, North-Holland Publ. Co., Amsterdam, p. 602.
Gringauz, K. I., Bezrukikh, V. V., Musatov, L. S., Rybchinsky, R. E., and Sheronova, S. M.: 1964, in *Space Research*, vol. IV, North-Holland Publ. Co., Amsterdam, p. 621.
Gringauz, K. I., Bezrukikh, V. V., Khokhlov, M. Z., Musativ, L. S., and Reminzov, A. R.: 1966, *Dokl. Akad. Nauk. SSSR Geofiz.* **170**, 570.
Heppner, J. P., Ness, N. F., Scearce, C. S., and Skillman, T. L.: 1963, *J. Geophys. Res.* **68**, 1.
Heppner, J. P., Sugiura, M., Skillman, T. L., Ledley, B. G., and Campbell, M.: 1967, *J. Geophys. Res.* **72**, 5417.
Hess, W. N.: 1968, *The Radiation Belt and Magnetosphere*, Blaisdell Publ. Co., Waltham, Mass.
Hess, W. N. and Mead, G. D.: 1968, *Introduction to Space Science*, 2nd ed., Gordon and Breach, Science Publishers, New York.
Holzer, R. E., McLeod, M. G., and Smith, E. J.: 1966, *J. Geophys. Res.* **71**, 1481.

Hones, E. W., Jr., Asbridge, J. R., Bame, S. J., and Strong, I. B.: 1967, *J. Geophys. Res.* **72**, 5879.
I. G. Bulletin: 1964, *Trans. Am. Geophys. Union* **45**, 501.
Intriligator, D., Wolfe, J., McKibbin, D., Collard, H., Scarf, F., Greenstadt, E., Ness, N., and Mariani, F.: 1968, *Symposium on the Physics of the Magnetosphere*, Book of Abstracts, Washington, D.C., Sept. 3–13.
Intriligator, D. S., Wolfe, J. H., McKibbin, D. D., and Collard, H. R.: 1969a, *Planetary Space Sci.* **17**, 321.
Intriligator, D. S., Wolfe, J. H., and McKibbin, D. D.: 1969b (to be published).
Johnson, F. S.: 1960, *J. Geophys. Res.* **65**, 3049.
Jokipii, J. R.: 1966, *J. Geophys. Res.* **71**, 3173.
Jokipii, J. R.: 1968, *J. Geophys. Res.* **73**, 931.
Kellogg, P. J.: 1962, *J. Geophys. Res.* **67**, 3805.
Kennel, C. F. and Sagdeev, R. Z.: 1967, *J. Geophys. Res.* **72**, 3303 and 3327.
Konradi, A.: 1966, *J. Geophys. Res.* **71**, 2317.
Krimigis, S. M., Van Allen, J. A., and Armstrong, T. P.: 1967, *Phys. Rev. Letters* **18**, 1204.
Lin, R. P.: 1968, *J. Geophys. Res.* **73**, 3066.
Lin, R. P. and Anderson, K. A.: 1966, *J. Geophys. Res.* **71**, 4213.
Mackin, R. J., Jr. and Neugebauer, M.: 1966, *The Solar Wind*, Pergamon Press, New York.
McDiarmid, I. B. and Burrows, J. R.: 1965, *J. Geophys. Res.* **70**, 3031.
McKibbin, D. D., Wolfe, J. H., Card, D. H., and Intriligator, D. S.: 1969 (to be published).
Mead, G. D. and Beard, D. B.: 1964, *J. Geophys Res.* **69**, 1169.
Michel, F. C. and Dessler, A. J.: 1965, *J. Geophys. Res.* **70**, 4305.
Mihalov, J. D. and Sonett, C. P.: 1968, *J. Geophys. Res.* **73**, 6837.
Mihalov, J. D., Colburn, D. S., Currie, R. G., and Sonett, C P.: 1968, *J. Geophys. Res.* **73**, 943.
Mihalov, J. D., Sonett, C. P., and Wolfe, J. H.: 1969, *J. Plasma Phys.* **3**, 449.
Montgomery, M. D.: 1968, *J. Geophys. Res.* **73**, 871.
Montgomery, M. D., Singer, S., Conner, J. P., and Stogsdill, E. E.: 1965, *Phys. Rev. Letters* **14**, 209.
Murayama, T.: 1966, *J. Geophys. Res.* **71**, 5547.
Murayama, T. and Simpson, J. A.: 1968, *J. Geophys. Res.* **73**, 891.
Ness, N. F.: 1965, *J. Geophys. Res.* **70**, 2989.
Ness, N. F.: 1967, *Solar-Terrestrial Physics*, Academic Press, Inc., London, p. 57.
Ness, N. F.: 1969, *Rev. of Geophys.* (in press).
Ness, N. F., Scearce, C. S., and Seek, J. B.: 1964, *J. Geophys. Res.* **69**, 3531.
Ness, N. F., Scearce, C. S., and Cantarano, S.: 1966, *J. Geophys. Res.* **71**, 3305.
Ness, N. F., Scearce, C. S., and Cantarano, S. C.: 1967, *J. Geophys. Res.* **72**, 3769.
Neugebauer, M. and Snyder, C. W.: 1962, Jet Propulsion Laboratory, Tech. Mem. 33-111.
Neugebauer, M. and Snyder, C. W.: 1966, *The Solar Wind*, Pergamon Press, New York, p. 3.
Obayashi, T : 1964, *J. Geophys. Res.* **69**, 861.
Ogilvie, K. W., Burlaga, L. F. and Wilkerson, T. D.: 1968, Goddard Space Flight Center Preprint No. X-616-68-441.
Olbert, S.: 1968, M.I.T. preprint CSR-P-68-6.
Piddington, J. H.: 1960, *J. Geophys. Res.* **65**, 93.
Scarf, F. L., Crook, G. M., Green, I. M., and Virobik, P. F.: 1968, *J. Geophys. Res.* **73**, 6665.
Serlemitsos, P.: 1966, *J. Geophys. Res.* **71**, 61.
Shklovskiy, I. S., Moroz, V. I., and Kurt, V. G.: 1960, *Astron. Zh.* **37**, 931.
Siscoe, G. L., Davis, L., Jr., Smith, E. J., Coleman, P. J., Jr., and Jones, D. E.: 1967, *J. Geophys. Res.* **72**, 1.
Smith, E. J.: 1962, *J. Geophys. Res.* **67**, 2045.
Smith, E. J., Coleman, P. J., Judge, D. L., and Sonett, C. P., 1960: *J. Geophys. Res.* **65**, 1858.
Smith, E. J., Holzer, R. E., McLeod, M. G., and Russell, C. T.: 1967, *J. Geophys. Res.* **72**, 4803.
Snyder, C. W. and Neugebauer, M.: 1964, in *Space Research*, vol IV, North-Holland Publ. Co., Amsterdam p. 89.
Sonett, C. P.: 1959, *Proc. Astron. Soc. Pacific* **71**, 390.
Sonett, C. P. and Abrams, I. J.: 1963, *J. Geophys. Res.* **68**, 1233.
Sonett, C. P., Judge, D. L., Sims, A. R., and Kelso, J. M.: 1960, *J. Geophys. Res.* **65**, 55.
Sonett, C. P., Colburn, D. S., Davis, L., Jr., Smith, E. J., and Coleman, P. J., Jr.: 1964, *Phys. Rev. Letters* **13**, 153.

Sonett, C. P., Colburn, D. S., Currie, R. G., and Mihalov, J. D.: 1968, in *Physics of the Magnetosphere* (ed. by R. L. Carovillano *et al.*), D. Reidel Pub. Co., Dordrecht, Holland, p. 461.
Speiser, T. W.: 1968, *Earth's Particles and Fields*, Reinhold Book Corp., New York, p. 393.
Speiser, T. W., and Ness, N. F.: 1967, *J. Geophys. Res.* **72**, 131.
Spreiter, J. R. and Alksne, A. Y.: 1968, *Planetary Space Sci.* **16**, 971.
Spreiter, J. R. and Alksne, A. Y.: 1969, *Planetary Space Sci.* (in press).
Spreiter, J. R. and Briggs, B. R.: 1962, *J. Geophys. Res.* **67**, 37.
Spreiter, J. R. and Jones, W. P.: 1963, *J. Geophys. Res.* **68**, 3555.
Spreiter, J. R., Summers, A. L., and Alksne, A. Y.: 1966, *Planetary Space Sci.* **14**, 223.
Spreiter, J. R., Summers, A. L., and Alksne, A. Y.: 1968, *J. Geophys. Res.* **73**, 1851.
Sugiura, M., Skillman, T. L., Ledley, B. G., and Heppner, J. P.: 1968, *J. Geophys. Res.* **73**, 6699.
Tidman, D. A.: 1967, *J. Geophys. Res.* **72**, 1799.
Van Allen, J. A.: 1966, *J. Geophys. Res.* **71**, 2406.
Vasyliunas, V. M.: 1968, *J. Geophys. Res.* **73**, 2839.
Vernov, S. N., Melnikov, V. V., Savenko, I. A., and Savin, B. I.: 1966, in *Space Research*, vol. VI, p. 746.
Wilcox, J. M.: 1968, *Space Sci. Rev.* **8**, 258.
Wolfe, J. H. and McKibbin, D. D.: 1968, *Planetary Space Sci.* **16**, 953.
Wolfe, J. H. and Silva, R. W.: 1965, *J. Geophys. Res.* **70**, 3575.
Wolfe, J. H., Silva, R. W., and Myers, M. A.: 1966a, *J. Geophys. Res.* **71**, 1319.
Wolfe, J. H., Silva, R. W., and Myers, M. A.: 1966b, in *Space Research*, vol. VI, Macmillan, London, p. 680.
Wolfe, J. H., Silva, R. W., McKibbin, D. D., and Mason, R. H.: 1967, *J. Geophys. Res.* **72**, 4577.